

# SEISMIC RESPONSE OF JACK-UPS

AN IMPROVED PROCEDURE USING TIME HISTORY ANALYSIS

S.B. LATOOIJ





# Seismic response of jack-ups

An improved earthquake screening procedure using  
time history analysis

by

**S.B. Latooi**

to obtain the degree of

**Master of Science**

at the Delft University of Technology

Student number: 1396951

**Educational institution:**

Delft University of Technology  
Faculty of Civil Engineering and Geosciences  
Section Offshore Engineering

Stevinweg 1  
2628CN Delft  
The Netherlands

**Graduation committee:**

An electronic version of this thesis will be available at <http://repository.tudelft.nl/>.



# Abstract

Jack-ups are used for offshore wind turbine installation (OWTI). To assess whether a jack-up can safely operate in a desired geographic location with known seismic activity, an earthquake response analysis is required for structural verification. This analysis is generally carried out according to the codes of the International Organization for Standardization (ISO). The prescribed procedure is called extreme level earthquake (ELE) screening and is performed using response spectrum analysis (RSA). This method is intended to be conservative and should produce higher utilization results than more detailed assessments. With offshore wind farm development moving into regions with greater seismic activity, more detailed assessments are required to demonstrate safe operation in those geographic locations.

The aim of this research was to improve the accuracy of earthquake screening of OWTI jack-ups in order to increase their geographic operability. A new ELE-screening procedure was proposed that uses time-history analysis (THA) and spectrum matched acceleration time history records (THR). For the development and benchmarking of the new method, an earthquake analysis was performed using both the new ELE-screening procedure with THA and the existing ELE-screening procedure with RSA. The analysis was performed for an OWTI jack-up based on the GJ-3750C located in a region offshore Japan. The RSA simulations were performed using Minifem; a new tool was developed in OpenSees for the THA simulations. To assess the effect of various parameters, simulations were run with different soil-structure connections, levels of damping, and design response spectra. The performance is evaluated using the global maximum action effects; limited to the forces and moments at the lower guide and footing. A soil-structure interaction analysis was performed on an equivalent single degree of freedom system to validate the soil-structure interface model, and the use of free field ground motions. A procedure and accompanying tools were developed for acceleration time history record selection and modification. The resulting spectrum matched THR are used for seismic excitation in the THA simulations.

The simulation results showed a reduction in the magnitude of calculated action effects when using the new ELE-screening procedure. A reduction of 10 to 20 percent in the global maximum shear force and moment was observed in the simulations best describing the jack-up and site-specific soil conditions. A small reduction of the global maximum normal force was also observed. The new ELE-screening procedure with THA can be used to demonstrate compliance with earthquake performance requirements when a jack-up does not satisfy the ELE-screening assessment criteria using RSA. Since safe operation can be demonstrated for more areas, the geographic operability of OWTI jack-ups is increased.



# Contents

Abstract	iii
List of abbreviations	ix
List of Figures	xi
List of Tables	xvii
1 Introduction	1
1.1 Background information . . . . .	1
1.2 Problem definition . . . . .	1
1.3 Research aim, objectives, and questions . . . . .	2
1.4 Research methodology . . . . .	2
1.5 Structure of report . . . . .	3
2 Seismic analysis procedure	5
2.1 ISO Seismic design procedures . . . . .	5
2.2 Existing earthquake analysis procedures . . . . .	7
2.3 New ELE-screening procedure using THA. . . . .	8
2.4 Benchmarking considerations . . . . .	9
3 Structural model	13
3.1 Model under consideration . . . . .	13
3.2 Structural model of the jack-up . . . . .	14
3.3 System damping . . . . .	16
3.4 Foundation modeling. . . . .	17
3.5 Verification of structural models . . . . .	18
4 Ground motions	21
4.1 Local site conditions . . . . .	21
4.2 ISO acceleration design response spectrum. . . . .	22
4.3 DRS used for simulations . . . . .	24
4.4 Ground motion selection . . . . .	25
4.5 Principal axes . . . . .	26
4.6 Spectrum matching. . . . .	26
5 Soil-structure interaction	31
5.1 Soil-structure interaction analysis methods. . . . .	31

5.2	SSI analysis of SDOF system . . . . .	32
5.3	SSI Simulations and Results. . . . .	35
6	Simulations . . . . .	37
6.1	Simulation cases . . . . .	37
6.2	Earthquake rotation. . . . .	38
6.3	Assessment criteria . . . . .	39
6.4	RSA simulation process in Minifem . . . . .	40
6.5	THA simulation process in OpenSees . . . . .	41
7	Results . . . . .	43
7.1	Simulation results. . . . .	43
7.2	Effect of vertical radiation damping. . . . .	49
7.3	Effect of time development . . . . .	50
7.4	Remarks on simulations . . . . .	53
8	Discussion . . . . .	55
8.1	Structural model . . . . .	55
8.1.1	Hull model. . . . .	55
8.1.2	Leg model . . . . .	56
8.2	Ground motions . . . . .	57
8.2.1	THR selection and spectrum matching bias . . . . .	57
8.2.2	Period range for spectrum matching . . . . .	58
8.3	Soil-structure interaction . . . . .	58
8.4	Simulation cases . . . . .	60
8.4.1	Soil-structure connection . . . . .	60
8.4.2	SRSS rule in RSA . . . . .	60
8.5	Simulation results. . . . .	62
8.5.1	Global maximum action effects . . . . .	62
8.5.2	Number of THR . . . . .	64
8.5.3	Earthquake angle of incidence. . . . .	65
8.5.4	Time development THA . . . . .	66
9	Conclusion and Recommendations . . . . .	69
9.1	Conclusion . . . . .	69
9.2	Recommendations . . . . .	73
A	Rayleigh damping ratio . . . . .	75
B	Site seismic maps . . . . .	77

---

C	Analysis methods	79
C.1	Response spectrum analysis . . . . .	79
C.2	Time history analysis . . . . .	82
D	Spectrum matching quality	83
E	Eigenmodes	87
E.1	Fixed case. . . . .	87
E.2	Pinned case. . . . .	89
E.3	Spring case . . . . .	91
F	Time development graphs	93
	Bibliography	95



# List of abbreviations

Abbreviation	Definition
ALE	abnormal level earthquake
ALS	accidental limit state
CQC	complete quadratic combination
DOF	degrees of freedom
DRS	design response spectrum
DSHA	deterministic seismic hazard analysis
ELE	extreme level earthquake
FT	footing
ISO	International Organization for Standardization
LG	lower guide
MDOF	multiple degrees of freedom
MMS	mean matched spectrum
MSL	mean sea level
OWTI	offshore wind turbine installation
PSHA	probabilistic seismic hazard analysis
RSA	response spectrum analysis
SDOF	single degree of freedom
SRC	seismic risk category
SRSS	square root of sum of squares
THA	time history analysis
ULS	ultimate limit state



# List of Figures

3.1	Side view of the jack-up unit in operational condition . . . . .	14
3.2	Side view of lumped parameter beam model consisting of nodes and elements . . . . .	14
3.3	Top view of the jack-up unit in operational condition . . . . .	14
3.4	Top view of lumped parameter beam model consisting of nodes and elements . . . . .	14
3.5	Cross section of the hull and two jack-houses. The axial force $F_V$ , shear force $F_H$ , and bending moment $M$ of the leg at the lower guide are shown. . . . .	15
3.6	Damping ratio when fitted to modes 1 and 4, and damping ratios when fitted to mode 1 and 10, for the fixed condition . . . . .	17
3.7	Mode 1 of fixed case in Minifem . . . . .	19
3.8	Mode 1 of fixed case in OpenSees . . . . .	19
3.9	Mode 2 of fixed case in Minifem . . . . .	19
3.10	Mode 2 of fixed case in OpenSees . . . . .	19
3.11	Mode 3 of fixed case in Minifem . . . . .	19
3.12	Mode 3 of fixed case in OpenSees . . . . .	19
4.1	Earthquake hypocentres in Japan [1] . . . . .	22
4.2	Lithosperic plates [1] . . . . .	22
4.3	Seismic acceleration design response spectrum for 5% damping according to ISO 19901-2[2] . . . . .	23
4.4	Vertical to horizontal spectral amplification function[2] . . . . .	23
4.5	5% H and 5% V damped DRS, T = 0 to 10[s] . . . . .	24
4.6	5% H and 5% V damped DRS, T = 0 to 2[s] . . . . .	24
4.7	5% H and 15%V damped DRS, T = 0 to 10[s] . . . . .	24
4.8	5% H and 15%V damped DRS, T = 0 to 2[s] . . . . .	24
4.9	Response spectra of the unmatched principal component of 4 earthquake time histories, and the 5% damped horizontal design response spectrum . . . . .	28
4.10	Response spectra of the matched principal component of 4 earthquake time histories, and the 5% damped horizontal design response spectrum. The time traces are matched over a period range from 0.1 to 3 seconds . . . . .	29
4.11	Original and matched acceleration, velocity, and displacement time history of the principal component of the RSN332 Coalinga earthquake . . . . .	29
5.1	Equivalent SDOF system resting on top of a homogeneous soil half space in the initial state and the deformed state [3] . . . . .	33
5.2	Motion of structure with and without SSI for $G=66e5$ . . . . .	36
5.3	SSI induced motion under base for $G=66e5$ . . . . .	36

5.4	Motion of structure with and without SSI for $G=66e6$ . . . . .	36
5.5	SSI induced motion under base for $G=66e6$ . . . . .	36
5.6	Motion of structure with and without SSI for $G=66e7$ . . . . .	36
5.7	SSI induced motion under base for $G=66e7$ . . . . .	36
6.1	OpenSees framework . . . . .	41
7.1	Max shear force $F_{H,LG}$ at the lower guide per EQ incidence angle for the Fixed connection . . . . .	44
7.2	Max shear force $F_{H,FT}$ at the footing per EQ incidence angle for the Fixed connection . . . . .	44
7.3	Max normal force $V_{LG}$ at the lower guide per EQ incidence angle for the Fixed connection . . . . .	44
7.4	Max normal force $V_{FT}$ at the footing per EQ incidence angle for the Fixed connection . . . . .	44
7.5	Max moment $M_{LG}$ at the lower guide per EQ incidence angle for the Fixed connection . . . . .	44
7.6	Max moment $M_{FT}$ at the footing per EQ incidence angle for the Fixed connection . . . . .	44
7.7	Max shear force $F_{H,LG}$ at the lower guide per EQ incidence angle for the Pinned connection . . . . .	45
7.8	Max shear force $F_{H,FT}$ at the footing per EQ incidence angle for the Pinned connection . . . . .	45
7.9	Max normal force $V_{LG}$ at the lower guide per EQ incidence angle for the Pinned connection . . . . .	45
7.10	Max normal force $V_{FT}$ at the footing per EQ incidence angle for the Pinned connection . . . . .	45
7.11	Max moment $M_{LG}$ at the lower guide per EQ incidence angle for the Pinned connection . . . . .	45
7.12	Max moment $M_{FT}$ at the footing per EQ incidence angle for the Pinned connection . . . . .	45
7.13	Max shear force $F_{H,LG}$ at the lower guide per EQ incidence angle for the Spring5 connection . . . . .	46
7.14	Max shear force $F_{H,FT}$ at the footing per EQ incidence angle for the Spring5 connection . . . . .	46
7.15	Max normal force $V_{LG}$ at the lower guide per EQ incidence angle for the Spring5 connection . . . . .	46
7.16	Max normal force $V_{FT}$ at the footing per EQ incidence angle for the Spring5 connection . . . . .	46
7.17	Max moment $M_{LG}$ at the lower guide per EQ incidence angle for the Spring5 connection . . . . .	46
7.18	Max moment $M_{FT}$ at the footing per EQ incidence angle for the Spring5 connection . . . . .	46
7.19	Max shear force $F_{H,LG}$ at the lower guide per EQ incidence angle for the Spring15 connection . . . . .	47
7.20	Max shear force $F_{H,FT}$ at the footing per EQ incidence angle for the Spring15 connection . . . . .	47
7.21	Max normal force $V_{LG}$ at the lower guide per EQ incidence angle for the Spring15 connection . . . . .	47
7.22	Max normal force $V_{FT}$ at the footing per EQ incidence angle for the Spring15 connection . . . . .	47
7.23	Max moment $M_{LG}$ at the lower guide per EQ incidence angle for the Spring15 connection . . . . .	47
7.24	Max moment $M_{FT}$ at the footing per EQ incidence angle for the Spring15 connection . . . . .	47
7.25	Max shear force $F_{H,LG}$ at the lower guide per EQ incidence angle for the Spring15ISO connection . . . . .	48
7.26	Max shear force $F_{H,FT}$ at the footing per EQ incidence angle for the Spring15ISO connection . . . . .	48
7.27	Max normal force $V_{LG}$ at the lower guide per EQ incidence angle for the Spring15ISO connection . . . . .	48
7.28	Max normal force $V_{ft}$ at the footing per EQ incidence angle for the Spring15ISO connection . . . . .	48
7.29	Max moment $M_{LG}$ at the lower guide per EQ incidence angle for the Spring15ISO connection . . . . .	48
7.30	Max moment $M_{LG}$ at the footing per EQ incidence angle for the Spring15ISO connection . . . . .	48
7.31	Max $F_{H,LG}$ per leg per FKS01 EQ incidence angle found in time for the Fixed connection . . . . .	50

7.32 Max $F_{H,LG}$ per leg per FKS01 EQ incidence angle found from $F_{X,max}, F_{Y,max}$ for the Fixed connection . . . . .	50
7.33 Max $M_{LG}$ per leg per FKS01 EQ incidence angle found in time for the Fixed connection . . . . .	50
7.34 Max $M_{LG}$ per leg per FKS01 EQ incidence angle found from $M_{X,max}, M_{Y,max}$ for the Fixed connection . . . . .	50
7.35 Max $F_{H,LG}$ per leg per FKS01 EQ incidence angle found in time for the Pinned connection . . . . .	51
7.36 Max $F_{H,LG}$ per leg per FKS01 EQ incidence angle found from $F_{X,max}, F_{Y,max}$ for the Pinned connection . . . . .	51
7.37 Max $M_{LG}$ per leg per FKS01 EQ incidence angle found in time for the Pinned connection . . . . .	51
7.38 Max $M_{LG}$ per leg per FKS01 EQ incidence angle found from $M_{X,max}, M_{Y,max}$ for the Pinned connection . . . . .	51
7.39 Max $F_{H,LG}$ per leg per FKS01 EQ incidence angle found in time for the Spring5 connection . . . . .	51
7.40 Max $F_{H,LG}$ per leg per FKS01 EQ incidence angle found from $F_{X,max}, F_{Y,max}$ for the Spring5 connection . . . . .	51
7.41 Max $M_{LG}$ per leg per FKS01 EQ incidence angle found in time for the Spring5 connection . . . . .	52
7.42 Max $M_{LG}$ per leg per FKS01 EQ incidence angle found from $M_{X,max}, M_{Y,max}$ for the Spring5 connection . . . . .	52
7.43 Max $F_{H,LG}$ per leg per FKS01 EQ incidence angle found in time for the Spring15 connection . . . . .	52
7.44 Max $F_{H,LG}$ per leg per FKS01 EQ incidence angle found from $F_{X,max}, F_{Y,max}$ for the Spring15 connection . . . . .	52
7.45 Max $M_{LG}$ per leg per FKS01 EQ incidence angle found in time for the Spring15 connection . . . . .	52
7.46 Max $M_{LG}$ per leg per FKS01 EQ incidence angle found from $M_{X,max}, M_{Y,max}$ for the Spring15 connection . . . . .	52
8.1 Structural model of the hull . . . . .	56
8.2 Mode 4 of spring case . . . . .	56
8.3 Basis for new structural model 1 . . . . .	56
8.4 Basis for new structural model 2 . . . . .	56
8.5 The existing structural model of the leg and leg-hull interface at the jack-house . . . . .	57
8.6 Proposed new structural model of the leg and leg-hull interface incorporating the jack-house . . . . .	57
8.7 Max normal force $V_{LG}$ at the lower guide per EQ incidence angle for the Spring15 connection . . . . .	63
8.8 Max normal force $V_{FT}$ at the footing per EQ incidence angle for the Spring15 connection . . . . .	63
8.9 Max shear force $F_{H,LG}$ at the lower guide per EQ incidence angle for the Pinned connection . . . . .	64
8.10 Max moment $M_{LG}$ at the lower guide per EQ incidence angle for the Pinned connection . . . . .	64
8.11 Max shear force $F_{H,LG}$ at the lower guide per EQ incidence angle for the Fixed connection . . . . .	65
8.12 Max moment $M_{LG}$ at the lower guide per EQ incidence angle for the Fixed connection . . . . .	65
8.13 Max shear force $F_{H,FT}$ at the footing per EQ incidence angle for the Spring15 connection . . . . .	65
8.14 Max moment $M_{FT}$ at the footing per EQ incidence angle for the Spring15 connection . . . . .	65
8.15 Max shear force $F_{H,LG}$ at the lower guide per EQ incidence angle for the Spring15 connection (time) . . . . .	66
8.16 Max shear force $F_{H,LG}$ at the lower guide per EQ incidence angle for the Spring15 connection (XY) . . . . .	66

8.17	Max moment $M_{LG}$ at the lower guide per EQ incidence angle for the Spring15 connection (time)	67
8.18	Max moment $M_{LG}$ at the lower guide per EQ incidence angle for the Spring15 connection (XY)	67
8.19	Max shear force $F_{H,LG}$ at the lower guide per EQ incidence angle for the Spring15 connection; FKS01	67
8.20	Max moment $M_{LG}$ at the lower guide per EQ incidence angle for the Spring15 connection; FKS01	67
A.1	Damping ratio when fitted to modes 1 and 4, and damping ratios when fitted to mode 1 and 10, for the Fixed condition	75
A.2	Damping ratio when fitted to modes 1 and 4, and damping ratios when fitted to mode 1 and 10, for the Pinned condition	75
A.3	Damping ratio when fitted to modes 1 and 4, and damping ratios when fitted to mode 1 and 10, for the Spring conditions	76
B.1	Map of spectral accelerations offshore Japan for 0.2[s] oscillator period	77
B.2	Map of spectral accelerations offshore Japan for 1.0[s] oscillator period	78
C.1	Schematic illustration of the construction of the displacement response spectrum of a SDOF with 2% damping for the El Centro earthquake of 1940 [4]	80
E.1	Mode 1 of fixed case	87
E.2	Mode 2 of fixed case	87
E.3	Mode 3 of fixed case	88
E.4	Mode 4 of fixed case	88
E.5	Mode 5 of fixed case	88
E.6	Mode 6 of fixed case	88
E.7	Mode 7 of fixed case	88
E.8	Mode 8 of fixed case	88
E.9	Mode 9 of fixed case	89
E.10	Mode 10 of fixed case	89
E.11	Mode 1 of pinned case	89
E.12	Mode 2 of pinned case	89
E.13	Mode 3 of pinned case	89
E.14	Mode 4 of pinned case	89
E.15	Mode 5 of pinned case	90
E.16	Mode 6 of pinned case	90
E.17	Mode 7 of pinned case	90
E.18	Mode 8 of pinned case	90
E.19	Mode 9 of pinned case	90
E.20	Mode 10 of pinned case	90
E.21	Mode 1 of spring case	91
E.22	Mode 2 of spring case	91

---

E.23 Mode 3 of spring case . . . . .	91
E.24 Mode 4 of spring case . . . . .	91
E.25 Mode 5 of spring case . . . . .	91
E.26 Mode 6 of spring case . . . . .	91
E.27 Mode 7 of spring case . . . . .	92
E.28 Mode 8 of spring case . . . . .	92
E.29 Mode 9 of spring case . . . . .	92
E.30 Mode 10 of spring case . . . . .	92
F1 Max shear force $F_{H,LG}$ at the lower guide per EQ incidence angle for the Spring15 connection; FKS01 . . . . .	93
F2 Max moment $M_{LG}$ at the lower guide per EQ incidence angle for the Spring15 connection; FKS01	93
F3 Max shear force $F_{H,LG}$ at the lower guide per EQ incidence angle for the Spring15 connection; RSN33 . . . . .	94
F4 Max moment $M_{LG}$ at the lower guide per EQ incidence angle for the Spring15 connection; RSN33	94
F5 Max shear force $F_{H,LG}$ at the lower guide per EQ incidence angle for the Spring15 connection; RSN57 . . . . .	94
F6 Max moment $M_{LG}$ at the lower guide per EQ incidence angle for the Spring15 connection; RSN57	94
F7 Max shear force $F_{H,LG}$ at the lower guide per EQ incidence angle for the Spring15 connection; RSN73 . . . . .	94
F8 Max moment $M_{LG}$ at the lower guide per EQ incidence angle for the Spring15 connection; RSN73	94



# List of Tables

2.1	Seismic risk category for manned offshore structures based on seismic zone . . . . .	6
2.2	Seismic design requirements for each seismic risk category . . . . .	6
2.3	Advantages and limitations of the ELE-screening method using RSA and the ALE method using THA . . . . .	8
3.1	Eigenvalue, eigenfrequency, and eigenperiod of the Fixed model . . . . .	20
3.2	Eigenvalue, eigenfrequency, and eigenperiod of the Pinned model . . . . .	20
3.3	Eigenvalue, eigenfrequency, and eigenperiod of the models with Springs . . . . .	20
4.1	Correction factor for acceleration $C_a$ . . . . .	22
4.2	Correction factor for velocity $C_v$ . . . . .	22
4.3	Earthquake time histories selected from PEER database [5] . . . . .	25
4.4	Eigenvalue, eigenfrequency, and eigenperiod of the first mode of the structure with fixed, pinned, and spring connection . . . . .	27
5.1	SSI analysis simulation cases . . . . .	35
7.1	Global maximum action effects for the Fixed connection . . . . .	44
7.2	Global maximum action effects for the Pinned connection . . . . .	45
7.3	Global maximum action effects for the Spring5 connection . . . . .	46
7.4	Global maximum action effects for the Spring15 connection . . . . .	47
7.5	Global maximum action effects for the Spring15ISO connection . . . . .	48
7.6	Global maximum action effects for the Spring5 connection . . . . .	49
7.7	Global maximum action effects for the Spring15 connection . . . . .	49
7.8	Global maximum action effects for the Spring15ISO connection . . . . .	49
8.1	Natural periods and damping ratios of the Fixed model for the first 10 modes . . . . .	61
8.2	Natural periods and damping ratios of the Pinned model for the first 10 modes . . . . .	61
8.3	Natural periods and damping ratios of the Spring15 model for the first 10 modes . . . . .	61
8.4	Global maximum action effects from the Fixed, Pinned, Spring5, Spring15, and Spring15ISO simulations . . . . .	62
9.1	Advantages and limitations of the ELE-screening method using RSA and the ALE method using THA . . . . .	70
D.1	Match quality of the major principal axis earthquake component time traces to the 5% damped horizontal design response spectrum . . . . .	83

---

D.2	Match quality of the intermediate principal axis earthquake component time traces to the 5% damped horizontal design response spectrum . . . . .	84
D.3	Match quality of the minor principal axis earthquake component time traces to the 5% damped vertical design response spectrum . . . . .	84
D.4	Match quality of the minor principal axis earthquake component time traces to the 15% damped vertical design response spectrum . . . . .	85

# 1

## Introduction

### 1.1. Background information

Site specific analysis is performed for mobile offshore structures to demonstrate safe operation in a desired geographic location. Earthquake response analysis is required for structural verification in areas with seismic activity. The objective of such an earthquake analysis is to develop a quantitative measure that converts strong ground motions at the base of the structure to loading and displacement demands. This analysis is generally carried out according to the codes of the International Organization for Standardization (ISO) as these are applicable worldwide. With offshore wind farm development moving into regions with higher and stronger seismic activity, offshore wind turbine installation (OWTI) jack-ups need to demonstrate safe operation for the conditions in those geographic locations.

### 1.2. Problem definition

When performing seismic analysis according to ISO-19905[6], the jack-up is assessed to its ultimate limit state (ULS) for strength and stiffness, whilst subjected to earthquake actions derived from a design spectrum for a return period of 1000 years. The ULS seismic design event is called an extreme level earthquake (ELE) and the earthquake assessment is referred to as ELE-screening. During such an event the structure should sustain little or no damage; only localized and limited non-linear behaviour is permitted. ELE-screening is performed using linear response spectrum analysis (RSA). The screening is intended to be a conservative method and should produce higher utilization results than more detailed assessments. If the jack-up does not satisfy the 1000 year ELE-screening assessment criteria, a more detailed method is used to evaluate compliance with earthquake performance requirements. The structure is assessed to its accidental limit state (ALS) for an abnormal level earthquake (ALE) using non-linear time history analysis (THA).

The current method being employed for earthquake response analysis of a jack-up is the "ELE-screening procedure using response spectrum analysis" from the ISO 19905 standard. This method is relatively straight forward and computationally efficient, however RSA only calculates the maximum displacement and member forces and moments in each mode without sign information. The method is purely linear and does not take P-delta effects (geometric non-linearities) into account. For large lateral displacements this can have a significant effect. It should also be noted that there is no time development in the RSA method.

When the structure does not satisfy the design checks of ELE-screening with RSA a more detailed method is required. The non-linear ALE analysis using THA is more accurate, however it is complex and requires several additional site-specific studies that are often not available. The method is also computationally very demanding. The development of an ELE-screening procedure using linear THA is proposed as an intermediate step. Improving the accuracy of ELE-screening is expected to result in lower action effects, thus increasing the operability of the structure, without having to perform non-linear ALE analysis. The model and tools required for ELE-screening with linear THA are very similar to those required for non-linear ALE analysis, and form the foundation of future development of more complex methods.

### 1.3. Research aim, objectives, and questions

The aim of this research is to improve the accuracy of earthquake screening of OWTI jack-ups in order to increase their geographic operability. In order to achieve this aim, a research methodology was designed to accomplish the following objectives:

- Obj. 1** Develop an improved earthquake screening procedure for jack-ups using time history analysis that will result in a more accurate assessment of the seismic action effects of the structure.
- Obj. 2** Develop a numerical tool to perform earthquake screening of jack-ups using linear time history analysis, and spectrum matched acceleration time history records.
- Obj. 3** Develop a procedure and accompanying tools for acceleration THR selection and modification for seismic excitation in THA simulations.
- Obj. 4** Assess the performance of the new ELE-screening procedure using THA by benchmarking it against the existing RSA procedure.

The following research questions were posed to aid in the development of the new method, and to evaluate whether the objectives of the research are achieved.

- RQ. 1** What are the advantages and limitations of the different earthquake analysis procedures?
- RQ. 2** Is the barstool structural model of the jack-up that has been used for RSA adequate for THA?
- RQ. 3** What are requirements for using spectrum matched THR in ELE-screening?
- RQ. 4** Do soil-structure interaction effects need to be included in ELE-screening with THA?
- RQ. 5** Does the jack-up have predetermined critical angles of earthquake incidence?
- RQ. 6** What are the benefits of time development in seismic analysis?
- RQ. 7** Does the new ELE-screening procedure result in lower action effects?
- RQ. 8** Does the new ELE-screening procedure achieve the aim of this research?

### 1.4. Research methodology

The ISO codes applicable to earthquake analysis of jack-ups were studied in order to define the framework in which the new procedure should fit. As these ISO codes are not very mature, other codes such as Eurocode-8 [7] and ASCE 7-16 [8] were consulted for reference. This was complemented with a literature study on the state of the art of earthquake engineering for mobile offshore structures. Following the literature study a new ELE-screening method that uses THA was developed and tested. The steps taken in the development of the new method consist of:

- Constructing a lumped parameter equivalent beam model for jack-up structures
- Selecting and modifying recorded ground motions to be used as seismic input for simulations
- Performing a soil-structure interaction analysis to validate the use of free field ground motions, and to validate the assumptions made for the interface connection between the soil and structure.
- Developing a THA simulation and analysis tool in the software framework OpenSees
- Developing Matlab scripts to analyze the output from the THA simulations

- Benchmarking the performance of the new THA procedure against the existing RSA procedure and analyzing the results.

A unit based on the GJ-3750C OWTI jack-up was used in the development of the method. The structural model, consisting of a rectangular hull and four cylindrical legs, was taken from previous RSA studies. For the site-specific data the unit was taken to be situated offshore Japan in a location where previous earthquake analysis studies have been performed by GustoMSC. Simulations were run with different soil-structure connections to represent different fixity conditions. The connections used are: fixed, pinned, and spring connection with different levels of damping. The GustoMSC program Minifem is used to perform RSA simulations, and OpenSees is used for THA simulations. The quantities used for benchmarking are the forces and moments at the lower guide and the footing.

## 1.5. Structure of report

**Chapter 2** looks at the seismic analysis procedure. The seismic design procedures of the International Organisation for Standardisation are examined. An overview of the two existing earthquake analysis procedures for jack-ups, as prescribed by ISO, are presented and their application and limitations discussed. The new earthquake analysis procedure is presented followed by the development and benchmarking considerations.

**Chapter 3** looks at the structural model for earthquake analysis using response spectrum analysis and time history analysis. A description is given of the jack-up and the operational condition under consideration. The method in which the jack-up is modeled as a lumped parameter beam model is discussed and the implementation of damping and the modeling of the foundation are described. The chapter concludes with the verification of the structural models.

**Chapter 4** looks at the ground motions. The local site conditions for the geographic design case are presented and the design response spectra used for the simulations are constructed according to the ISO standards. The criteria used for ground motion selection are discussed and the earthquake time histories are selected from the PEER strong motion database. The records are transformed to their principal axes, and spectrum matched to the design response spectra used for the time history analysis.

**Chapter 5** looks at the soil structure interaction. First the basics of soil-structure interaction are explained and the methods of analysis are presented. A SSI analysis is performed for an equivalent single degree of freedom system. The simulations that were run, and the results are presented.

**Chapter 6** looks at the earthquake analysis simulations that are used to assess the performance of the new ELE-screening procedure using THA against the existing ELE-screening procedure using RSA. First the different simulation cases and the rationale behind them are discussed, followed by an explanation on how different earthquake orientations are applied to the models. The assessment criteria for a jack-up subject to an ELE event and the corresponding action effects are presented. The RSA simulation process in Minifem and the THA simulation process in OpenSees conclude the chapter.

**Chapter 7** looks at the results of the simulations. First the format of the results are discussed and the results of the different simulation cases are presented. This is followed by an assessment on the effect of vertical radiation damping on the response of the structure. The effect of time development on the magnitude of the action effects is analyzed. The chapter concludes with some remarks on simulations that utilized one of the alternative solution algorithms, and which simulation cases did not converge to a solution.

**Chapter 8** discusses the results and findings of the previous chapters. First the choice of structural model and its influence on the action effects are discussed. This is followed by a discussion on the ground motions and on the soil-structure interaction. The chapter concludes with remarks on the simulation cases and a discussion on the simulation results.

**Chapter 9** concludes the report by answering the research questions and providing recommendations for future work.



# 2

## Seismic analysis procedure

Before a jack-up is mobilized to a location, a site-specific analysis is performed to ensure operational safety of the unit. When this location is in an area of seismic activity an earthquake assessment is required as part of the site-specific analysis. This chapter looks at the seismic analysis procedure. First the seismic design procedures of the International Organisation for Standardisation are examined in Section 2.1. The ISO codes are used due to their international applicability. An overview of the two existing earthquake analysis procedures for jack-ups, as prescribed by ISO, are presented in Section 2.2 and their application and limitations discussed. The new ELE-screening procedure using linear THA is presented in Section 2.3. The development and benchmarking considerations of the new procedure are described in Section 2.4.

### 2.1. ISO Seismic design procedures

The series of International Standards applicable to types of offshore structure, ISO 19900 to ISO 19906, addresses design requirements and assessments for all offshore structures used by the petroleum and natural gas industries worldwide. For earthquake response analysis of jack-ups, particular interest is paid to ISO 19901-2[2], ISO 19902[9], and ISO 19905-1[6]. ISO 19901-2 is intended to provide general seismic design procedures for different types of offshore structures, and a framework for the derivation of seismic design criteria. ISO 19902 specifies requirements and provides recommendations applicable to fixed steel offshore structures. ISO 19905-1, which has been developed from the Society of Naval Architects and Marine Engineers (SNAME) Technical & Research Bulletin 5-5A (2002), gives general principles and basic requirements for site-specific assessment of mobile jack-ups.

The seismic design procedure according to ISO can be split into several different parts. One is the procedure for determining the earthquake actions where the forces to be used for structural analysis are calculated. Another is the method of structural analysis, this can be either static or dynamic, and in the frequency- or time-domain. The last one is the method used for the evaluation of seismic activity, which can be done empirically, statistically, or deterministically. The parts are summarized as:

- Earthquake action procedure
- Structural analysis method
- Evaluation of seismic activity

For the seismic design of offshore structures ISO 19901-2 provides two alternative procedures for determining earthquake actions: a simplified seismic action procedure, and a detailed seismic action procedure. The simplified method may be used where seismic considerations are unlikely to govern the design of a structure. The detailed method is used where seismic considerations have a significant impact on the design. The selection of the appropriate procedure depends on the exposure level of the structure and the expected intensity and characteristics of seismic events. The simplified procedure allows the use of generic seismic maps, while the detailed procedure requires a site-specific seismic hazard study. The simplified procedure can be used in all cases to perform appraisal and concept screening for a new offshore development.

The complexity of a seismic action evaluation and the associated design procedure depend on the structure's seismic risk category (SRC). The seismic risk category is determined by the structure's exposure level and the severity of the ground motion. All manned offshore structures have an exposure level L1 for seismic actions, as it is not possible to evacuate prior to an earthquake. The severity of ground motion is determined from seismic maps of spectral accelerations for the offshore areas of the world and categorized into site seismic zones. These seismic maps are provided in Annex B of ISO 19901-2[2]; a copy of the seismic maps of Japan is included in Appendix B. An overview of the seismic risk categories for manned offshore structures depending on the seismic zones is given in Table 2.1.

**Table 2.1:** Seismic risk category for manned offshore structures based on seismic zone

$S_{a,map}$ (1.0)	< 0.03 g	0.03 g - 0.10 g	0.11 g - 0.25 g	0.26 g - 0.45 g	> 0.45 g
Seismic zone	0	1	2	3	4
Seismic risk category	SRC 1	SRC 3	SRC 4	SRC 4	SRC 4

For areas on the site seismic maps where the spectral acceleration is higher than 0.1[g] the structure will have an SRC4, and an SRC3 for areas with accelerations between 0.03[g] and 0.10[g]. These areas generally require a site-specific detailed seismic action procedure using non-linear analysis for abnormal level earthquake design (ALE). The seismic design requirements for the different seismic risk categories are given in Table 2.2. The seismic action procedure refers to the method of derivation of the actions to be used in a load and resistance factor design (LRFD), which is the design methodology employed by ISO. Evaluation of seismic activity can either be done using regional/ISO maps or by performing a site specific analysis. For the site specific evaluation of seismic activity a probabilistic seismic hazard analysis is performed (PSHA).

**Table 2.2:** Seismic design requirements for each seismic risk category

SRC	Seismic action procedure	Evaluation of seismic activity	Non-linear ALE analysis
1	None	None	None
2	Simplified	ISO maps or regional maps	Permitted
3	Simplified	Site-specific, ISO/regional maps	Recommended
4	Detailed	Site-specific	Recommended
4	Detailed	Site-specific	Required

Structures in seismically active areas are designed to their ultimate limit state (ULS) for low-intensity frequent earthquakes. The ULS seismic design event is called an extreme level earthquake or ELE. During such an event the structure should sustain little or no damage; only localized and limited non-linear behavior is permitted. As a result the ELE design procedures are mainly based on linear elastic methods of structural analysis where non-linear effects, such as those in soil-structure interaction, are linearised. These methods are not applicable to structures that employ seismic isolation or passive energy dissipation devices due to strong non-linear behavior. The two methods of analysis that are used for the ELE design check are: the response spectrum analysis method, and the time history analysis method.

Structures are designed to their Abnormal Limit State (alternatively referred to as Accidental Limit State) for high-intensity rare earthquakes. The ALS seismic design event is called the abnormal level earthquake or ALE. The structure should be able to sustain large inelastic displacement reversals without complete loss of integrity and avoid collapse that could lead to loss of life or major environmental damage. As the structural elements are allowed to behave plastically, the ALE design check employs non-linear methods of analysis. The two methods used are: the static pushover or extreme displacement method, and the non-linear time history analysis method. The latter is recommended as it is the most accurate method of ALE analysis.

The ISO standards allow the use of different procedures that are more thorough. Care needs to be taken that these procedures do not result in an unsafe assessment of the structure.

## 2.2. Existing earthquake analysis procedures

For jack-ups there are currently two methods for earthquake analysis prescribed by the ISO codes. The first is ELE-screening using response spectrum analysis; used as a first step in assessing a structures response to seismic loading. When the structure does not pass the ELE screening checks a non-linear ALE analysis using time history analysis can be performed.

### ELE-screening with RSA procedure

Earthquake analysis of an existing jack-up is part of the site-specific assessment of mobile offshore units that fall within the provisions of ISO 19905 [6]. Earthquake assessment is done by assessing the structure to its ultimate limit state for strength and stiffness, whilst subjected to earthquake actions derived from a design spectrum for a return period of 1000 years. This earthquake assessment is referred to as ELE-screening. The screening is intended to be a conservative method and should produce higher utilization results than more detailed assessments. ELE-screening is performed using response spectrum analysis.

Response spectrum analysis is a linear-dynamic statistical analysis method that makes use of a response spectrum. It measures the contribution from each natural mode of vibration and combines them to calculate the most probable maximum seismic response of an elastic structure. A detailed explanation of response spectrum analysis is provided in Appendix C.

The ELE-screening procedure using response spectrum analysis consists of the following steps:

- Determine site-specific parameters
- Create a lumped parameter stick model of the structure
- Construct site-specific design response spectrum
- Perform response spectrum analysis
- Use modal combination rule (SRSS/CQC) to construct actions
- Evaluate actions

### Non-linear ALE THA procedure

When a jack-up does not satisfy the 1000 year ELE-screening to ULS assessment criteria, a more detailed method can be used to evaluate compliance with the earthquake performance requirements. A site specific non-linear time history analysis is performed for the ALE case to assess the structure to its ALS. This assessment method is referred to as non-linear ALE analysis.

Time history analysis is an analysis method in which the state of a system is evaluated at successive time increments. The seismic input for time-history analysis are time history records. The response of the system is evaluated at each time step using the initial conditions of the previous time step and the loading history at the current time step. The equation of motion and initial conditions of a damped multiple degree of freedom system excited by an earthquake input acceleration are rewritten to state space form. The problem is transformed from a coupled system of  $2^{nd}$  order differential equations to a system of first order differential equations that can be solved by commercial software packages. A detailed explanation of time-history analysis is provided in Appendix C.

The non-linear ALE method using time-history analysis consists of the following steps:

- Determine site-specific parameters
- Create structural model of the jack-up
- Perform probabilistic seismic hazard analysis (PSHA)
- Complement PSHA results with deterministic seismic hazard analysis (DSHA)
- Construct uniform hazard spectrum of mean spectral accelerations
- Perform site response analysis and modify spectrum
- Acquire representative acceleration time-histories
- Modify acceleration time-histories
- Perform non-linear time history analysis
- Evaluate actions

## Limitations of existing procedures

The ELE-screening method using RSA has the advantage that it is relatively straight forward to perform and is computationally efficient. This is why it is used for the first test of the seismic response of a structure. On the other hand there are several well documented drawbacks to using this method. There is no sign information in the RSA procedure: the maximum displacement and member forces in each mode are calculated without sign information. There is no time development in this procedure: all actions are combined from global maxima which do not necessarily occur at the same time. The lack of sign information and time development can result in an overly conservative analysis of the structure. Another limitation of the ELE-screening method using RSA is that it can not take non-linearities into account, including geometric non-linearities (P-delta effect). Especially with large lateral displacement this can have a significant effect on the result.

The non-linear ALE method using time history analysis is a very detailed method which allows all non-linearities to be taken into account. Since time history analysis evaluates the state of a system at successive time increments, sign information and time development are preserved. From the steps of the non-linear ALE THA procedure it is evident that this method requires additional analyses to be performed, such as the PSHA and DSHA, requiring additional site specific data. The method is complex, computationally demanding and time consuming, and requires a detailed soil model.

**Table 2.3:** Advantages and limitations of the ELE-screening method using RSA and the ALE method using THA

Assessment	Analysis	Advantages	Limitations
ELE	RSA	+ Computationally efficient + Straight forward method	- No sign information - No time development - No non-linearities
ALE	THA	+ Very detailed + Non-linearities + Sign information + Time development	- Requires PSHA - Requires DSHA - Complex method - Computationally very demanding - Requires detailed soil modeling

An overview of the main advantages and limitations of the existing earthquake analysis procedures are given in Table 2.3. The ELE-screening method using RSA can be considered conservative as it produces higher utilization results than more detailed assessments, while the non-linear ALE method using THA can be considered complex. For the earthquake analysis of jack-ups there is a need for a new method which does not have the limitations of the ELE RSA method while being less complex than the non-linear ALE method.

## 2.3. New ELE-screening procedure using THA

Based on a literature study a new ELE-screening procedure was proposed that uses time history analysis. It combines elements from the ELE-screening using RSA and the non-linear ALE THA procedure described in Section 2.2. The new method complies with the seismic design procedures of ISO 19901-2 [2]. In addition elements have been taken from more mature codes such as ASCE 7-16 [8] and EC8 [7].

The ELE-screening procedure using THA consists of the following steps:

- Determine site-specific parameters
- Create structural model of the jack-up
- Construct site-specific design response spectrum
- Acquire representative acceleration time-histories and compute principal components
- Spectrum match acceleration time-histories to the design response spectrum
- Perform linear time history analysis
- Evaluate actions

The first step in the new ELE-screening procedure is to determine the site-specific parameters of the desired operational location. A structural model is created based on the physical properties of the jack-up and the site-specific parameters. The new method uses time history analysis for which the seismic inputs are time history records. To ensure adequate loading demand on the jack-up the time history records are modified. In accordance with seismic analysis requirements in more mature codes, the ground motions are modified through spectrum matching. The selection and modification of the time history records are done using the design response spectrum. The DRS is constructed using the site specific parameters and structural properties of the jack-up. The period range over which the time history records are spectrum matched to the DRS depends on the modes of the structure. The modes are derived from the structural model. Simulations are run for different orientations of the ground motions on the structure. Response quantities are analyzed for the legs at the lower guide and the leg to spudcan connection. These areas on jack-ups are critical with regard to structural strength.

The new ELE-screening THA method can be used to demonstrate acceptability when the structure fails the ELE-screening using RSA. If the structure does not pass the ELE-screening using THA a non-linear ALE using THA needs to be performed. The new ELE-screening method has been designed so that it forms the basis for the non-linear ALE THA. The structural model of the new ELE-screening procedure can be updated to incorporate all non-linearities and a detailed soil model. The procedure for modifying the time history records remains the same, however use is made of a different response spectrum for the non-linear ALE method.

The assumption is that by incorporating sign information and time development into the analysis of the new procedure, this will result in a more accurate assessment of the structure, ultimately resulting in better operability. To demonstrate the performance gain of the new ELE-screening method using THA it is benchmarked against the existing RSA method.

## 2.4. Benchmarking considerations

For the development and benchmarking of the new method an earthquake analysis was performed using both the new ELE-screening procedure with THA and the existing ELE-screening procedure with RSA. The analysis was performed for a jack-up based on the GJ-3750C located in a region offshore Japan where previous studies have been performed by GustoMSC. The response spectrum analysis simulations were performed using the GustoMSC in-house developed software tool "Minifem". A new tool was built in OpenSees[10] for the time history analysis simulations. The performance evaluation was done using the global maximum action effects; limited to forces and moments at the lower guide and footing.

### Local site conditions

The site specific properties of the selected offshore location are:

- Water depth: 30 [m]
- Soil density: 2000 [ $kg/m^3$ ]
- Shear wave velocity: 180 [m/s]
- Dynamic shear modulus of the soil: 66.24 [ $MN/m^2$ ]

### Soil-structure connection

The fixity of the structure in the soil depends on the foundation type of the jack-up and the site-specific conditions. The model was evaluated using the site specific fixity condition, and for a low and high fixity condition. In the structural model the fixities are implemented at the soil-structure connection. The different soil-structure connections used for the structural model are:

- Pinned - Low fixity condition
- Fixed - High fixity condition
- Spring - Site specific fixity condition

## Simulations

Due to the different implementations of damping in the two software environments, simulations are run with several levels of damping. This is to either include or exclude the influence of the different damping implementations in the analysis. For RSA the damping is implemented through the DRS; for THA the damping is implemented through Rayleigh damping and linear viscous dampers. This is described in detail in Chapter 3. Due to software limitations with regard to the interpretation of the vertical DRS in Minifem, THA simulations are run with THR matched to the vertical DRS as interpreted by Minifem and the vertical DRS prescribed by ISO. This is described in detail in Chapter 4.

The simulations that are run for the ELE-screening using RSA are:

RSA Fixed; 5% damped horizontal DRS; 5% damped vertical DRS

RSA Pinned; 5% damped horizontal DRS; 5% damped vertical DRS

RSA Spring; 5% damped horizontal DRS; 5% damped vertical DRS

RSA Spring; 5% damped horizontal DRS; 15% damped vertical DRS

The simulations that are run for the ELE-screening using THA are:

THA Fixed; 5% Rayleigh damping & Minifem DRS matched THR

THA Pinned; 5% Rayleigh damping & Minifem DRS matched THR

THA Spring; 5% Rayleigh damping & Minifem DRS matched THR

THA Spring; 5% Rayleigh damping + vertical linear viscous damper & Minifem DRS matched THR

THA Spring; 5% Rayleigh damping + vertical linear viscous damper & Minifem DRS matched horizontal THR and ISO DRS matched vertical THR

## Performance evaluation

The parameters used to evaluate the performance of the two models are the forces and moments at the leg-hull connection and at the soil structure interface. The soil structure interface is also referred to as footing. As mentioned previously these areas are critical with regard to structural strength for jack-ups.

## Soil structure interaction

A soil-structure interaction analysis is performed on an equivalent single degree of freedom system to demonstrate the validity of the soil-structure interface model that is used in the new ELE-screening procedure. In addition the soil-structure interaction analysis demonstrates that the induced motion from soil-structure interaction can be neglected for the cases considered and the free-field acceleration can be used. This is discussed in detail in Chapter 5.

## Requirements

- The structure being analysed shall be modelled in three spatial dimensions and 6 degrees of freedom.
- Inherent and accidental torsion shall be included in the analysis by offsetting the centre of mass of the structure.
- The ground motions shall be comprised of three simultaneously acting mutually perpendicular components.
- The same THR component shall not be used simultaneously along both horizontal directions.

- 
- Earthquake time history records shall be selected such that they represent the dominating ELE events.
  - Four sets of time history records shall be used to capture the randomness in seismic motions [2].
  - Spectrum matched ground motions shall be used for seismic analysis using THA.
  - P-delta effects shall be included directly in the analysis.



# 3

## Structural model

The jack-up is modeled as a lumped parameter beam model in both the response spectrum analysis and time history analysis method. Use is made of elastic Timoshenko-beams as they can account for shear deformations. This chapter looks at the structural model used for earthquake analysis with RSA and THA. First a basic description is given of the jack-up and the operational condition under consideration in Section 3.1. This is followed by the method in which the jack-up is modeled as a lumped parameter beam model in Section 3.2. Section 3.3 explains how damping is implemented in the models, and Section 3.4 describes how the foundation of the jack-up is modeled. The chapter concludes in Section 3.5 with a verification of the structural models built in Minifem and OpenSees to demonstrate equivalence.

### 3.1. Model under consideration

The jack-up used for development and benchmarking of the new method is based on the GJ3750-C designed by GustoMSC. The unit consists of a rectangular hull, four tubular legs and four continuous hydraulic jacking systems. The general configuration and dimensions are displayed in Fig. 3.1. Note that the figure is for illustration purposes only and is not to scale. The unit stands in water with a mean sea level (MSL) of 30 [m] and the deck has an airgap of 11[m]. The maximum bearing capacity of the spudcan is 2.2m below the seabed. The level of maximum bearing capacity is taken as the origin of the vertical axis. The main crane is arranged on a pedestal on the starboard side of the unit. An accommodation deck-house is arranged at the forward end of the unit, as well as a helicopter landing deck. The mass distribution of the unit is determined based on the mass estimation of the basic design of the jack-up and an estimation of the operational mass. For earthquake analysis a variable load of 75% is considered as part of the total elevated weight. For the static load an eccentricity of the elevated weight of  $\pm 1.5$ [m] in longitudinal and  $\pm 2.3$ [m] in transverse direction is included as shown in Fig. 3.3, which is due to the 75% variable load.

The general configuration of the hull is given by:

- Length at main deck: 73.0 [m]
- Width: 40.0 [m]
- Depth: 6.5 [m]
- Longitudinal leg spacing: 45.0 [m]
- Transverse leg spacing: 33.0 [m]

The general configuration of the legs is given by:

- Number of legs: 4
- Type of legs: tubular
- Leg diameter: 3.5 [m]
- Overall leg length: 86.0 [m]
- Footing area: 45.0 [ $m^2$ ]

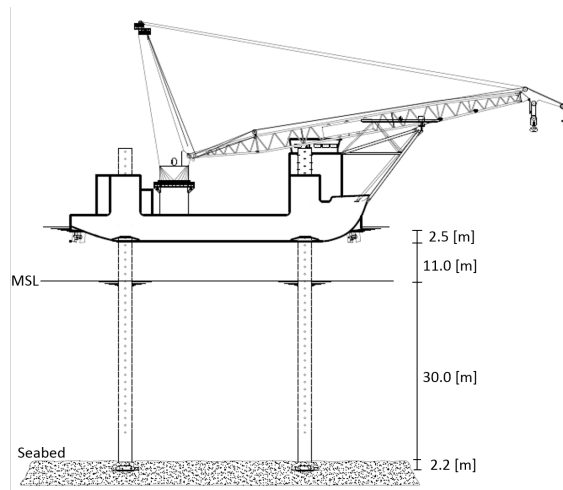


Figure 3.1: Side view of the jack-up unit in operational condition

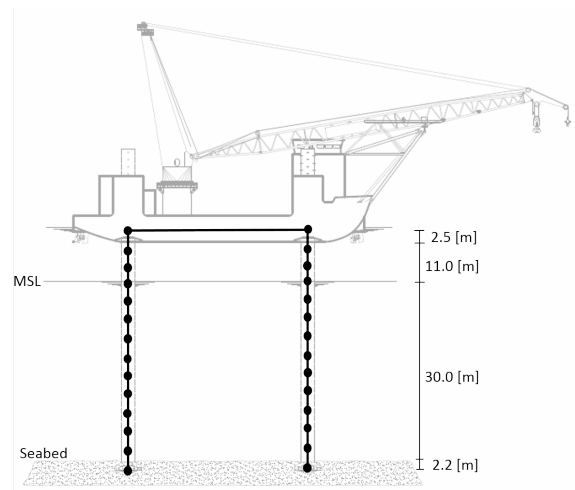


Figure 3.2: Side view of lumped parameter beam model consisting of nodes and elements

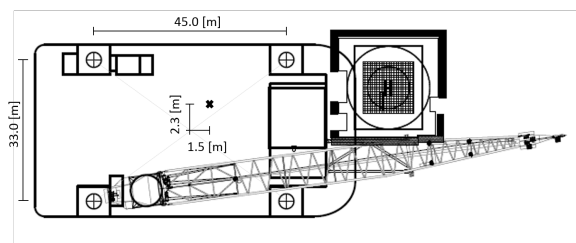


Figure 3.3: Top view of the jack-up unit in operational condition

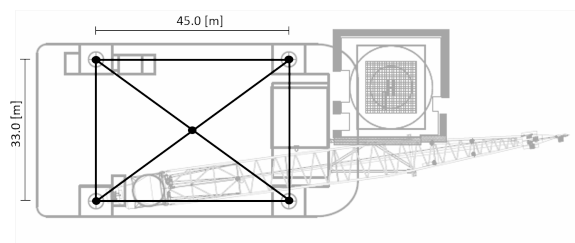


Figure 3.4: Top view of lumped parameter beam model consisting of nodes and elements

### 3.2. Structural model of the jack-up

This section looks at how to model the jack-up into a lumped parameter finite element model for use in the simulation programs Minifem and OpenSees. Both software packages require the model to be represented in the form of nodes and elements. The mass of the structure is discretised into a finite number of nodes. The nodes are connected by elements which have shear area and moment of inertia properties assigned to them. Figures 3.2 and 3.4 show the side and top view of the finite element model overlain over the jack-up unit. The amount of nodes, and hence elements, that are required to represent the legs depends on the solution methods being used in the simulation. If too few nodes are used the solution will not converge. Initially the legs were represented by 15 nodes above MSL and 30 nodes at and below MSL. After observing that for particular simulation cases the solution did not converge, the choice was made to increase the amount of nodes to 30 above MSL and 60 at and below MSL. The more nodes and elements that are being used, the higher the computational intensity of the simulation, and the longer it takes to run the simulation.

#### Modeling the leg

The legs of the jack-up are modeled as equivalent beams. The bending stiffness of the leg is determined by the modulus of elasticity  $E$  and the moment of inertia  $I_{xx}$ ,  $I_{yy}$  of the leg cross section. In the case of circular legs the moment of inertia  $I_{xx}$  and  $I_{yy}$  are equal and given in Eq. (3.1).

$$I_{xx} = I_{yy} = \frac{\pi}{4} \rho_{leg} g \left( D_0^4 - (D_o - 2t_{leg})^4 \right) \quad (3.1)$$

The mass of the leg above MSL is taken as the mass of the steel that comprises the leg. The mass of the leg below MSL additionally includes added mass. The added mass is calculated as the product of the displaced volume of the leg and an added mass coefficient  $C_A$ . The horizontal added mass coefficient  $C_{A,H}$  is 2 and

the vertical added mass coefficient  $C_{A,V}$  is 1. The vertical added mass contribution comes from the water enclosed in the tubular leg. Vertical added mass due to wall friction between the leg and water is considered negligible for tubular legs. The mass of the legs is lumped into nodes: 30 above MSL, one at MSL, and 59 below MSL.

The leg weight per unit length is given by Eq. (3.2) and the leg buoyancy per unit length is given by Eq. (3.3).

$$F_{W,leg} = \frac{\pi}{4} \rho_{steel} g (D_o^2 - D_i^2) \quad (3.2)$$

$$F_{B,leg} = \frac{\pi}{4} \rho_w g (D_o^2 - D_i^2) \quad (3.3)$$

Due to limitations in the software used for RSA, the part of the legs that is above the level of the hull can not be simulated. The software used to perform THA does not have this limitation and the option to model the part of the legs above the hull has been included in the OpenSees tool. To ensure the models of the RSA and THA procedure are identical the current solution is to lump the mass of the leg above the hull to the leg node at hull level, which will become the highest node of the leg. This approximation has an influence on the dynamic behavior of the structure ; the mode shapes and mass participation are different. Since this research is focused on the difference between the RSA and THA method of analysis for earthquake response of the structure and the same model is used for both, the effect of modeling the legs above the hull is not researched further. It is recommended that the effects are investigated of modeling the legs in this manner on the response of the jack-up.

### Modeling the hull

The hull is modeled by four edge beams that are connected in the corners by the hull corner nodes, and four cross beams that connect the four corner nodes to a hull center node, as shown in Fig. 3.4. The edge beams are modeled such that they represent the structural properties of the hull. The cross beams are modeled so as to not affect the stiffness of the hull, while their main purpose is to connect a hull center node to the rest of the hull. 50% of the elevated mass is concentrated in the center node while the remaining mass is distributed over the four corner nodes. The eccentricity of the elevated weight is modeled by subtracting mass from one corner node and adding it to another corner node. The mass is distributed over the four nodes so that they produce an equivalent moment to that of the eccentricity of the elevated weight.

### Modeling the leg-hull connection

The legs of the jack-up are connected to the hull via the lower guide, jacking systems, and upper guide. The leg-to-hull connection modeling is of extreme importance to the analysis since it controls the distribution of leg bending moments and shears carried between the upper and lower guide structures and the jacking or fixation system [6]. Figure 3.5 shows a cross section of the hull and two jack-houses. In the equivalent beam model this connection is modeled by means of springs in 6 degrees of freedom.

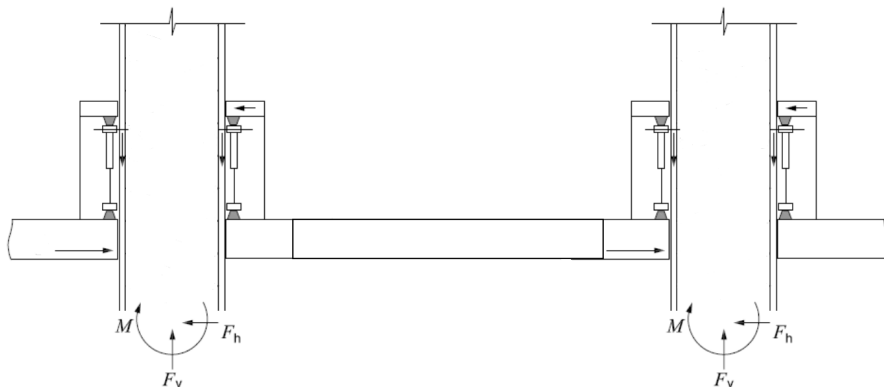


**Figure 3.5:** Cross section of the hull and two jack-houses. The axial force  $F_v$ , shear force  $F_h$ , and bending moment  $M$  of the leg at the lower guide are shown.

### Modeling the spudcan

The spudcan is modeled as the lowest node in the leg. The mass of the spudcan and the mass of part of the leg are lumped into this node. The added mass of the spudcan in vertical direction is considered significant and taken to be equal to the product of the displacement of the spudcan and the vertical added mass coefficient.

The support point of the jack-up is located at 0.8 [m] above the spudcan tip; this is the maximum bearing area of the spudcan. The spudcan tip is embedded 3 [m] into the soil, so that the support point is located 2.2 [m] below the seabed level. For the purpose of this research the spudcan was modeled as a flat circular plate on a homogeneous half-space. How the spudcan is modeled is of particular importance for soil-structure interaction as detailed in Chapter 5.

- Spudcan submerged weight:  $-0.4885$ [MN]
- Spudcan mass: 80[t]
- Spudcan added mass: 83.8[t]
- Spudcan volume:  $81.8$ [ $m^3$ ]
- Recommended footing vertical mass: 163.8[t]
- Type of foundation: pinned/fixed/spring

Note that the spudcan submerged weight has a negative sign. This indicates that the net force is directed upward, and the spudcan has a net buoyancy. The spudcan submerged weight is the algebraic sum of:

- Spudcan weight: 0.785[MN]
- Spudcan buoyancy:  $-0.822$ [MN]
- Lower leg buoyancy:  $-0.451$ [MN]

The lower leg buoyancy is due to the part of the leg above the spudcan that is watertight. The length of the leg above the spudcan that is watertight is approximately 5 [m]. This extra buoyancy from the leg is added to the spudcan node. As the spudcans of this jack-up are relatively small, and the weight of the spudcan is located near the hinge point, it should not have a large impact on the motion of the structure.

### 3.3. System damping

The structural damping in the model is implemented differently depending on the analysis method being used. For the RSA damping is incorporated in the design response spectrum as explained in Section 4.2. For the time history analysis the damping is implemented using Rayleigh damping. In both methods the system damping is taken as 5%. Additional damping in the form of radiation damping is implemented in the model as described in Section 3.4.

#### Rayleigh damping

Classic Rayleigh damping is a form of viscous damping which is proportional to mass and stiffness. The damping matrix is described by Eq. (3.4) in which  $a_0$  is the mass proportional coefficient and  $a_1$  the stiffness proportional coefficient. The damping ratio of the  $n^{th}$  mode of such a system is given by Eq. (3.5) [11].

$$\mathbf{C} = a_0 \mathbf{M} + a_1 \mathbf{K} \quad (3.4)$$

$$\zeta_n = \frac{a_0}{2} \frac{1}{\omega_n} + \frac{a_1}{2} \omega_n \quad (3.5)$$

The coefficients  $a_0$  and  $a_1$  are determined from specified damping ratios  $\zeta_i$  and  $\zeta_j$  for the  $i^{th}$  and  $j^{th}$  nodes. This is expressed in Eq. (3.6). If both modes are assumed to have the same damping ratio  $\zeta$ , then  $a_0$  and  $a_1$  are given by Eq. (3.7).

$$\frac{1}{2} \begin{bmatrix} 1/\omega_i & \omega_i \\ 1/\omega_j & \omega_j \end{bmatrix} \begin{bmatrix} a_0 \\ a_1 \end{bmatrix} = \begin{bmatrix} \zeta_i \\ \zeta_j \end{bmatrix} \quad (3.6)$$

$$a_0 = \zeta \frac{2\omega_i\omega_j}{\omega_i + \omega_j} \quad a_1 = \zeta \frac{2}{\omega_i + \omega_j} \quad (3.7)$$

Having determined the coefficients  $a_0$  and  $a_1$ , the damping matrix can be constructed according to Eq. (3.4). The damping ratio for any other mode, than the selected modes  $i$  and  $j$ , will vary according to Eq. (3.5). It

is therefore important to select modes  $i$  and  $j$  in such a manner that it ensures reasonable values for the damping ratios of all the modes contributing significantly to the response.

To ensure the model is not overly damped the Rayleigh damping is fitted to modes 1 and 10. As can be seen in Fig. 3.6 the damping ratios are close to 0.05 for all modes except modes 3 and 4. When fitting the Rayleigh damping to modes 1 and 4 the higher modes have a damping ratio greater than 0.05. Although the first four modes contribute most to the response of the structure, and a reasonable result could be achieved by fitting Rayleigh damping to modes 1 and 4, the higher order modes would be overly damped and not adequately taken into account. The choice was made to fit the damping to modes 1 and 10. How the damping ratio varies when fitted to modes 1 and 4 versus modes 1 and 10 is displayed in Appendix A for the Fixed, Pinned, and Spring cases in Figs. A.1 to A.3 respectively.

mode	freq [rad/s]	$\zeta$ (m1-m4)	$\zeta$ (m1-m10)
1	2.45	0.050	0.050
2	2.47	0.050	0.050
3	3.76	0.043	0.037
4	8.44	0.050	0.029
5	22.89	0.109	0.048
6	23.17	0.110	0.049
7	23.43	0.112	0.049
8	23.76	0.113	0.050
9	23.94	0.114	0.050
10	23.97	0.114	0.050

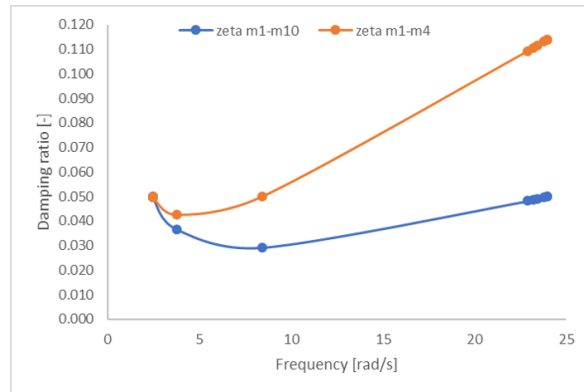


Figure 3.6: Damping ratio when fitted to modes 1 and 4, and damping ratios when fitted to mode 1 and 10, for the fixed condition

### 3.4. Foundation modeling

The jack-up is modeled to have circular footings resting on a homogeneous half-space. The interface of the spudcan with the underlying soil is modeled with equivalent springs and dampers. The springs and dampers connect the lowest node in the leg to a node fixed in space in 6 degrees of freedom.

#### Foundation stiffness

Vertical and horizontal stiffnesses of the foundation are based on the elastic solutions for a rough flat-based circular rigid disk on an elastic half-space. The elastic stiffness factors are calculated assuming full contact of the spudcan with the seabed, and are derived for a homogeneous, linear, isotropic soil. The vertical, horizontal, and rotational stiffnesses, as calculated by ISO [6], are given in Eqs. (3.8) to (3.10).

$$K_1 = K_{d1} \frac{2GB}{(1-\nu)} \quad (\text{vertical stiffness}) \quad (3.8)$$

$$K_2 = K_{d2} \frac{16GB(1-\nu)}{(7-8\nu)} \quad (\text{horizontal stiffness}) \quad (3.9)$$

$$K_3 = K_{d3} \frac{GB^3}{3(1-\nu)} \quad (\text{rotational stiffness}) \quad (3.10)$$

$K_{d1}$ ,  $K_{d2}$ ,  $K_{d3}$  are depth factors for vertical, horizontal, and rotational foundation stiffness respectively.  $G$  is the shear modulus of the foundation soil,  $B$  is the effective spudcan diameter at the uppermost part of bearing area in contact with the soil, and  $\nu$  is the Poisson's ratio of the soil. As the foundation is modeled as circular footings resting on the half space the depth factors are taken to be 1.

### Radiation damping

Foundation radiation damping from wave propagation is included for vertical motion of the spudcan. The additional contribution of vertical radiation damping to the linear damping ratio for the vertical mode only is calculated using Eq. (3.11). This equation is based on the work by Lysmer and Richart [12].

$$C_{RD} = R \left( 0.85 \frac{B^2}{(1-\nu)} \right) \sqrt{\rho G_0} \quad (3.11)$$

$C_{RD}$  is the radiation damping coefficient of a dashpot (force per unit velocity),  $R$  is a reduction factor applied to avoid unconservatism and normally taken as 0.5,  $B$  is the equivalent spudcan diameter at uppermost bearing contact with the soil,  $\nu$  is the Poisson's ratio of the foundation soil,  $G_0$  is the shear modulus of the foundation soil, and  $\rho$  is the total (saturated) density of the foundation soil. For non-linear dynamic analyses, or in linear time domain dynamic analyses using direct time integration, ISO suggests to use Eq. (3.11) to establish the damping coefficients for the foundation dashpots. In linear modal dynamic analysis the vertical radiation damping contribution to the linear damping ratio is calculated by Eq. (3.12)

$$\zeta_{RD} = 0.213 R N_S B \omega_n \sqrt{\frac{\rho}{G_0}} \quad (3.12)$$

### 3.5. Verification of structural models

A structural model of the jack-up is built in Minifem and in OpenSees. To verify that the models are equivalent several checks are performed including: mass, self weight, and mode check.

#### Mass and load check

A mass counter has been built into both the Minifem and OpenSees tools that sums the masses in all degrees of freedom. The mass counter tool also provides a useful overview to quickly check whether added mass has been implemented correctly in the model. A difference between the two models will be flagged. Similarly the self weight (gravity load) in both models is summed and compared.

#### Mode check

To verify that the structural models used in Minifem and OpenSees are equivalent the eigenmodes are compared. The check is performed before the self weight (gravity load) is applied to the structures. This is done because gravity loads affect the elastic stability of tall structural systems by reducing their capacity to carry lateral loads, which lengthens the resonant periods. The loss of apparent lateral stiffness may be especially important in the case of high-rise buildings, since the columns in the lower elevations must then carry large axial forces[13]. This is commonly known as the  $\Pi-\Delta$  effect, and also referred to as inverted pendulum effect. The time-history model in OpenSees can directly take this effect into consideration.

The eigenmodes of the structural model in Minifem and OpenSees were observed to be identical. The eigenmodes of the structural model with fixed, pinned, and spring connection are given in Table 3.1, Table 3.2, and Table 3.3 respectively. For the case of the spring soil-structure connection, soil springs derived from small strain initial stiffnesses were used to determine the natural periods[6]. The first three mode shapes of the fixed model are given in Figs. 3.7, 3.9 and 3.11 for Minifem and in Figs. 3.8, 3.10 and 3.12 for OpenSees. Additional information on the mode shapes is provided in Appendix E.

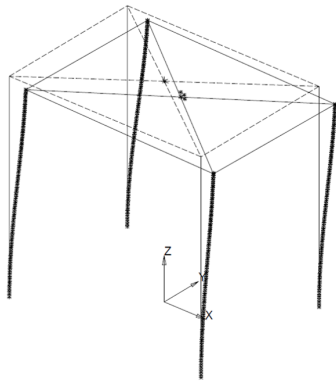


Figure 3.7: Mode 1 of fixed case in Minifem

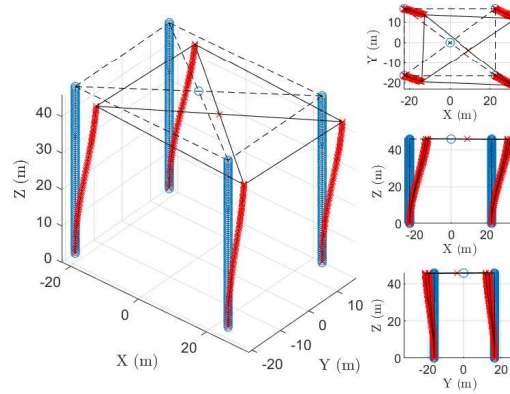


Figure 3.8: Mode 1 of fixed case in OpenSees

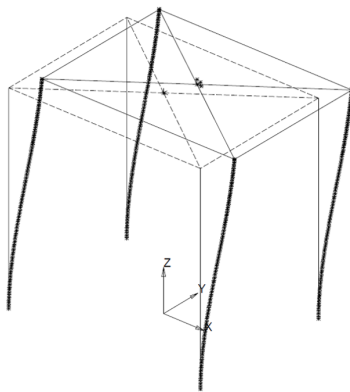


Figure 3.9: Mode 2 of fixed case in Minifem

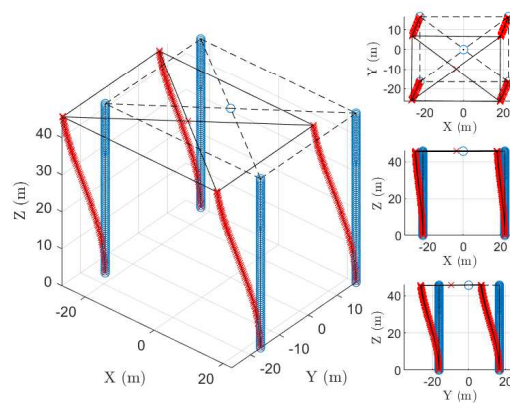


Figure 3.10: Mode 2 of fixed case in OpenSees

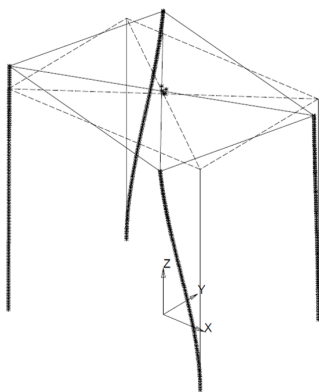


Figure 3.11: Mode 3 of fixed case in Minifem

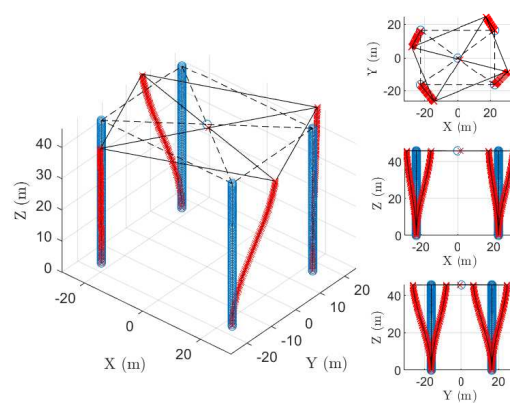


Figure 3.12: Mode 3 of fixed case in OpenSees

**Table 3.1:** Eigenvalue, eigenfrequency, and eigenperiod of the Fixed model

mode [-]	Eigenvalue [rad/s <sup>2</sup> ]	Eigenfrequency [rad/s]	Eigenfrequency [Hz]	Eigen Period [s]
1	6.01	2.45	0.39	2.56
2	6.08	2.47	0.39	2.55
3	14.16	3.76	0.60	1.67
4	71.19	8.44	1.34	0.74
5	523.91	22.89	3.64	0.27
6	536.86	23.17	3.69	0.27
7	549.00	23.43	3.73	0.27
8	564.60	23.76	3.78	0.26
9	572.93	23.94	3.81	0.26
10	574.32	23.97	3.81	0.26

**Table 3.2:** Eigenvalue, eigenfrequency, and eigenperiod of the Pinned model

mode (-)	Eigenvalue [rad/s <sup>2</sup> ]	Eigenfrequency [rad/s]	Eigenfrequency [Hz]	Eigen Period [s]
1	1.38	1.18	0.19	5.35
2	1.41	1.19	0.19	5.30
3	2.58	1.61	0.26	3.91
4	71.19	8.44	1.34	0.74
5	245.21	15.66	2.49	0.40
6	252.48	15.89	2.53	0.40
7	267.16	16.34	2.60	0.38
8	268.06	16.37	2.61	0.38
9	269.31	16.41	2.61	0.38
10	283.35	16.83	2.68	0.37

**Table 3.3:** Eigenvalue, eigenfrequency, and eigenperiod of the models with Springs

mode (-)	Eigenvalue [rad/s <sup>2</sup> ]	Eigenfrequency [rad/s]	Eigenfrequency [Hz]	Eigen Period [s]
1	3.38	1.84	0.29	3.42
2	3.41	1.85	0.29	3.40
3	8.44	2.90	0.46	2.16
4	65.62	8.10	1.29	0.78
5	292.55	17.10	2.72	0.37
6	306.20	17.50	2.78	0.36
7	313.54	17.71	2.82	0.35
8	313.92	17.72	2.82	0.35
9	329.24	18.15	2.89	0.35
10	329.65	18.16	2.89	0.35

# 4

## Ground motions

Ground motions are the seismic input in earthquake analysis. They depend on the geographic location, the method of seismic action evaluation, and the earthquake analysis method. Response spectrum analysis requires design response spectra while time history analysis requires representative acceleration time histories. In Section 4.1 the local site conditions are presented for the geographic design case. How the acceleration DRS is constructed according to ISO is described in Section 4.2. The DRS used for the simulations are presented in Section 4.3. The response spectrum is also used to select suitable earthquake time history records from the PEER strong motion database. The selection criteria and the selected earthquake time histories are presented in Section 4.4. The records were transformed to their principal axes, and spectrum matched to the design response spectrum. Principal axis transformation is performed to ensure the most conservative assumption regarding the incident earthquake wave as explained in Section 4.5. The transformed time histories are spectrum matched to ensure compatibility with the site-specific elastic design response spectra representing the seismic events. Section 4.6 concludes the chapter with an explanation of the spectrum matching process and presents the spectrum matched acceleration time histories used in the time history analysis simulations.

### 4.1. Local site conditions

A location offshore Japan where previous earthquake analysis studies have been performed is taken as the geographic design case. Japan lies in the collision zone of four major lithospheric plates shown in Fig. 4.2: the Eurasian plate, the North American plate, the Philippine Sea plate, and the Pacific plate. The plates form a subduction zone where the plate with higher density slides underneath the plate with lower density. Due to friction this sliding is not smooth; energy is built up over time and released in the form of earthquakes. These earthquakes are known as subduction-type earthquakes and are usually classified as deep-earthquakes. Figure 4.1 shows earthquake hypocentres of magnitude 5 and greater earthquakes from 1964-2007, and the 2011 Tohoku earthquake and aftershocks.

For the location of interest the following properties are known:

- Dynamic shear modulus:  $66.24 [MN/m^2]$
- Soil density:  $2000 [kg/m^3]$
- Shear wave velocity:  $182 [m/s]$

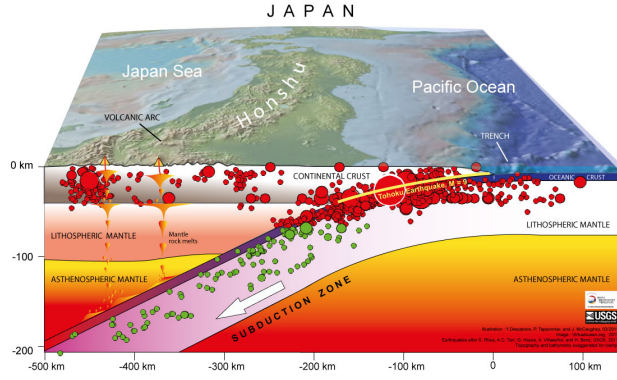


Figure 4.1: Earthquake hypocentres in Japan [1]

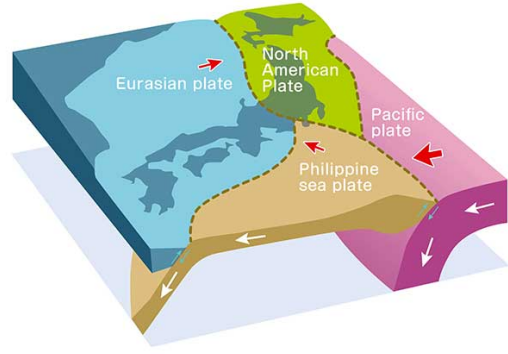


Figure 4.2: Lithospheric plates [1]

## 4.2. ISO acceleration design response spectrum

The seismic input for a response spectrum analysis is the acceleration design response spectrum (DRS). The design response spectrum is also used to find suitable earthquake acceleration time histories for use in the time history analysis method. The ISO site-specific acceleration design response spectrum corresponding to a 1000 year return period is constructed by:

1. Obtaining rock outcrop spectral accelerations from seismic maps
2. Determining site class based on the average representative shear wave velocity
3. Determining the site coefficients  $C_a$  and  $C_v$
4. Determining the site 1000 year horizontal acceleration spectrum
5. Deriving the vertical acceleration spectrum using the V/H amplification function
6. Modifying the spectrum for damping values other than 5%

The rock outcrop spectral accelerations are obtained from seismic maps. Use can be made of the maps provided in ISO 19901-2 [2] or of regional seismic maps. For the purpose of this research the ISO seismic maps have been used. The spectral acceleration for the 0.2[s] oscillator period is taken to be 1.0[g] and the spectral acceleration for the 1.0[s] oscillator period is taken as 0.4[g]. After the rock outcrop spectral accelerations are obtained, the average representative shear wave velocity is calculated using Eq. (4.1) where  $n$  is the amount of distinct soil layers in the effective seabed,  $d_i$  is the thickness of layer  $i$  in [m], and  $v_{s,i}$  is the representative shear wave velocity of layer  $i$  in [m/s].

$$\bar{v}_s = \frac{30}{\sum_{i=1}^n \frac{d_i}{v_{s,i}}} \quad (4.1)$$

The shear wave velocity is used to determine the site class of the location. The different site classes are:

**Class A/B:** Hard rock/rock, thickness of soft sediment <5 [m];  $\bar{v}_s > 750$  [m/s]

**Class C:** Very dense hard soil and soft rock;  $350 < \bar{v}_s \leq 750$  [m/s]

**Class D:** Stiff to very stiff soil;  $180 < \bar{v}_s \leq 350$  [m/s]

**Class E:** Soft to firm soil;  $120 < \bar{v}_s \leq 180$  [m/s]

The site coefficients  $C_a$  and  $C_v$  are taken from Tables 4.1 and 4.2 respectively.  $C_a$  is the correction factor applied to the acceleration part (shorter periods) of the response spectrum.  $C_v$  is the correction factor applied to the velocity part (longer periods) of the response spectrum.

Table 4.1: Correction factor for acceleration  $C_a$

Site class	$S_{a,map}(0.2)$					
	$\leq 0.25$ g	0.50 g	0.75 g	1.0 g	1.25 g	$\geq 1.5$ g
A	0.9	0.9	0.9	0.9	0.9	0.9
B	0.9	0.9	0.9	0.9	0.9	0.9
C	1.3	1.3	1.2	1.2	1.2	1.2
D	1.6	1.4	1.2	1.1	1.0	1.0
E	2.4	1.7	1.3	1.1	1.0	0.8

Table 4.2: Correction factor for velocity  $C_v$

Site class	$S_{a,map}(1.0)$					
	$\leq 0.25$ g	0.50 g	0.75 g	1.0 g	1.25 g	$\geq 1.5$ g
A	0.8	0.8	0.8	0.8	0.8	0.8
B	0.8	0.8	0.8	0.8	0.8	0.8
C	1.5	1.5	1.5	1.5	1.5	1.4
D	2.4	2.2	2	1.9	1.8	1.7
E	4.2	3.3	2.8	2.4	2.2	2

The horizontal DRS is calculated using Eqs. (4.2) to (4.5), and graphically represented in Fig. 4.3.

$$S_{a,site}(T) = (3T + 0.4) C_a \cdot S_{a,map}(0.2) \quad \text{for: } 0.0 \leq T \leq 0.2 \quad (4.2)$$

$$S_{a,site}(T) = \frac{C_v}{T} \cdot S_{a,map}(1.0) \quad \text{for: } 0.2 < T \leq 4.0 \quad (4.3)$$

$$S_{a,site}(T) \leq C_a \cdot S_{a,map}(0.2) \quad \text{for: } 0.2 < T \leq 4.0 \quad (4.4)$$

$$S_{a,site}(T) = \frac{C_v}{T^2} \cdot S_{a,map}(1.0) \quad \text{for: } 4.0 < T \quad (4.5)$$

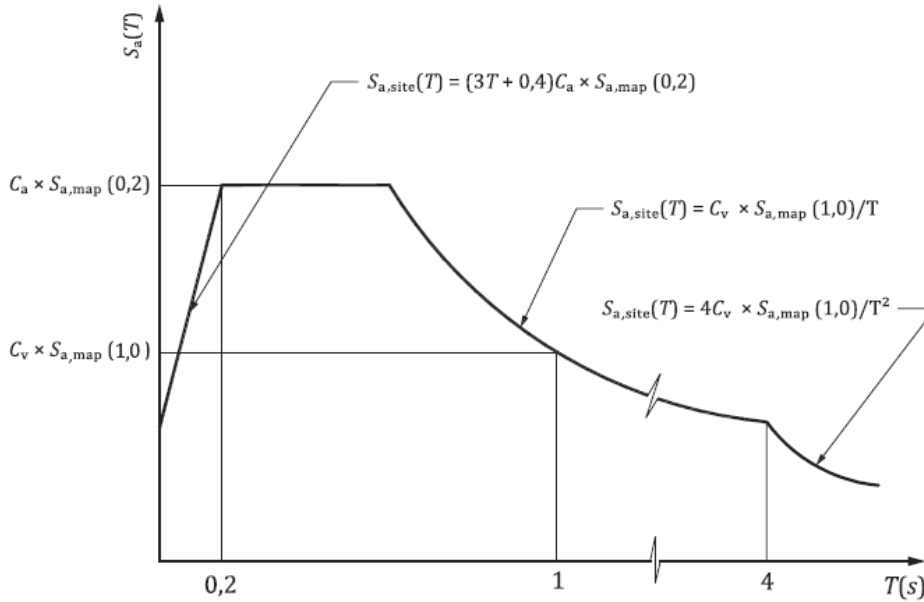


Figure 4.3: Seismic acceleration design response spectrum for 5% damping according to ISO 19901-2[2]

The spectra used for the two orthogonal horizontal directions are assumed identical while the vertical spectrum has very distinct characteristics and a different shape compared to the horizontal spectrum. In design codes the vertical design response spectrum is constructed from the horizontal design response spectrum using a period dependent scaling factor. The period dependence of this scaling factor is shown in Fig. 4.4.

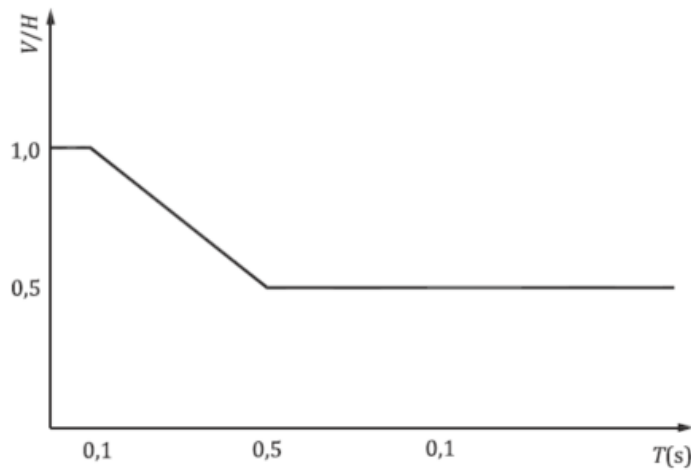


Figure 4.4: Vertical to horizontal spectral amplification function[2]

The horizontal and vertical acceleration design spectra obtained using these methods are for a damping of 5%. Acceleration spectra corresponding to different damping values are obtained by scaling the 5% spectrum with the correction factor  $D$ , as given in Eq. (4.6) where  $\eta$  is the percent of critical damping.

$$D = \frac{\ln\left(\frac{100}{\eta}\right)}{\ln(20)} \quad (4.6)$$

### 4.3. DRS used for simulations

For the simulations being run several differently damped design response spectra are used. The simulations that are being run require a:

- 5% damped horizontal DRS
- 5% damped vertical DRS
- 15% damped vertical DRS

The program Minifem that is used to run the RSA simulations has several limitations in the input of the DRS. It is limited to 10 sets of period and spectral acceleration pairs, and linearly interpolates between these points on a log-log scale. Minifem is also not able to use a period dependent scale factor to define the vertical DRS from the horizontal DRS, but uses a constant factor. This results in a higher vertical DRS than prescribed by the codes. For a fair comparison between the RSA and THA method the same DRS as used by Minifem is used for selecting and spectrum matching the time history records used for the THA in Sections 4.4 and 4.6. To see what the effect is of using the Minifem DRS, a THA is also done using the ISO DRS for comparison.

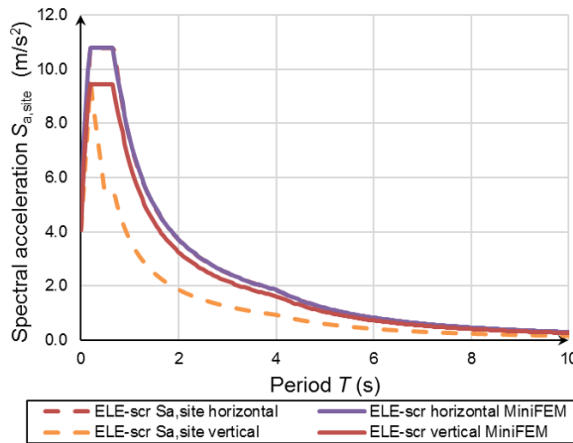


Figure 4.5: 5% H and 5% V damped DRS,  $T = 0$  to 10[s]

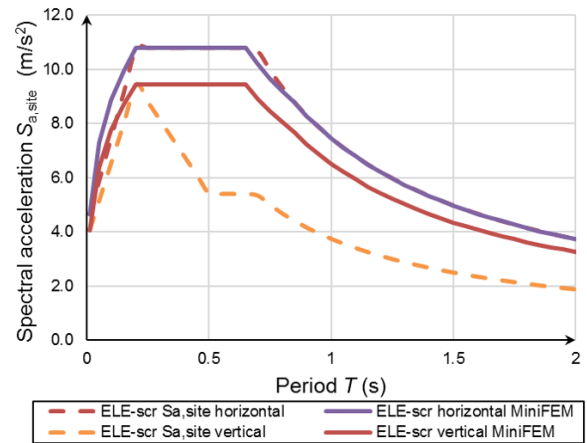


Figure 4.6: 5% H and 5% V damped DRS,  $T = 0$  to 2[s]

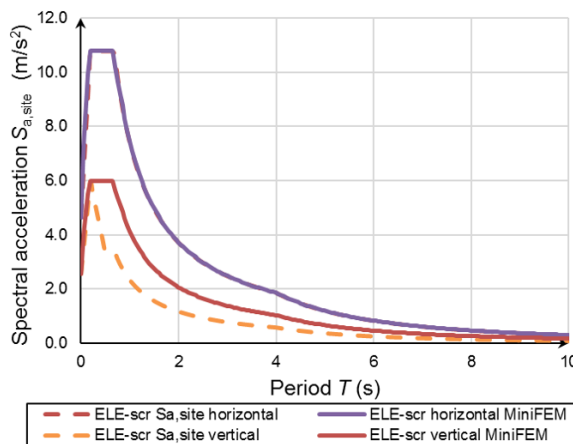


Figure 4.7: 5% H and 15%V damped DRS,  $T = 0$  to 10[s]

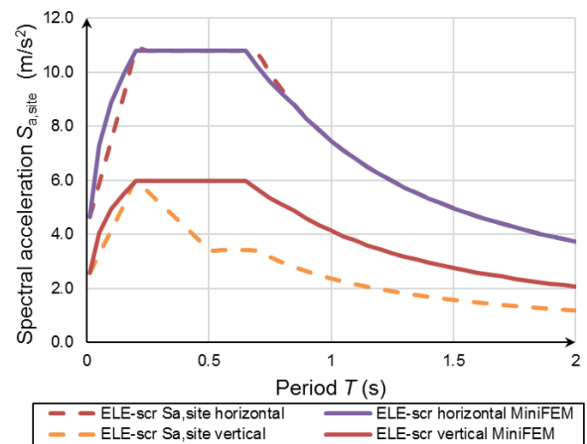


Figure 4.8: 5% H and 15%V damped DRS,  $T = 0$  to 2[s]

Figure 4.5 shows the ISO 5% damped horizontal and 5% damped vertical DRS in dashed lines, and the Minifem 5% damped horizontal and 5% damped vertical DRS in solid lines for a period range from 0 to 10 seconds. The same data is plotted in Fig. 4.6 zoomed in on the period range from 0 to 2 seconds to emphasize the difference between the ISO and Minifem vertical DRS. In Figs. 4.7 and 4.8 the ISO and Minifem DRS are plotted for the 5% horizontal and 15% vertical damping case for a period from 0 to 10 and 0 to 2 seconds respectively.

#### 4.4. Ground motion selection

The inputs required for time history analysis are acceleration time history records. The most important factor in selecting ground motions for scaling to a target spectrum is spectral shape over the period range of interest [14]. Initial selection is based on an approximate match to the earthquake magnitude and the spectral shape using the RMS of the difference in normalised spectral acceleration [14] given in Eq. (4.7)

$$\Delta SAN_{RMS} = \sqrt{\frac{1}{N_p} \sum_{i=1}^{N_p} \left( \frac{PSA_0(T_i)}{PGA_0} - \frac{PSA_s(T_i)}{PGA_s} \right)^2} \quad (4.7)$$

$N_p$  is the number of periods,  $PSA_0(T_i)$  is the pseudo spectral acceleration from the record at period  $T_i$ ,  $PSA_s(T_i)$  is the target pseudo spectral acceleration at the same period;  $PGA_0$  and  $PGA_s$  are the peak ground acceleration of the accelerogram and the zero-period anchor point of the target spectrum. Earthquake time histories were selected from the PEER NGA-West2 database using the selection tool [5]. The NGA-West2 database is of shallow crustal earthquakes and does not include deep earthquakes and subduction type earthquakes. Shallow earthquakes generally result in greater damage to structures; it is assumed that using earthquakes from this database will not result in an unconservative assessment. The earthquake time history selection criteria are:

- Response spectrum: Minifem 5% damped horizontal DRS
- Shear wave velocity range: 180-350 [m/s]
- Distance to rupture: 50-350 [km]
- Magnitude: minimum moment magnitude of 6
- Effective duration of motion D5-95: 15-35 [s]
- Fault type: reverse/oblique

The earthquake time history records need to be spectrum matched to the DRS as described in Section 4.6. It was found that some earthquakes would not match well to the target spectrum, especially when matching over a large period range as required for the pinned soil-structure connection. To ensure a fair comparison between the two ELE-screening methods, time histories were selected that produced a good matching quality. As required by ISO, four sets of time history records were selected to capture the randomness in seismic motion. Note that adopting an ensemble of earthquakes reduces the effects of frequency content and of particular characteristics of the individual earthquake ground motions [4]. By using more time histories the statistical uncertainty is reduced. The recorded earthquake time history records selected are given in Table 4.3, and are referred to in this report by their record sequence number (RSN); in graphs dropping the last digit for compactness.

**Table 4.3:** Earthquake time histories selected from PEER database [5]

RSN	Earthquake Name	Year	Mw	D5-95 [s]
332	Coalinga-01	1983	6.36	19.2
579	Taiwan SMART1(45)	1986	7.3	21.9
737	Loma Prieta	1989	6.93	27.5
FKS012	Fukushima Hamadori	2011	6.7	31.2

## 4.5. Principal axes

Ground motions are typically recorded in three orthogonal translational directions: two horizontal and one vertical. The horizontal components are often referred to as North-South and East-West, although in practice the recorders are not necessarily aligned in these directions. The ‘as-recorded’ time histories depend on the orientation of the recorders. By applying linear transformations to these time-histories the ground motion for different recorder orientations can be found.

It is prudent to use the most conservative assumption regarding the direction of incident earthquake wave for the calculation of structural response during seismic analysis. This is achieved by decomposing the recorded ground motions into a set of principal axes. The principal axes are a set of three orthogonal axes for which the ground accelerations  $a_1$ ,  $a_2$ , and  $a_3$  along those axes are uncorrelated. For ground motions that are not shallow and near-field, the principal components are defined as:

- $a_1$  is the major principal component of the ground motion; it is horizontal and oriented fault normal.
- $a_2$  is the intermediate principal component; it is horizontal and oriented fault parallel.
- $a_3$  is the minor principal component of the ground motion corresponding and oriented near vertically.

The first step in finding the principal components is composing the covariance matrix of the ground motions with entries  $\mu_{ij}$  given by Eq. (4.8). The diagonal terms of this matrix represent the mean square intensities of the three components, and the off-diagonal terms represent the cross correlation between pairs of components [11].

$$\mu_{ij} = \frac{1}{t_d} \int_0^{t_d} a_i(t) a_j(t) dt \quad i, j = x, y, z \quad (4.8)$$

Generally speaking  $\mu_{ij} \neq 0$  for  $i \neq j$  implying the three components are correlated. The ground motions are transformed to a new orthogonal set of axes 1, 2, and 3 such that the  $a_1$ ,  $a_2$ , and  $a_3$  along these axes are uncorrelated and  $\mu_{ij} = 0$  for  $i \neq j$  where  $i, j = 1, 2, 3$ . The eigenvalue problem is solved so that the eigenvalues and eigenvectors correspond to the principal axes. The eigenvalues are calculated by setting the determinant of the correlation matrix equal to zero, and sorted so that  $\mu_{11} > \mu_{22} > \mu_{33}$ . The major principal component corresponds to the largest eigenvalue, and the intermediate and minor principal components correspond to the second largest and smallest eigenvalue respectively. In the case of seismic events that are not near-field and/or shallow it is reasonable to assume that the vertical component can be treated separately. Decomposition into the principal axes  $a_1$  and  $a_2$  is done using Eq. (4.10) where  $a_x$  and  $a_y$  are the two recorded horizontal ground motions, and the angle of rotation is calculated by Eq. (4.9).

$$\theta = \frac{1}{2} \tan^{-1} \left( \frac{2\mu_{xy}}{\mu_{xx} - \mu_{yy}} \right) + k \frac{\pi}{2} \quad (4.9)$$

$$\begin{bmatrix} a_1 \\ a_2 \end{bmatrix} = \begin{bmatrix} \cos(\theta) & \sin(\theta) \\ -\sin(\theta) & \cos(\theta) \end{bmatrix} \begin{bmatrix} a_x \\ a_y \end{bmatrix} \quad (4.10)$$

The time histories selected in Section 4.4 were decomposed to their principal axes in Matlab using Eqs. (4.8) to (4.10). A Matlab script was used to read PEER strong motion files using *readPEER.m* [15], and output modified time series data.

## 4.6. Spectrum matching

The seismic input for time-history analysis is defined in the form of acceleration time histories. The time-histories need to be compatible with the site-specific elastic response spectra representing the seismic action. These can be obtained using different methods including generation of artificial time histories, and scaling or spectrum matching existing time histories. Artificial time histories can be generated from a reference response spectrum, as described in the method proposed by Shin and Song [16]. They have been widely

adopted in the past however due to several documented disadvantages [17] the trend has moved towards using modified real time histories. This is clear for instance from the linear response history procedure of ASCE 7-16 [8], where one of the principal differences with the older ASCE 7-10 code it replaces is that spectrum matched ground motions are now required for seismic analysis instead of being allowed. Spectrum matching is a method in which each individual ground motion is manipulated in the time domain by addition of wave packets [4]. The records are scaled with different factors in different frequency ranges such that the response spectrum of the record approximates the target design response spectrum.

After the earthquakes obtained in Section 4.4 from the NGA-West2 database were decomposed to their principal axes as described in Section 4.5 they were spectrum matched using SeismoMatch. This software application adjusts earthquake accelerograms to match a target response spectrum using the wavelets algorithm proposed by Hancock et al.[18]. The algorithm modifies the acceleration record to match the design response spectrum in a way that ensures no long period drifts are introduced in the corresponding velocity and displacement time histories. This has the advantage that no baseline corrections are required after each iteration.

When spectrum matching the acceleration time histories to the design response spectrum it is important to choose a suitable range for the period between which the spectral matching is carried out. The period range over which the acceleration records are matched depends on the fundamental period of the structure. ASCE 7-16 requires that each component of ground motion be spectrally matched over the period range  $0.8T_{lower}$  to  $1.2T_{upper}$ [8].  $T_{lower}$  is the period of vibration at which 90% of the structural mass has been recovered in each of the two orthogonal directions of response, and  $T_{upper}$  is the fundamental period corresponding to mode 1. Over the same period range and in each direction of response, the average of the 5% damped pseudo acceleration ordinates computed using the spectrum matched records shall not fall above or below the target spectrum by more than 10% in each direction of response [8]. The fundamental period of the jack-up depends on the soil-structure connection being modeled. The fundamental periods for the different soil-structure connections are given in Table 4.4.

**Table 4.4:** Eigenvalue, eigenfrequency, and eigenperiod of the first mode of the structure with fixed, pinned, and spring connection

Connection	Eigenvalue [rad/s <sup>2</sup> ]	Frequency [rad/s]	Frequency [Hz]	Period [s]
Fixed	6.01	2.45	0.39	2.56
Spring	3.38	1.84	0.29	3.42
Pinned	1.38	1.18	0.19	5.35

The different cases for which simulations are being run are:

- Fixed connection with 5% damped horizontal spectrum and 5% damped vertical spectrum
- Pinned connection with 5% damped horizontal spectrum and 5% damped vertical spectrum
- Spring connection with 5% damped horizontal spectrum and 5% damped vertical spectrum
- Spring connection with 5% damped horizontal spectrum and 15% damped vertical spectrum
- Spring connection with 5% damped horizontal spectrum and 15% damped vertical ISO spectrum

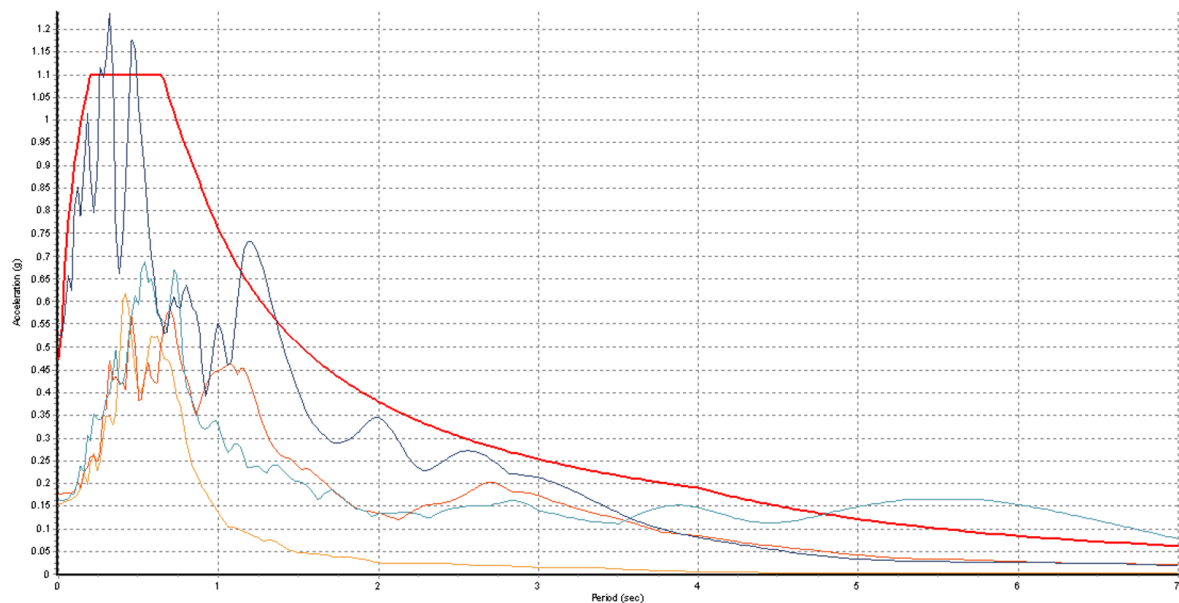
For each case the earthquake time traces are matched to different parameters. The major and intermediate principal time traces are matched to the 5% damped horizontal design response spectrum. The minor principal time traces are matched to both the vertical design response spectrum with 5% damping and 15% damping. For the fixed case the time traces are matched from 0.1 to 3 seconds, for the pinned case the time traces are matched from 0.1 to 5.5 seconds, and for the spring condition the time traces are matched from 0.1 to 4 seconds. Taking the different DRS into account this results in 44 unique spectrum matched time history records, and 20 unique sets of time history records.

Note that the period ranges above do not conform to the  $1.2T_{upper}$  rule as described by ASCE 7-16. They are chosen so that the fundamental period is within the matching period range and the quality of the match is

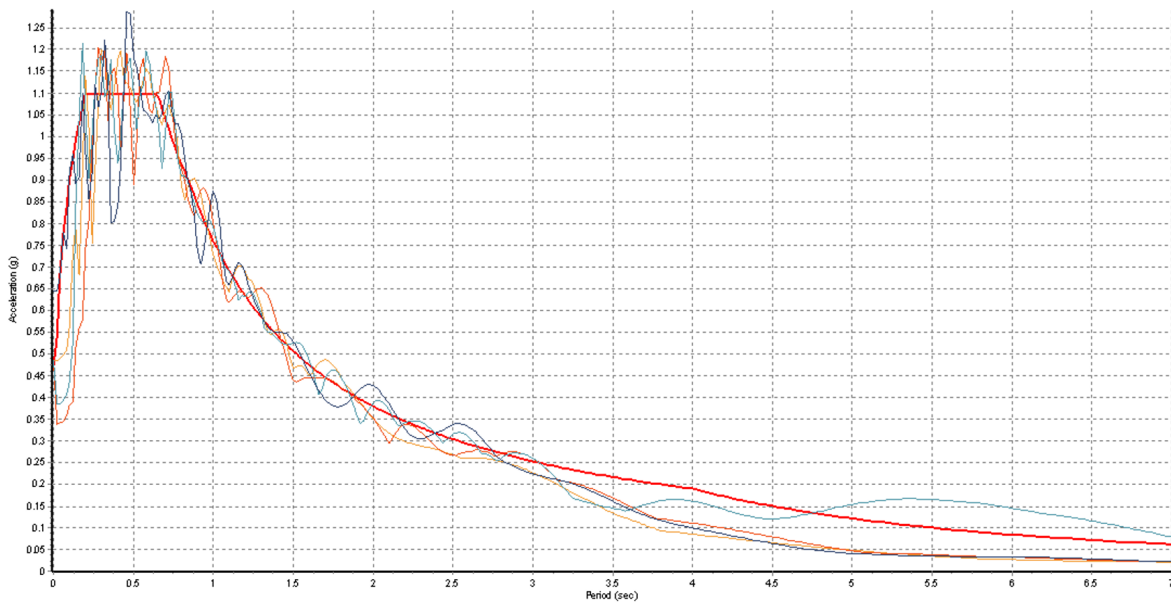
within an acceptable tolerance. During testing some issues were encountered when matching time traces for the pinned condition using the ASCE 7-16 range; which would run from 0.1 to 7 seconds. Some records from the NGA-West2 database could not be matched over this period range or had a very poor fit to the design response spectrum. An inverse relationship was observed between period range and matching quality.

Figure 4.9 shows the response spectrum of the major principal component of the original acceleration time histories for the 4 selected earthquakes, and the 5% damped horizontal DRS. The response spectra of the time history records matched for the fixed case ( $T=0.1-3[s]$ ) are shown in Fig. 4.10 next to the 5% damped horizontal DRS. The matching quality of all component time traces is provided for reference in Appendix D. In Fig. 4.11 the original acceleration, velocity, and displacement time trace of the major principal component of RSN332 are shown in blue; the modified time signals, after spectrum matching has been performed, are shown in red.

When the fundamental period of the structural model is changed, for instance when taking different soil spring stiffnesses, it is important to ensure the input time traces are matched to the corresponding period range. Not doing so can result in an unsafe assessment of the structure.



**Figure 4.9:** Response spectra of the unmatched principal component of 4 earthquake time histories, and the 5% damped horizontal design response spectrum



**Figure 4.10:** Response spectra of the matched principal component of 4 earthquake time histories, and the 5% damped horizontal design response spectrum. The time traces are matched over a period range from 0.1 to 3 seconds

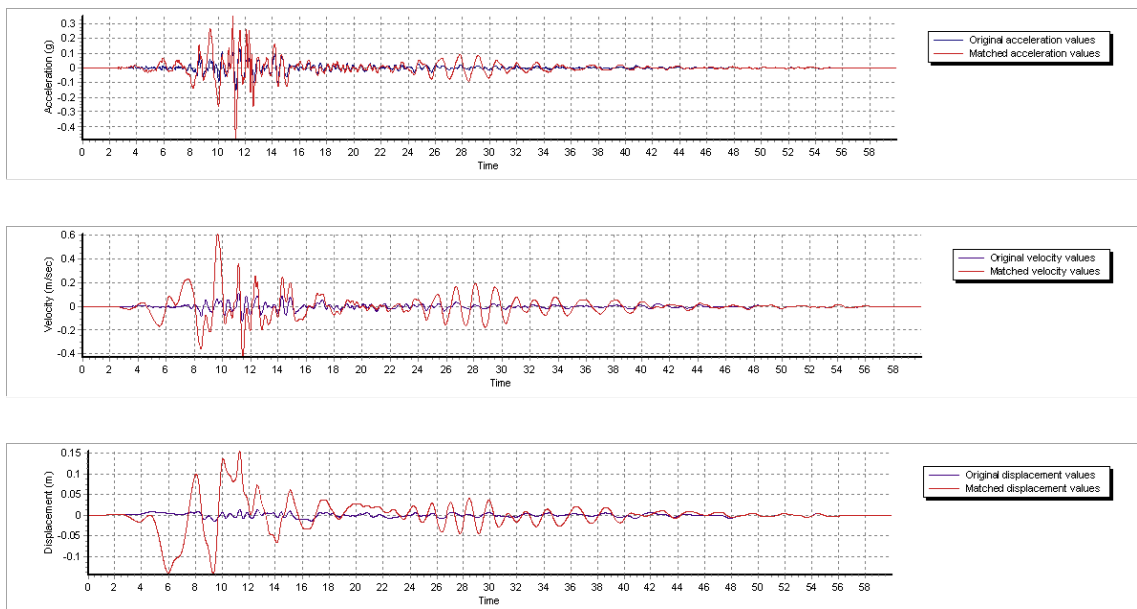


**Figure 4.11:** Original and matched acceleration, velocity, and displacement time history of the principal component of the RSN332 Coalinga earthquake



# 5

## Soil-structure interaction

In the new ELE-screening method using time-history analysis the soil-structure interface is modeled using a system of linear springs and dampers. The seismic input used in this method is the free-field acceleration. A soil-structure interaction analysis is performed on an equivalent single degree of freedom system to validate the use of a soil-structure interface model with linear springs and dampers in the new ELE-screening procedure. The soil-structure interaction analysis also demonstrates that the induced motion from soil-structure interaction is negligible for the cases considered and hence the free-field acceleration can be used. In Section 5.1 the basics of soil-structure interaction analysis are explained, and the two methods of analysis are presented. Section 5.2 describes how a soil-structure interaction analysis is performed for an equivalent single degree of freedom system. The simulations that were run and the results of the simulations are detailed in Section 5.3.

### 5.1. Soil-structure interaction analysis methods

Soil-structure interaction (SSI) analysis estimates the collective response of the entire soil-foundation-structure system to specified ground motions by determining the effects of: kinematic interaction (normally by site-response analysis), soil-foundation flexibility (foundation impedance), and inertia reaction (seismic analysis)[4]. The motion of soil is different in the presence of the foundation of the structure compared to the free field motion, and the motion of the structure is different due to the interaction with the soil. The importance of SSI is demonstrated by the fact that:

1. The structural response to an earthquake of a structure on deformable soils can be significantly different from that of a structure supported on a rigid foundation.
2. The ground motion at and around the base of a structure can be different from the free-field ground motion.

Even for relatively rigid structures supported on hard soils SSI can still be important in that the relative stiffness between the structure and foundations can significantly influence the energy and force transferring from the foundation to the structure. There are two types of approaches to SSI analysis: the direct analysis approach, and the substructure approach. The direct approach is suitable for both linear and non-linear formulations while the substructure approach is limited to linear formulation.

#### Direct analysis method

In the direct analysis approach the structure and the surrounding soil are modelled as an integrated system. A finite element model is made of the structure, the foundation, and the soil medium through which the seismic waves are transmitted. With this method it is possible to include the kinematic interaction, subgrade

impedance, and inertial reaction into one analysis. The solution is typically obtained in the time-domain by direct numerical integration.

The mesh size of the model needs to be small enough to capture the shortest wavelength, and the soil domain needs to be large enough to model the longest wavelength. This is achieved by using a large model with a fine mesh, which is computationally very demanding. The use is therefore often restricted to strongly non-linear systems in which non-linearities of the structure and the soil need to be taken into account.

### Substructure approach

The substructure approach can be used when the focus is on the linear response of the structure. This method divides the total system into distinct substructures: the superstructure, and the soil-foundation system. These two substructures are connected at the common soil-structure interface by imposing force equilibrium and kinematic compatibility at all times. The procedure for solving the problem is [19]:

1. Deriving the impedance matrix (dynamic stiffness matrix) of the soil-foundation system
2. Separating the structural from the foundation degrees of freedom
3. Formulating the equations of motion of the structure in partitioned form
4. Formulation of the equilibrium conditions at the soil-structure interface:
  - Force equilibrium
  - Displacement compatibility
5. Finding the solution of the coupled problem to determine:
  - Structural response
  - Motion at the interface

The dynamic stiffness matrix of the soil-foundation system can either be derived, or it can be constructed from tabulated data such as those in the works of Gazetas [20]. The equilibrium conditions at the soil-structure interface are usually formulated in the frequency domain as the soil impedance functions are obtained in the frequency domain.

The substructure approach is normally limited to linear behaviour and results in frequency dependent equations that are solved by use of Fourier synthesis. The interaction effects are typically accounted for by adding a number of frequency dependent springs and dashpots to the fixed base structural model. These represent the flexibility of the soil and the radiation of energy away from the foundation.

The advantages of the substructure approach are the convenience regarding both the modelling and computation. The approach requires little modifications to the fixed base structural model and hence allows for the possibility of using well-established techniques to derive the solution [4].

## 5.2. SSI analysis of SDOF system

The OpenSees tool built for the new ELE-screening procedure using THA does not take frequency dependent effects of SSI into account. The model uses the free-field input motions, and does not modify the ground motion input resulting from soil-structure interaction. To demonstrate the validity of the soil-structure interface model used in the new ELE-screening procedure, an SSI analysis was performed on an equivalent single degree of freedom system. The soil-structure interaction analysis also demonstrates that the induced motion from soil-structure interaction can be neglected for the cases considered and hence the free-field acceleration can be used. The substructure approach was used for the SSI analysis.

The jack-up described in Section 3.1 was modelled as an equivalent single degree of freedom system consisting of a structure with mass  $m$ , and a foundation block with mass  $m_0$ . The soil beneath the foundation block is homogeneous and extends to infinity in all direction below the foundation block, called a homogeneous

half-space. The equivalent SDOF system is shown in Fig. 5.1 in initial state and deformed state. The analysis procedure described in this section is taken from the works of Tsouvalas [19] and Clough [3].

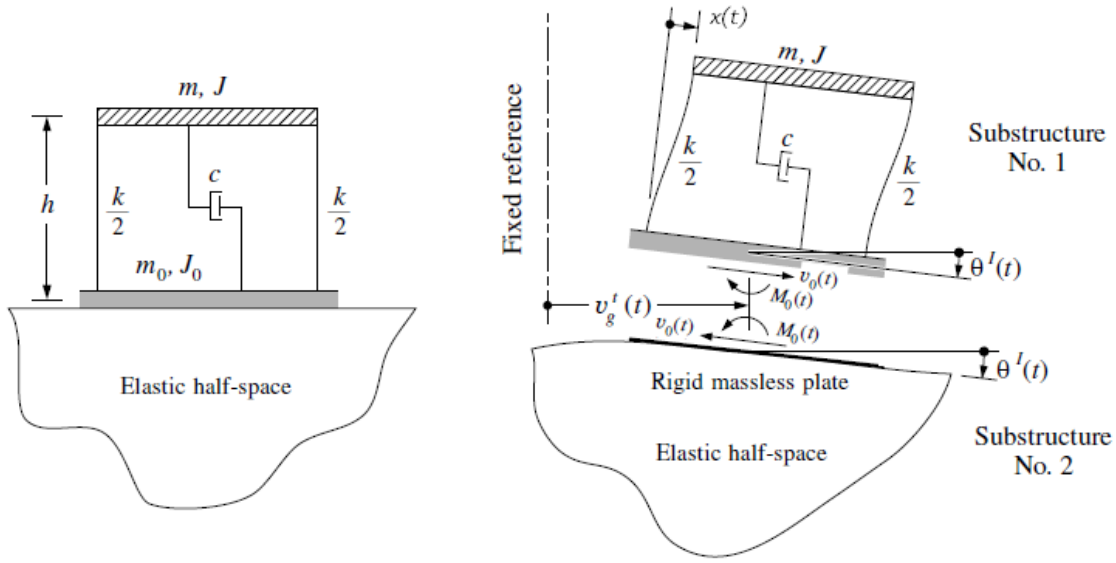


Figure 5.1: Equivalent SDOF system resting on top of a homogeneous soil half space in the initial state and the deformed state [3]

### Analysis procedure

The total translational motion imposed at the foundation level is built up of the free-field ground motion and the induced translational motion at the foundation level caused by soil-structure interaction, as shown in Eq. (5.1). The total rotational motion imposed at the foundation level is composed of the free-field incident rocking motion and the induced rocking motion caused by soil-structure interaction, as given in Eq. (5.2). The free-field incident rocking motion  $\theta_g(t)$  is assumed to be zero in this case.

$$u_g^t(t) = u_g(t) + u_g^I(t) \quad (5.1)$$

$$\theta_g^t(t) = \theta_g(t) + \theta_g^I(t) \quad (5.2)$$

The total acceleration of the structure mass is given by Eq. (5.3) and the equation of motion of the structure is given by Eq. (5.4)

$$\ddot{u}^{tot}(t) = \ddot{x}(t) + \ddot{u}_g(t) + \ddot{u}_g^I(t) + h\ddot{\theta}_g(t) + h\ddot{\theta}_g^I(t) \quad (5.3)$$

$$m\ddot{x}(t) + c\dot{x}(t) + kx(t) + m\ddot{u}_g(t) + m\ddot{u}_g^I(t) + mh\ddot{\theta}_g^I(t) = 0 \quad (5.4)$$

The translational balance of momentum at the soil structure interface is given by Eq. (5.5). The balance of moments at the soil structure interface is given by Eq. (5.6)

$$m\ddot{u}^{tot}(t) + m_0\ddot{u}_g^t(t) = V_0(t) \implies m\ddot{x}(t) + (m + m_0)\ddot{u}_g(t) + (m + m_0)\ddot{u}_g^I(t) + mh\ddot{\theta}_g^I(t) = V_0(t) \quad (5.5)$$

$$mh\ddot{u}^{tot}(t) + (J + J_0)\ddot{\theta}_g^I(t) = M_0(t) \implies mh\ddot{x}(t) + mh\ddot{u}_g(t) + mh\ddot{u}_g^I(t) + (mh^2 + J + J_0)\ddot{\theta}_g^I(t) = M_0(t) \quad (5.6)$$

By using the integral Fourier transform pair in Eq. (5.7) the equation of motion, the translational balance of momentum, and the balance of moments in Eqs. (5.4) to (5.6) can be transformed from the time domain to the frequency domain.

$$\begin{aligned}\bar{x}(\omega) &= \int_{-\infty}^{+\infty} x(t) e^{-i\omega t} dt \\ x(t) &= \frac{1}{2\pi} \int_{-\infty}^{+\infty} \bar{x}(\omega) e^{i\omega t} d\omega\end{aligned}\quad (5.7)$$

The equation of motion, the translational balance of momentum, and the balance of moments in the frequency domain are given in Eqs. (5.8) to (5.10)

$$(-\omega^2 m + i\omega c + k) \bar{x}(\omega) - \omega^2 m \bar{u}_g^I(\omega) - \omega^2 m h \bar{\theta}_g^I(\omega) = -m \bar{a}_g(\omega) \quad (5.8)$$

$$-\omega^2 m \bar{x}(\omega) - \omega^2 (m + m_0) \bar{u}_g^I(\omega) - \omega^2 m h \bar{\theta}_g^I(\omega) - \tilde{V}_0(\omega) = -(m + m_0) \bar{a}_g(\omega) \quad (5.9)$$

$$-\omega^2 m h \bar{x}(\omega) - \omega^2 m h \bar{u}_g^I(\omega) - \omega^2 (m h^2 + J + J_0) \bar{\theta}_g^I(\omega) - M_0(\omega) = -m h \bar{a}_g(\omega) \quad (5.10)$$

The equations of motion of the soil foundation system, which is substructure 2, depend only on  $\theta_g^I(t)$  and  $u_g^I(t)$  and can be expressed using the soil impedance matrix as shown in Eq. (5.11).

$$\begin{bmatrix} \tilde{V}_0(\omega) \\ M_0(\omega) \end{bmatrix} = \begin{bmatrix} \tilde{G}_{xx} & \tilde{G}_{xr} \\ \tilde{G}_{rx} & \tilde{G}_{rr} \end{bmatrix} \begin{bmatrix} u_g^I(\omega) \\ \theta_g^I(\omega) \end{bmatrix} \quad (5.11)$$

The force and moment in Substructure 1 are equal and opposite to the force and moment in Substructure 2. This is given in Eq. (5.12); note that here the superscripts I and II denote the Substructures 1 and 2.

$$\begin{aligned}\tilde{V}_0^{II}(\omega) &= -\tilde{V}_0^I(\omega) \\ \tilde{M}_0^{II}(\omega) &= -\tilde{M}_0^I(\omega)\end{aligned}\quad (5.12)$$

Substituting Eqs. (5.11) and (5.12) into Eqs. (5.8) to (5.10) yields the following set of equations:

$$(-\omega^2 m + i\omega c + k) \bar{x}(\omega) - \omega^2 m \bar{u}_g^I(\omega) - \omega^2 m h \bar{\theta}_g^I(\omega) = -m \bar{a}_g(\omega) \quad (5.13)$$

$$-\omega^2 m \bar{x}(\omega) - \omega^2 (m + m_0) \bar{u}_g^I(\omega) - \omega^2 m h \bar{\theta}_g^I(\omega) + \tilde{G}_{xx}(\omega) \bar{u}_g^I(\omega) + \tilde{G}_{xr}(\omega) \bar{\theta}_g^I(\omega) = -(m + m_0) \bar{a}_g(\omega) \quad (5.14)$$

$$-\omega^2 m h \bar{x}(\omega) - \omega^2 m h \bar{u}_g^I(\omega) - \omega^2 (m h^2 + J + J_0) \bar{\theta}_g^I(\omega) + \tilde{G}_{rx}(\omega) \bar{u}_g^I(\omega) + \tilde{G}_{rr}(\omega) \bar{\theta}_g^I(\omega) = -m h \bar{a}_g(\omega) \quad (5.15)$$

Writing equations Eqs. (5.13) to (5.15) in matrix form results in:

$$\begin{bmatrix} \tilde{k}_{11} & \tilde{k}_{12} & \tilde{k}_{13} \\ \tilde{k}_{21} & \tilde{k}_{22} & \tilde{k}_{23} \\ \tilde{k}_{31} & \tilde{k}_{32} & \tilde{k}_{33} \end{bmatrix} \begin{bmatrix} \bar{x}(\omega) \\ \bar{u}_g^I(\omega) \\ \bar{\theta}_g^I(\omega) \end{bmatrix} = - \begin{bmatrix} m \\ m + m_0 \\ m h \end{bmatrix} \bar{a}_g(\omega) \quad (5.16)$$

The entries of the matrix in Eq. (5.16) are given in Eqs. (5.17) to (5.22)

$$\tilde{k}_{11} = (-\omega^2 m + i\omega c + k) \quad (5.17)$$

$$\tilde{k}_{12} = \tilde{k}_{21} = -\omega^2 m \quad (5.18)$$

$$\tilde{k}_{13} = \tilde{k}_{31} = -\omega^2 m h \quad (5.19)$$

$$\tilde{k}_{22} = -\omega^2 (m + m_0) + \tilde{G}_{xx}(\omega) \quad (5.20)$$

$$\tilde{k}_{23} = \tilde{k}_{32} = -\omega^2 m h + \tilde{G}_{xr}(\omega) \quad (5.21)$$

$$\tilde{k}_{33} = -\omega^2 (m h^2 + J + J_0) + \tilde{G}_{rr}(\omega) \quad (5.22)$$

The soil-structure interaction problem is formulated in Eq. (5.16) and can be solved to find  $\bar{x}(\omega)$ ,  $\bar{u}_g^I(\omega)$ ,  $\bar{\theta}_g^I(\omega)$  caused by the free-field ground acceleration  $\bar{a}_g(\omega)$ . The results can then be transformed into the time domain using the integral Fourier transform pair in Eq. (5.7).

### 5.3. SSI Simulations and Results

To demonstrate that the assumptions regarding the soil model in the OpenSees tool for the new ELE-screening procedure do not result in an unsafe assessment of the structure, simulations were run using a model based on the works of Tsouvalas[19]. The simulations were run for the fixed condition; according to literature[20] the effects of SSI are most severe for stiff structures on soft soils. The SMART1 earthquake is used for the free-field ground acceleration with a duration of 40 seconds. The dynamic stiffness of the soil, or soil impedance matrix, is acquired from site response analysis. For practical purposes, this research uses tabulated values from the works of Clough and Penzien [3].

The SSI analysis was performed using the same site-specific parameters as used in the earthquake analysis with the two ELE-screening procedures. The local site conditions are detailed in Section 4.1. The dynamic shear modulus of the soil was then varied in the SSI analysis to assess the effects of a more rigid soil and a less rigid soil on the assumptions. The different simulation cases are given in Table 5.1.  $G$  is the dynamic shear modulus of the soil [ $N/m^2$ ],  $\rho$  is the saturated soil density [ $kg/m^3$ ], and  $\bar{v}_s$  is the shear wave velocity [ $m/s$ ].

**Table 5.1:** SSI analysis simulation cases

	Case 1 "66e5"	Case 2 "66e6"	Case 3 "66e7"	
$G$	$66 \cdot 10^5$	$66 \cdot 10^6$	$66 \cdot 10^7$	[ $N/m^2$ ]
$\rho$	2000	2000	2000	[ $kg/m^3$ ]
$\bar{v}_s$	58	182	575	[ $m/s$ ]

For this research the parameters of interest in the SSI analysis are the:

- Response of the structure with SSI
- Response of the structure without SSI
- SSI induced ground motion below the foundation

A comparison of the response of the structure with and without soil-structure interaction demonstrates whether excluding SSI effects from the analysis, for the specific conditions in this research, results in an unsafe assessment of the structure or not. By comparing the SSI induced ground motion to the free-field ground motion an assessment can be made whether the free-field ground motion can be used in the research.

The response of the structure with and without SSI is shown in Fig. 5.4 for the site specific condition: *Case 2* with a soil shear modulus of  $66 \cdot 10^6 [N/m^2]$ . The response of the structure without SSI is larger which suggests that not taking SSI into consideration in the new ELE-screening method for this particular case will not result in an unsafe assessment of the structure.

The induced motion beneath the base of the structure with and without SSI is shown in Fig. 5.5 for the site specific condition *Case 2*. The induced motion is several orders of magnitude smaller than the free-field ground motion. It is therefore concluded that the unmodified free-field ground motion can be used in the new ELE-screening method for this particular case.

The response of the structure with and without SSI for a less rigid soil, *Case 1*, and a more rigid soil, *Case 3*, are shown in Fig. 5.2 and Fig. 5.6 respectively. The graphs suggest that the difference between the response of the structure with and without SSI becomes larger for a softer soil, while for a more rigid soil the difference becomes smaller. Comparing the induced motion below the foundation for the three soil conditions in Figs. 5.3, 5.5 and 5.7 suggests that the induced motion is inversely proportional to the soil shear modulus.

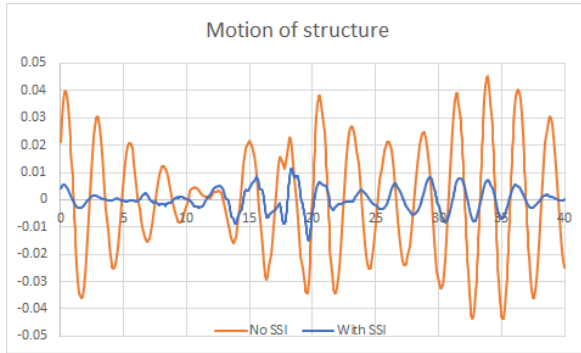


Figure 5.2: Motion of structure with and without SSI for G=66e5

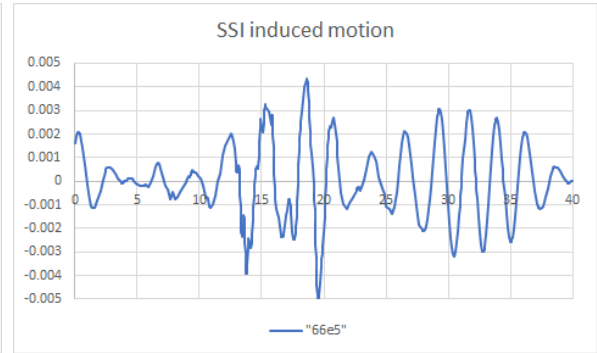


Figure 5.3: SSI induced motion under base for G=66e5

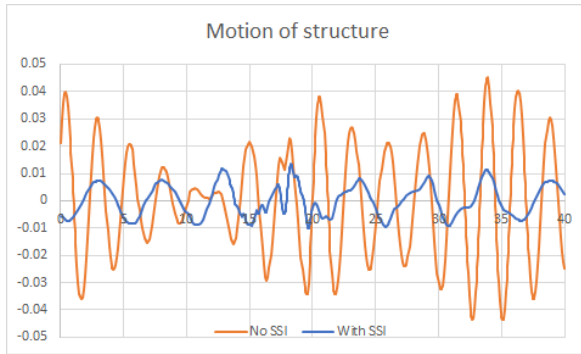


Figure 5.4: Motion of structure with and without SSI for G=66e6

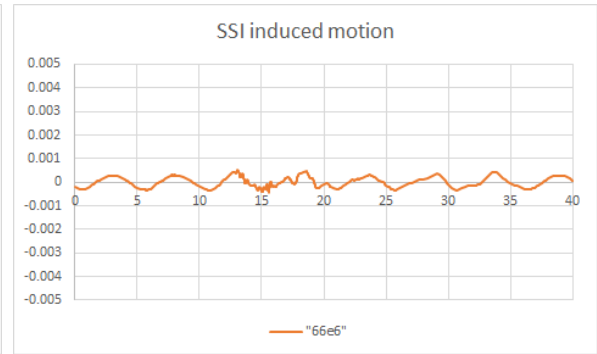


Figure 5.5: SSI induced motion under base for G=66e6

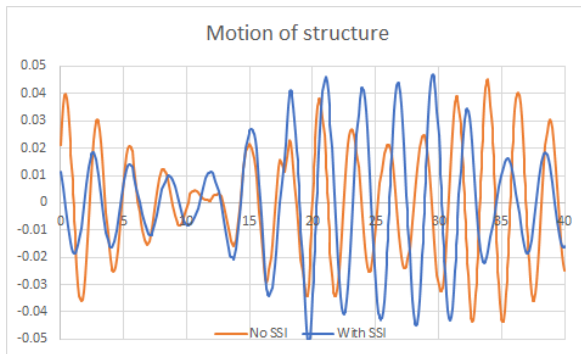


Figure 5.6: Motion of structure with and without SSI for G=66e7

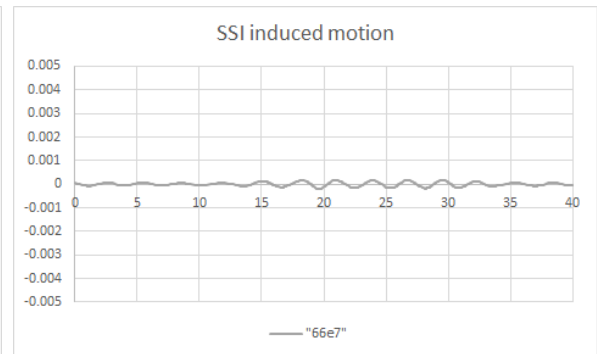


Figure 5.7: SSI induced motion under base for G=66e7

# 6

## Simulations

To assess the performance of the new ELE-screening procedure using THA against the existing ELE-screening procedure using RSA, an earthquake analysis was performed using both methods. This chapter looks at the different simulations that were run for the analysis and how they were performed. First the different simulations that were run and the rationale behind them are discussed in Section 6.1. How the different earthquake orientations are applied to the models is explained in Section 6.2. In Section 6.3 the assessment criteria are presented and the load quantities discussed that are used for evaluation. In Section 6.4 the Minifem simulation process used in the ELE-screening using RSA is discussed. The simulation process of the tool built in OpenSees for the new ELE-screening using THA is discussed in Section 6.5.

### 6.1. Simulation cases

To assess the performance of the new ELE-screening procedure using THA and compare it against the existing ELE-screening procedure using RSA, an earthquake analysis was performed using both methods. Several simulation cases were run to assess the effects of different parameters. The simulations differ in soil-structure connection, damping, and DRS.

The simulations that were run for the ELE-screening using RSA are:

RSA Fixed; 5% damped horizontal DRS; 5% damped vertical DRS

RSA Pinned; 5% damped horizontal DRS; 5% damped vertical DRS

RSA Spring; 5% damped horizontal DRS; 5% damped vertical DRS

RSA Spring; 5% damped horizontal DRS; 15% damped vertical DRS

The simulations that were run for the ELE-screening using THA are:

THA Fixed; 5% Rayleigh damping & Minifem DRS matched THR

THA Pinned; 5% Rayleigh damping & Minifem DRS matched THR

THA Spring; 5% Rayleigh damping & Minifem DRS matched THR

THA Spring; 5% Rayleigh damping + vertical linear viscous damper & Minifem DRS matched THR

THA Spring; 5% Rayleigh damping + vertical linear viscous damper & Minifem DRS matched horizontal THR and ISO DRS matched vertical THR

## Damping

One of the biggest differences in modelling the structure for the RSA and THA method is the implementation of damping. In the RSA method, damping is incorporated in the design response spectrum as explained in Section 4.2 and Appendix C. The horizontal and vertical DRS can each have different damping values. In the case of THA the damping is incorporated in the form of Rayleigh damping. One damping ratio is chosen and fit on 2 modes in such a manner that it ensures all other modes contributing significantly to the response have a reasonable damping value as explained in Section 3.3. It is not possible to select a different value for the vertical and horizontal modes as is done with RSA. To ensure a fair comparison between the RSA and THA, the damping is chosen to be 5% in both vertical and horizontal direction for the first three comparisons. This is done because this damping can accurately be implemented in both models. As shown in Fig. 3.6 the Rayleigh damping is 0.05 or less for the first ten modes. This implementation ensures that the level of damping of the THA is more conservative than that of the RSA.

For the in situ condition of the jack up the damping is taken as 5% in horizontal direction, and 15% in vertical direction. This additional vertical damping is due to radiation damping as explained in Section 3.4. The vertical design response spectrum is modified as explained in Section 4.2. As it is not possible to define two different damping ratios using Rayleigh damping, for the THA an additional viscous linear damper is implemented at the soil-structure interface aligned in the vertical direction.

## Soil-structure connection

In the usual procedure for SSA of jack-ups a representative soil condition is taken from where the unit is to operate. Additional simulations are run with higher and lower fixity values of the soil-structure connection. In the limit case of higher fixity is the Fixed condition where the structure is constrained in all 6 degrees of freedom. On the other end is the Pinned case, where the structure is constrained in lateral displacement directions but there is no rotational resistance. For the representative soil condition springs are used for the resistance. The different soil-structure connection cases being modeled are:

1. Fixed connection
2. Pinned connection
3. Spring connection
4. Spring connection with additional vertical viscous linear damper

The soil-structure connection influences the fundamental periods of the structure. The earthquake acceleration time histories are matched to the design response spectrum for a particular period range. This means that for different soil-structure interfaces the earthquake time histories are matched over a different range, resulting in different input acceleration time histories depending on the soil-structure connection, as discussed in Section 4.6.

## 6.2. Earthquake rotation

When a structural design is asymmetric in geometric configuration or directional capacity, additional analyses need to be done to demonstrate suitable performance in weaker directions. For time history analyses, this may require different orientations of the earthquake horizontal records to demonstrate performance requirements [2]. According to ASCE 7-16 each pair of ground motions should be applied simultaneously to the structure, considering the most disadvantageous location of eccentric masses [8]. As the orientation of the horizontal earthquake components that results in the highest action effects is not known a priori, the simulations are run for different earthquake orientations. This is done by rotating the set of orthogonal horizontal ground motions around the vertical axis in increments of 30 degrees, resulting in 12 directions. The orientation of the major principal component is used to indicate the orientation of the pair. An increment of 30 degrees was chosen as an optimum between simulation time and number of orientation cases. This increment was also chosen so that the cases are included in which: the major principal component is oriented in parallel with the diagonal of the legs, and where it is oriented perpendicular to the diagonal of the legs.

In OpenSees the ground motions are input in 3 directions:

- 1 - corresponds to translation along the global X axis
- 2 - corresponds to translation along the global Y axis
- 3 - corresponds to translation along the global Z axis

To input the differently oriented time traces into the OpenSees model, the horizontal components are decomposed to the translational X and Y axis. This is done using Eq. (6.1). The two horizontal components of an earthquake time trace,  $a_1$  and  $a_2$  are thus effectively decomposed into a set of 12 new time history pairs each representing an orientation. Each unique matched time history pair from Section 4.6 was decomposed in this manner.

$$\begin{bmatrix} a_{1,\theta} \\ a_{2,\theta} \end{bmatrix} = \begin{bmatrix} \cos\theta & -\sin\theta \\ \sin\theta & \cos\theta \end{bmatrix} \begin{bmatrix} a_1 \\ a_2 \end{bmatrix} \quad (6.1)$$

In the RSA simulation using Minifem, a RESOLV vector is used to simulate rotation of the earthquake around the structure. For details on this method the reader is referred to "*Dynamics of fixed marine structures*" [21].

### 6.3. Assessment criteria

Areas on jack-ups that are often critical with regard to structural strength are the legs at the lower guides, the legs between guides, the pinions and/or rack teeth, the fixation system and/or fixation system supports and the leg to spudcan connection [6]. The assessment criteria for a jack-up subject to an ELE event are:

- Overturning stability
- Leg strength
- Holding capacity of the jacking system
- Pre-load capacity
- Foundation bearing and sliding capacity

The forces and moments that are used to verify these criteria are the normal force, shear force, and moment in the leg at both the leg-hull connection, also called lower guide (LG), and the leg to spudcan connection or footing (FT). The naming convention for the load quantities is adopted from the ISO codes for ease and consistency. The shear force in the leg is referred to as  $F_H$  as it is the force in the horizontal plane of the global axis system.  $F_{H,LG}$  is the shear force in the leg at the lower guide, and  $F_{H,FT}$  the shear force in the leg at the footing. The normal force in the leg is referred to as  $V$  as this is the vertical force in the global axis system, with  $V_{LG}$  at the lower guide and  $V_{FT}$  at the footing. The moments  $M_{LG}$  and  $M_{FT}$  in the leg follow similarly.

$F_H$  is the resultant of the horizontal components  $F_X$  and  $F_Y$ . Similarly  $M$  is the resultant of  $M_X$  and  $M_Y$ . The maximum horizontal force  $F_{H,max}$  and maximum moment  $M_{max}$  are found differently in the RSA and THA method. In the RSA method  $F_{H,max}$  is the resultant of  $F_{X,max}$  and  $F_{Y,max}$  as shown in Eq. (6.2).  $M_{max}$  follows similarly in Eq. (6.3).

$$F_{H,max} = \sqrt{(F_{X,max})^2 + (F_{Y,max})^2} \quad (6.2)$$

$$M_{max} = \sqrt{(M_{X,max})^2 + (M_{Y,max})^2} \quad (6.3)$$

In the THA method the maximum horizontal force  $F_{H,max}$  and maximum moment  $M_{max}$  are found in time as shown in Eqs. (6.4) and (6.5) respectively.

$$F_{H,max} = \max \left( \sqrt{(F_X(t))^2 + (F_Y(t))^2} \right) \quad (6.4)$$

$$M_{max} = \max \left( \sqrt{(M_X(t))^2 + (M_Y(t))^2} \right) \quad (6.5)$$

## 6.4. RSA simulation process in Minifem

Minifem is a finite element simulation program developed in-house at GustoMSC. It was originally designed as a tool to perform checks on linear and non-linear finite element analyses. A tool has been built in Minifem to perform ELE-screening using response spectrum analysis. The tool works by reducing a multi-degree of freedom (MDOF) system to a number of uncoupled SDOF systems which can each be solved using the response spectrum.

The MDOF system is reduced using a normal mode analysis and transformation. The eigenfrequencies  $\omega_i$  and the normalized eigenshapes  $\Phi_i$  are obtained by solving the eigenvalue problem of the MDOF system. The equations of motion of the structure are transformed to the modal domain. The equation of motion of an MDOF system with damping is given in Eq. (6.6). The eigenfrequencies are the positive roots of the characteristic equation given in Eq. (6.7). It is assumed that the response can be expressed in terms of the undamped modes as given in Eq. (6.8), where  $\Phi$  is the real-valued eigenmatrix obtained by solving the undamped free vibration  $\mathbf{M}\ddot{\mathbf{x}} + \mathbf{K}\mathbf{x} = \mathbf{0}$ .

$$\mathbf{M}\ddot{\mathbf{x}}(t) + \mathbf{C}\dot{\mathbf{x}}(t) + \mathbf{K}\mathbf{x}(t) = -\mathbf{M}\mathbf{r}\ddot{x}_g(t) \quad (6.6)$$

$$\det(-\omega_i^2 \mathbf{M} + \mathbf{K}) = 0 \quad (6.7)$$

$$\mathbf{x}(t) = \Phi \mathbf{u}(t) = \sum_{i=1}^N \hat{\Phi}_i u_i(t) \quad (6.8)$$

Substituting the solution or  $\mathbf{x}(t)$  from Eq. (6.8) into the equation of motion results in Eq. (6.9). Pre-multiplying this equation with the transpose of the eigenmatrix gives Eq. (6.10).

$$\mathbf{M}\Phi\ddot{\mathbf{u}}(t) + \mathbf{C}\Phi\dot{\mathbf{u}}(t) + \mathbf{K}\Phi\mathbf{u}(t) = -\mathbf{M}\mathbf{r}\ddot{u}_g(t) \quad (6.9)$$

$$\mathbf{M}^*\ddot{\mathbf{u}}(t) + \mathbf{C}^*\dot{\mathbf{u}}(t) + \mathbf{K}^*\mathbf{u}(t) = -\Phi^T \mathbf{M}\mathbf{r}\ddot{u}_g(t) \quad (6.10)$$

The modal mass matrix  $\mathbf{M}^*$  and modal stiffness matrix  $\mathbf{K}^*$  are diagonal, while the modal damping matrix  $\mathbf{C}^*$  is fully populated. Rayleigh damping is used to force a diagonalised modal damping matrix. A decoupled equation of motion is obtained for each modal coordinate  $u_i(t)$ ,  $i = 1, 2, \dots, N$  as given in Eq. (6.11), with  $\zeta_i$  and  $\Gamma_i$  defined by Eqs. (6.12) and (6.13) respectively.

$$\ddot{u}_i(t) + 2\zeta_i\omega_i\dot{u}_i(t) + \omega_i^2 u_i(t) = -\Gamma_i\ddot{u}_g(t) \quad (6.11)$$

$$\zeta_i = \frac{c_{ii}^*}{2m_{ii}^*\omega_i} = \frac{c_{ii}^*}{c_{ii,crit}^*} \quad (6.12)$$

$$\Gamma_i = \frac{L_i}{m_{ii}^*} = \frac{\hat{\Phi}_i^T \mathbf{M}\mathbf{r}}{\hat{\Phi}_i^T \mathbf{M}\hat{\Phi}_i} \quad (6.13)$$

$u_i(t)$  is the modal displacement response in the  $i^{th}$  mode

$\zeta_i$  is the modal damping ratio in the  $i^{th}$  mode

$\Gamma_i$  is the modal participation factor in the  $i^{th}$  mode

The maximum modal displacement response for each modal degree of freedom is then calculated in Eq. (6.14) using the the design response spectrum.

$$u_{i,max} = |u_i(t)|_{max} = |\Gamma_i S_d(\zeta_i, T_i)| \quad (6.14)$$

The normal coordinate of each mode responds to the earthquake like a single degree of freedom oscillator. Each mode experiences a scaled version of the excitation determined by the participation factor. The maximum displacement response of the structure in the  $i^{th}$  mode is given by Eq. (6.15) and the maximum acceleration response of the structure in the  $i^{th}$  mode is given by Eq. (6.16).

$$x_{i,max} = \Phi_i u_{i,max} \quad (i = 1, 2, \dots, n) \quad (6.15)$$

$$\ddot{x}_{i,max} = \Phi_i \Gamma_i S_a(\zeta_i, T_i) \quad (i = 1, 2, \dots, n) \quad (6.16)$$

The individual responses are statistically combined to obtain the most probable peak response. The modal combination rule used is the square-root-of-sum-of-squares rule (SRSS) given in Eq. (6.17).

$$\ddot{x}_{max} = \left( \sum_{i=1}^N (\ddot{x}_{i,max})^2 \right)^{\frac{1}{2}} = \left( \sum_{i=1}^N (\Phi_i \Gamma_i S_a(\zeta_i, T_i))^2 \right)^{\frac{1}{2}} \quad (6.17)$$

The total structural response due to the seismic excitation from all three translational directions is obtained by spatial combination of the responses using SRSS.

## 6.5. THA simulation process in OpenSees

OpenSees is a software framework for building finite element applications in structural and geotechnical systems, using the Tcl programming language. Tcl is a string based command language consisting of variables and variable substitutions, expression evaluation, basic control structures, procedures, file manipulations, and file sourcing.

The main abstractions in OpenSees are the Model, Domain, Analysis, and Recorder as shown in Fig. 6.1. In the Model the objects are constructed and added to the Domain. The Domain holds the state of the model at time (t) and (t+dt). The Analysis moves the model from state at time (t) to state at time (t+dt). The Recorder monitors and stores user defined parameters in the model during the analysis.

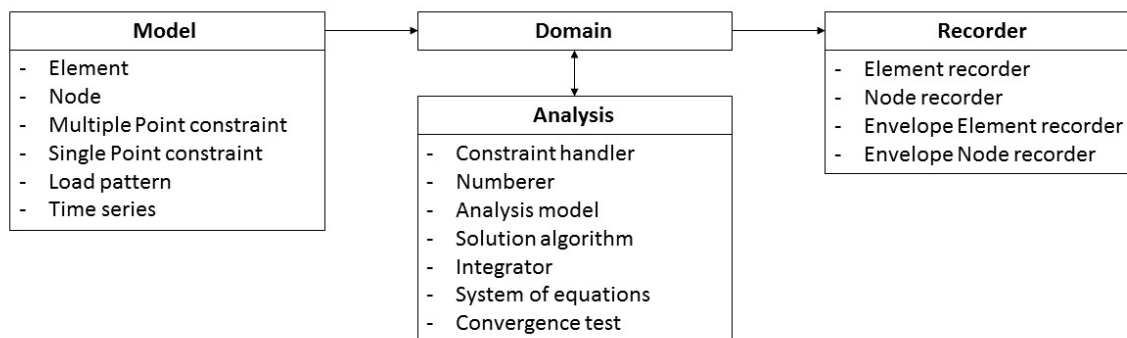


Figure 6.1: OpenSees framework

### Model

First the model is built by defining:

- Model dimensions and degrees-of-freedom
- Nodal coordinates
- Nodal constraints & boundary conditions
- Nodal masses
- Elements and element connectivity
- Recorders to capture and store output

For the elements use is made of elastic Timoshenko beams

The gravity load is then applied to the model by:

- Selecting nodal or element loads
- Setting static-analysis parameters (tolerances & load increments)
- Performing analyze command
- Holding gravity loads constant
- Resetting time to zero

The lateral loads are then defined and applied, consisting of:

- The load pattern: nodal loads for static analysis, and support ground motions for earthquake analysis.
- Lateral-analysis parameters: tolerances & displacement/time increments
- For Static Lateral-Load Analysis
  - define the displacement increments and displacement path
- Dynamic Lateral-Load Analysis
  - define the input motion and all associated parameters, such as scaling and input type
  - define analysis duration and time increment
  - define damping

The system is then analysed.

## Analysis

The analysis command is used to construct the analysis object which defines the type of analysis that will be performed. In this research use was made of the *Transient* analysis with constant time step.

The linear equation solver used in the OpenSees model is called *Sparse General*. This is a direct solver for unsymmetrical sparse matrices. The numbering of the degrees of freedom in the domain is done by the *RCM* method. This renumbers the DOF to minimize the matrix band-width using the Reverse Cuthill-McKee algorithm. The integrator used is the *Hilbert-Hughes-Taylor* method. This is an implicit method that allows for energy dissipation and second order accuracy, which is not possible with the regular Newmark method. Depending on choices of input parameters, the method can be unconditionally stable. The three parameter Hilbert-Hughes-Taylor time-stepping method is used to determine the next time step for the analysis including inertial effects. The iteration from the previous time step to the current time step is done using the *Modified Newton* method; this is the solution algorithm. This method uses the tangent at the first iteration to iterate to convergence. A convergence test is used to determine whether the current state of the domain is on the converged solution path. The convergence test used is the *Energy Increment Test* which uses the dot product of the solution vector and norm of the right hand side of the matrix equation to determine if convergence has been reached. If the analysis is not successful using the Modified Newton method, alternative solution algorithms are used. The model is programmed to consequently solve using the Newton with Initial Tangent method followed by the Broyden method.

## Recorder

The recorders are defined and built in the model. They record and store the state of the domain for each time step. For transient analysis, the response output recorded depends on the input:

- UniformExcitation Pattern (input acceleration record): Relative with respect to supports
- MultipleSupport Pattern (input displacement record): Absolute values

This means that since there is uniform excitation from the earthquake acceleration time histories that the recorded accelerations, velocities, and displacements are relative with respect to the supports. To get the absolute acc., vel., and disp. of a node, the respective acc., vel., disp., of the foundation node needs to be added. The input acceleration time history records are modified and consequently decomposed to implement the different angles of incidence of the earthquake on the structure as described in Section 4.6 and Section 6.2. It is important to ensure the correct earthquake motions are used to obtain the absolute values of the nodes. Recorders have been created in the OpenSees tools to record forces and motions.

- The recorders of motions of the nodes (acc., vel., disp.) are 3 in DOF: x,y,z.
- The recorders of the reaction forces of the elements are in 6 DOF.

For the comparison of the new ELE-screening method using THA with the existing ELE-screening method using RSA, the assessment criteria are focussed on the forces and moments as described in Section 6.3. The recorders for the motions have been included in the model to get a better understanding of how the model behaves, perform sanity checks, and for future developed use of the model.

# 7

## Results

Simulations were run to assess the performance of the new ELE-screening procedure using THA against the existing ELE-screening procedure using RSA. In this chapter the results of the response spectrum analysis and the time history analysis simulations are presented and analyzed. In Section 7.1 the format of the results is discussed and the results of the simulations for the Fixed, Pinned, Spring5, Spring15, and Spring15ISO cases are presented. The effect of vertical radiation damping on the results is presented in Section 7.2. One of the advantages of using time time history analysis over response spectrum analysis is time development. Section 7.3 looks at the effect of time development on the maximum horizontal force and the maximum moment. The chapter concludes in Section 7.4 with some remarks on the simulations that were run.

### 7.1. Simulation results

The assessment criteria for a jack-up subject to an ELE event are: overturning stability, leg strength, holding capacity of the jacking system, pre-load capacity, and foundation bearing and sliding capacity. As discussed in Section 6.3, the parameters used to verify these criteria are the normal force, shear force, and moment in the legs at the lower guide and footing.

During the THA these values are recorded at each time step for each leg. To compare the performance of the THA method with that of the RSA the same output is required. Results from the RSA are given as the maximum force or moment per leg per EQ direction. If one leg fails the whole structure fails, therefore the global maximum action effect per earthquake incidence angle are examined and not the maximum action effect per leg.

The maximum action effect per earthquake incidence angle are displayed in:

- Figs. 7.1 to 7.6. for the simulations with the Fixed connection.
- Figs. 7.7 to 7.12 for the simulations with the Pinned connection.
- Figs. 7.13 to 7.18 for the simulations with the Spring5 connection.
- Figs. 7.19 to 7.24 for the simulations with the Spring15 connection.
- Figs. 7.25 to 7.30 for the simulations with the Spring15ISO connection.

It is important to note that the lines connecting the data points in Figs. 7.1 to 7.30 do not have any physical meaning. They are merely drawn to help with visualization and do not indicate values for these intermediate earthquake incidence angles.

The quantities used for unity checks are the global maximum forces and moments, i.e. action effects, that the structure will experience irrespective of the earthquake incidence angle. These values are presented in Tables 7.1 to 7.5 for the Fixed, Pinned, Spring5, Spring15, and Spring15ISO simulations respectively.

### Fixed connection

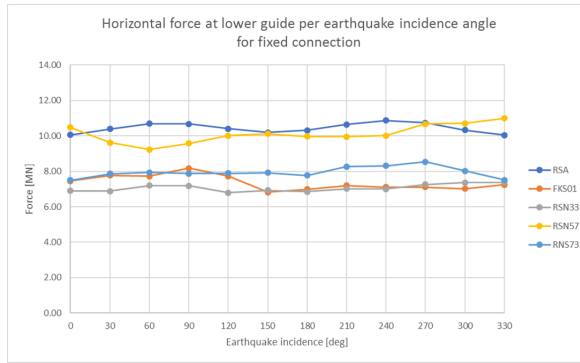


**Figure 7.1:** Max shear force  $F_{H,LG}$  at the lower guide per EQ incidence angle for the Fixed connection

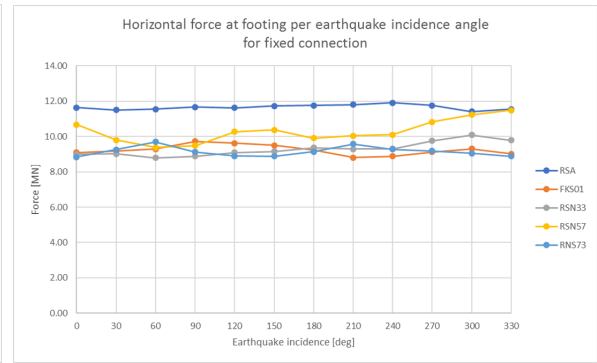


**Figure 7.2:** Max shear force  $F_{H,FT}$  at the footing per EQ incidence angle for the Fixed connection

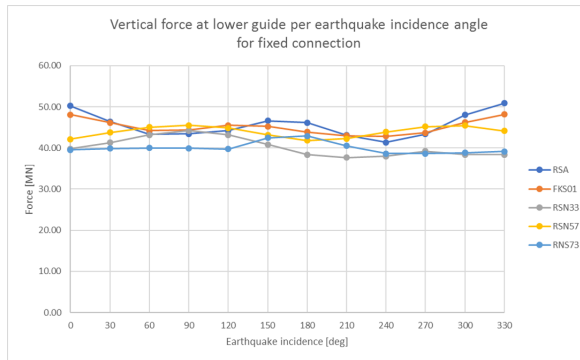


**Figure 7.3:** Max normal force  $V_{LG}$  at the lower guide per EQ incidence angle for the Fixed connection

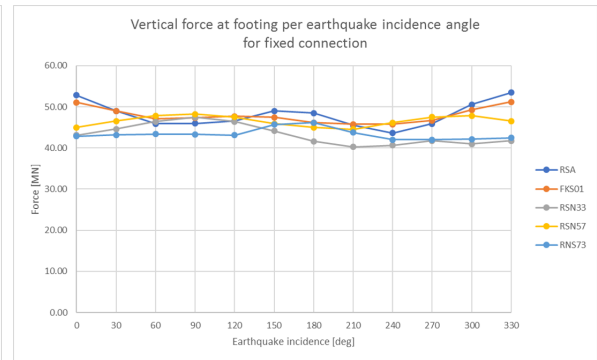


**Figure 7.4:** Max normal force  $V_{FT}$  at the footing per EQ incidence angle for the Fixed connection

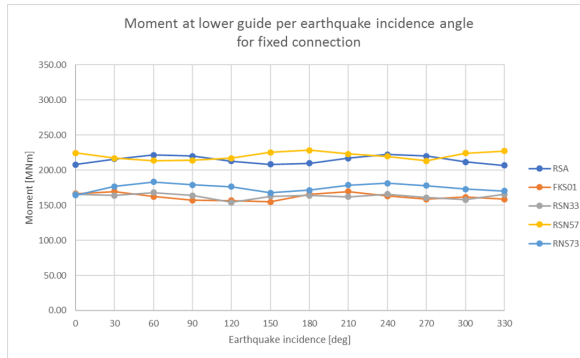


**Figure 7.5:** Max moment  $M_{LG}$  at the lower guide per EQ incidence angle for the Fixed connection

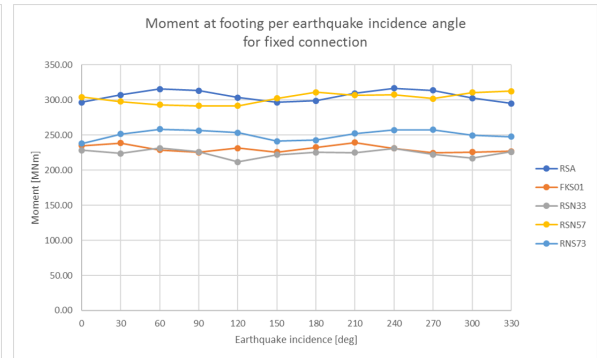


**Figure 7.6:** Max moment  $M_{FT}$  at the footing per EQ incidence angle for the Fixed connection

**Table 7.1:** Global maximum action effects for the Fixed connection

	RSA	FKS01	RSN33	RSN57	RSN73	
$F_{H,LG}$	10.87	8.18	7.38	11.00	8.54	MN
$V_{LG}$	50.87	48.15	44.21	45.52	42.89	MN
$M_{LG}$	222.15	169.69	168.19	228.44	183.32	MNm
$F_{H,FT}$	11.91	9.73	10.10	11.49	9.70	MN
$V_{FT}$	53.46	51.18	47.41	48.24	46.11	MN
$M_{FT}$	316.76	239.43	231.23	312.35	258.10	MNm

### Pinned connection

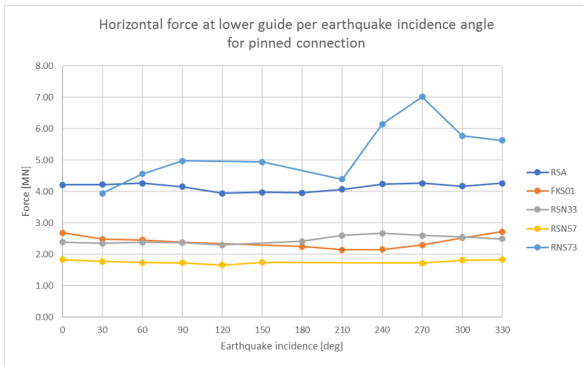


**Figure 7.7:** Max shear force  $F_{H,LG}$  at the lower guide per EQ incidence angle for the Pinned connection

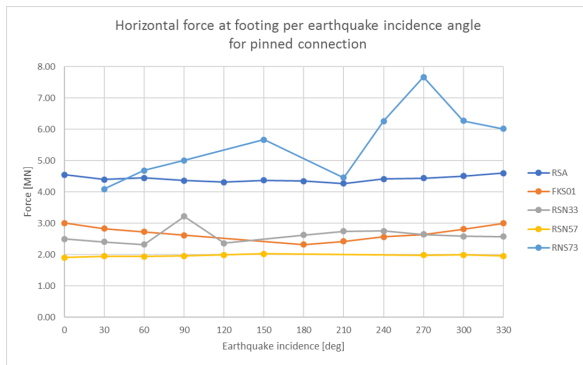


**Figure 7.8:** Max shear force  $F_{H,FT}$  at the footing per EQ incidence angle for the Pinned connection

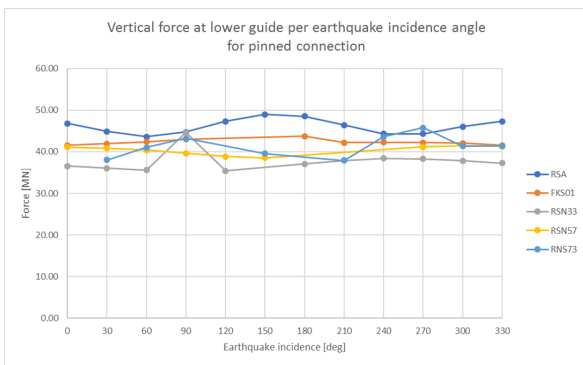


**Figure 7.9:** Max normal force  $V_{LG}$  at the lower guide per EQ incidence angle for the Pinned connection

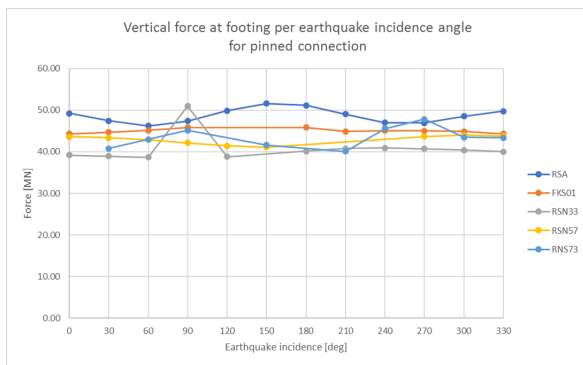


**Figure 7.10:** Max normal force  $V_{FT}$  at the footing per EQ incidence angle for the Pinned connection

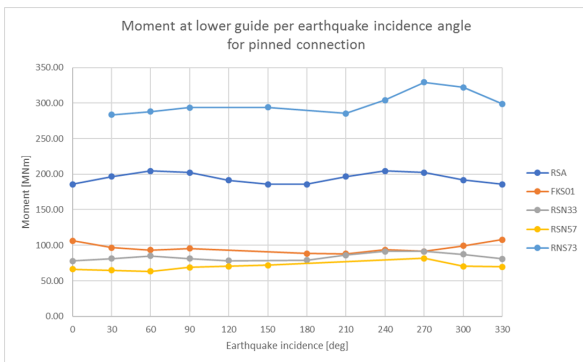


**Figure 7.11:** Max moment  $M_{LG}$  at the lower guide per EQ incidence angle for the Pinned connection

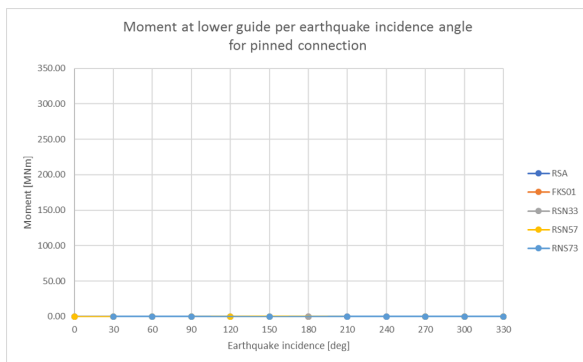


**Figure 7.12:** Max moment  $M_{FT}$  at the footing per EQ incidence angle for the Pinned connection

**Table 7.2:** Global maximum action effects for the Pinned connection

	RSA	FKS01	RSN33	RSN57	RSN73	
$F_{H,LG}$	4.26	2.72	2.67	1.83	7.01	MN
$V_{LG}$	48.99	43.71	44.65	41.44	45.80	MN
$M_{LG}$	204.62	107.70	91.55	81.66	329.27	MNm
$F_{H,FT}$	4.60	3.01	3.22	2.03	7.66	MN
$V_{FT}$	51.58	45.87	50.95	43.97	47.82	MN
$M_{FT}$	0.00	0.01	0.06	0.01	0.02	MNm

### Spring5 connection

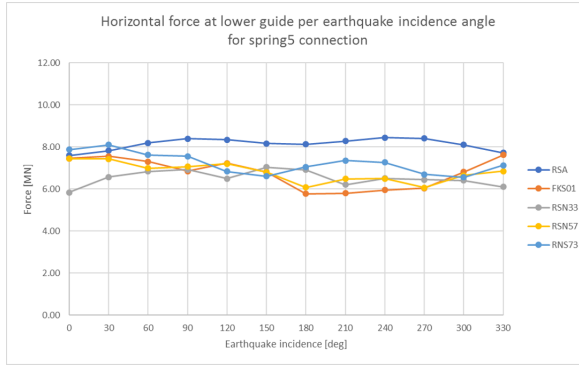


**Figure 7.13:** Max shear force  $F_{H,LG}$  at the lower guide per EQ incidence angle for the Spring5 connection

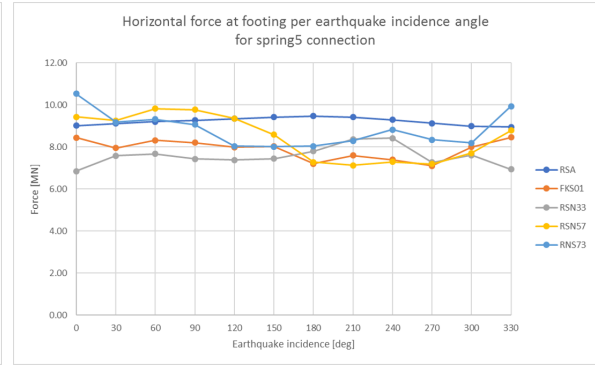


**Figure 7.14:** Max shear force  $F_{H,FT}$  at the footing per EQ incidence angle for the Spring5 connection

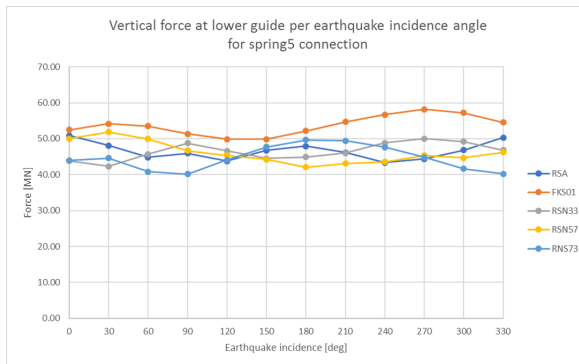


**Figure 7.15:** Max normal force  $V_{LG}$  at the lower guide per EQ incidence angle for the Spring5 connection

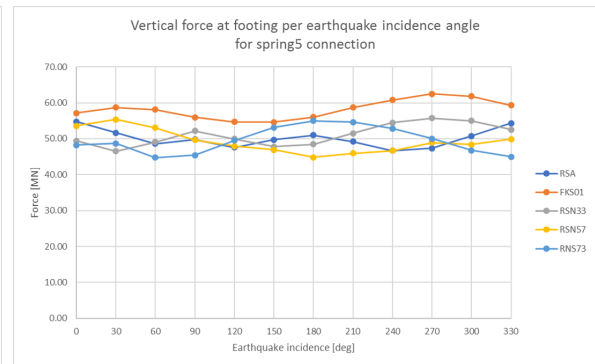


**Figure 7.16:** Max normal force  $V_{FT}$  at the footing per EQ incidence angle for the Spring5 connection

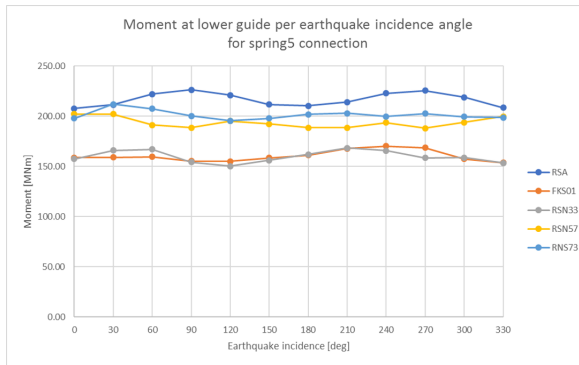


**Figure 7.17:** Max moment  $M_{LG}$  at the lower guide per EQ incidence angle for the Spring5 connection

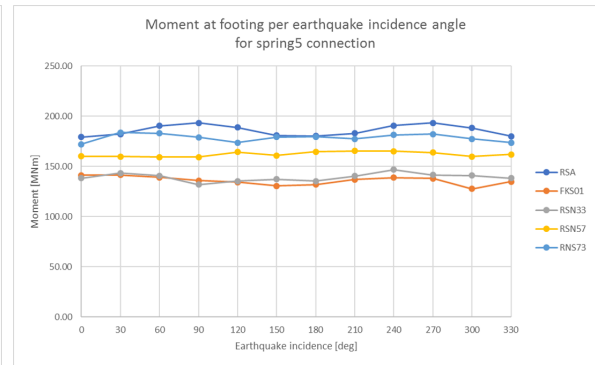


**Figure 7.18:** Max moment  $M_{FT}$  at the footing per EQ incidence angle for the Spring5 connection

**Table 7.3:** Global maximum action effects for the Spring5 connection

	RSA	FKS01	RSN33	RSN57	RSN73	
$F_{H,LG}$	8.45	7.62	7.03	7.44	8.10	MN
$V_{LG}$	50.93	58.17	50.03	51.90	49.63	MN
$M_{LG}$	226.25	170.20	168.34	202.10	212.00	MNm
$F_{H,FT}$	9.47	8.45	8.41	9.82	10.52	MN
$V_{FT}$	54.77	62.49	55.73	55.37	54.96	MN
$M_{FT}$	193.38	141.51	146.72	165.39	183.78	MNm

### Spring15 connection

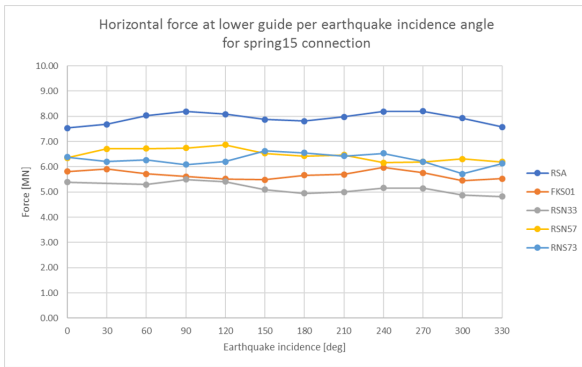


**Figure 7.19:** Max shear force  $F_{H,LG}$  at the lower guide per EQ incidence angle for the Spring15 connection

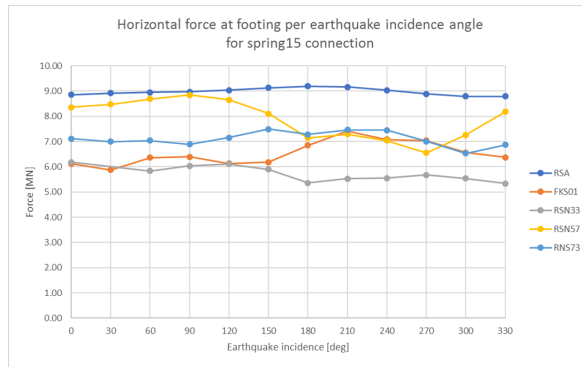


**Figure 7.20:** Max shear force  $F_{H,FT}$  at the footing per EQ incidence angle for the Spring15 connection

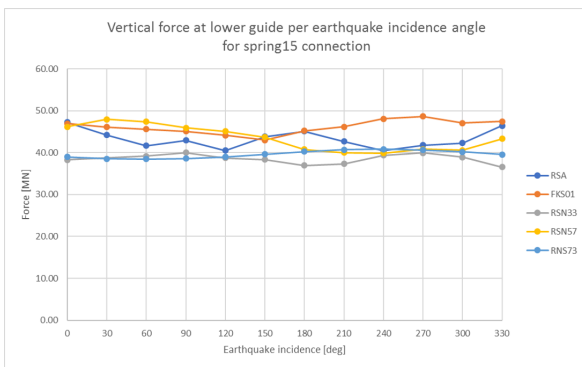


**Figure 7.21:** Max normal force  $V_{LG}$  at the lower guide per EQ incidence angle for the Spring15 connection

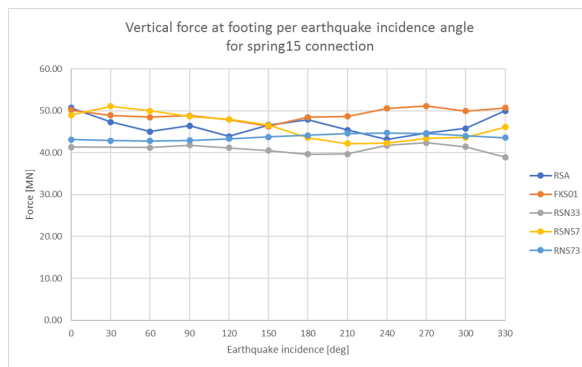


**Figure 7.22:** Max normal force  $V_{FT}$  at the footing per EQ incidence angle for the Spring15 connection

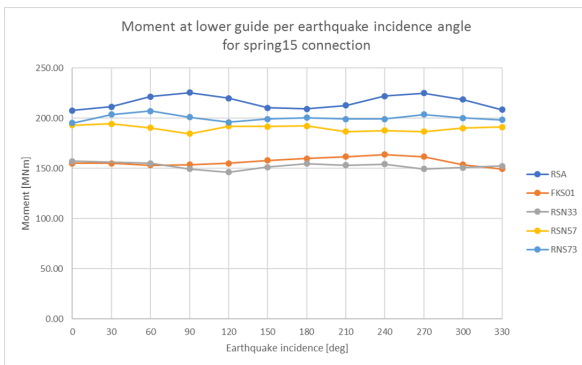


**Figure 7.23:** Max moment  $M_{LG}$  at the lower guide per EQ incidence angle for the Spring15 connection

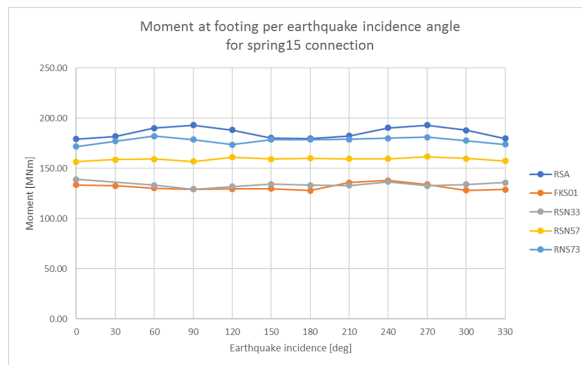


**Figure 7.24:** Max moment  $M_{FT}$  at the footing per EQ incidence angle for the Spring15 connection

**Table 7.4:** Global maximum action effects for the Spring15 connection

	RSA	FKS01	RSN33	RSN57	RSN73	
$F_{H,LG}$	8.20	5.97	5.50	6.87	6.62	MN
$V_{LG}$	47.28	48.67	40.02	47.98	40.86	MN
$M_{LG}$	225.42	163.88	157.22	194.41	207.06	MNm
$F_{H,FT}$	9.19	7.41	6.18	8.84	7.49	MN
$V_{FT}$	50.70	51.11	42.38	51.07	44.73	MN
$M_{FT}$	193.03	138.09	139.04	161.64	182.23	MNm

### Spring15ISO connection

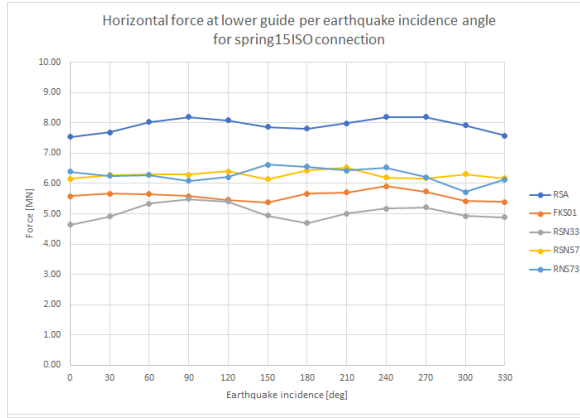


**Figure 7.25:** Max shear force  $F_{H,LG}$  at the lower guide per EQ incidence angle for the Spring15ISO connection

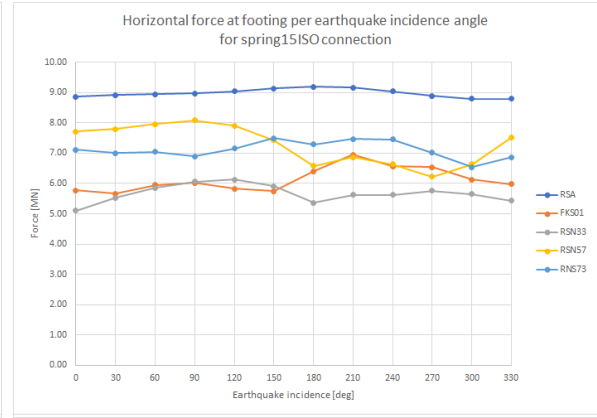


**Figure 7.26:** Max shear force  $F_{H,FT}$  at the footing per EQ incidence angle for the Spring15ISO connection

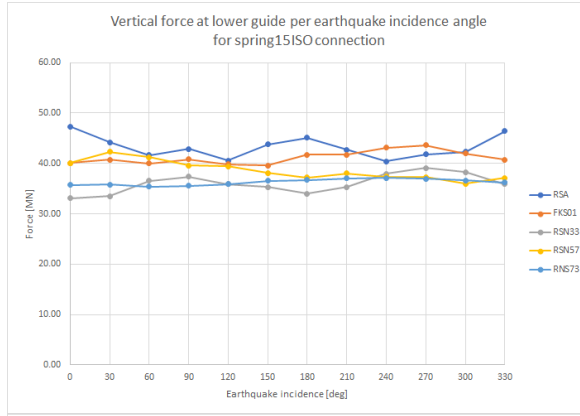


**Figure 7.27:** Max normal force  $V_{LG}$  at the lower guide per EQ incidence angle for the Spring15ISO connection

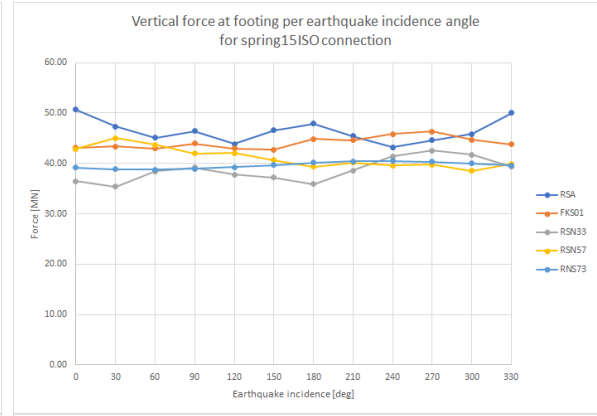


**Figure 7.28:** Max normal force  $V_{f_i}$  at the footing per EQ incidence angle for the Spring15ISO connection

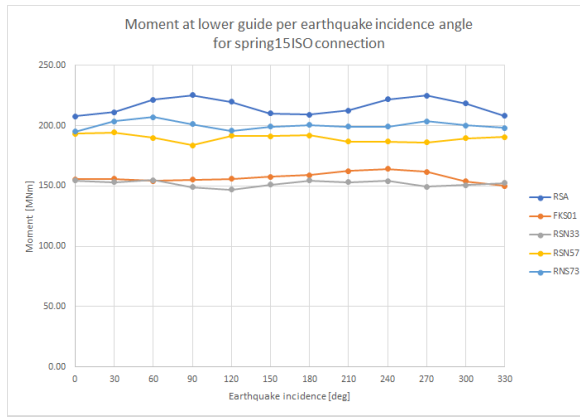


**Figure 7.29:** Max moment  $M_{LG}$  at the lower guide per EQ incidence angle for the Spring15ISO connection

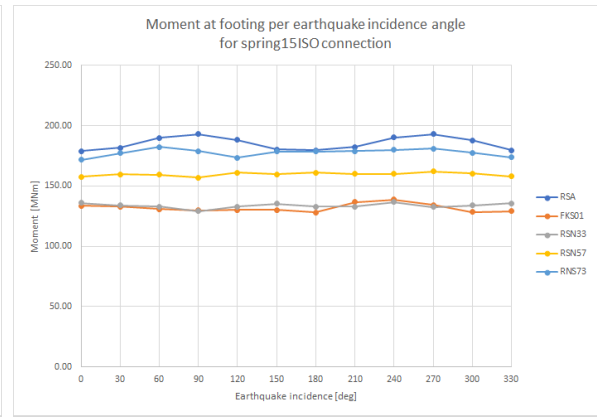


**Figure 7.30:** Max moment  $M_{LG}$  at the footing per EQ incidence angle for the Spring15ISO connection

**Table 7.5:** Global maximum action effects for the Spring15ISO connection

	RSA	FKS01	RSN33	RSN57	RSN73	
$F_{H,LG}$	8.20	5.92	5.49	6.52	6.63	MN
$V_{LG}$	47.28	43.60	39.07	42.30	37.14	MN
$M_{LG}$	225.42	164.12	154.86	194.40	207.16	MNm
$F_{H,FT}$	9.19	6.95	6.12	8.08	7.50	MN
$V_{FT}$	50.70	46.31	42.53	45.02	40.52	MN
$M_{FT}$	193.03	138.68	136.79	162.31	182.32	MNm

## 7.2. Effect of vertical radiation damping

To assess the effect of additional vertical radiation damping on the response of the structure the Spring5 and Spring15 simulations were used. In all simulations the horizontal damping is set to 5%. The Spring 5 case has vertical damping of 5%, and the Spring15 case has vertical damping of 15%. In the RSA simulations the damping is implemented in the spectrum, as described in Section 4.2. In the THA simulations the Rayleigh damping is set to 5% and there are additional vertical linear viscous dampers, as described in Section 3.3 and Section 3.4. The results of the Spring5 and Spring15 simulations are given in table Tables 7.6 and 7.7.

In addition the Spring15ISO case was used to assess the effect of using the vertical DRS as described by ISO instead of the Minifem vertical DRS. As described in Section 4.2 the Minifem DRS was used for a fair comparison between the RSA and THA methods. The results of the Spring15ISO simulations are given in Table 7.8.

**Table 7.6:** Global maximum action effects for the Spring5 connection

	RSA	FKS01	RSN33	RSN57	RSN73	THA <sub>max</sub>	THA <sub>avg</sub>	$\Delta_{max}$	$\Delta_{avg}$	
$F_{H,LG}$	8.45	7.62	7.03	7.44	8.10	8.10	7.55	0.34	0.90	MN
$V_{LG}$	50.93	58.17	50.03	51.90	49.63	58.17	52.43	-7.24	-1.50	MN
$M_{LG}$	226.25	170.20	168.34	202.10	212.00	212.00	188.16	14.25	38.10	MNm
$F_{H,FT}$	9.47	8.45	8.41	9.82	10.52	10.52	9.30	-1.05	0.17	MN
$V_{FT}$	54.77	62.49	55.73	55.37	54.96	62.49	57.14	-7.72	-2.37	MN
$M_{FT}$	193.38	141.51	146.72	165.39	183.78	183.78	159.35	9.60	34.03	MNm

**Table 7.7:** Global maximum action effects for the Spring15 connection

	RSA	FKS01	RSN33	RSN57	RSN73	THA <sub>max</sub>	THA <sub>avg</sub>	$\Delta_{max}$	$\Delta_{avg}$	
$F_{H,LG}$	8.20	5.97	5.50	6.87	6.62	6.87	6.24	1.33	1.96	MN
$V_{LG}$	47.28	48.67	40.02	47.98	40.86	48.67	44.38	-1.39	2.90	MN
$M_{LG}$	225.42	163.88	157.22	194.41	207.06	207.06	180.64	18.36	44.78	MNm
$F_{H,FT}$	9.19	7.41	6.18	8.84	7.49	8.84	7.48	0.35	1.71	MN
$V_{FT}$	50.70	51.11	42.38	51.07	44.73	51.11	47.32	-0.41	3.38	MN
$M_{FT}$	193.03	138.09	139.04	161.64	182.23	182.23	155.25	10.79	37.78	MNm

**Table 7.8:** Global maximum action effects for the Spring15ISO connection

	RSA	FKS01	RSN33	RSN57	RSN73	THA <sub>max</sub>	THA <sub>avg</sub>	$\Delta_{max}$	$\Delta_{avg}$	
$F_{H,LG}$	8.20	5.92	5.49	6.52	6.63	6.63	6.14	1.57	2.06	MN
$V_{LG}$	47.28	43.60	39.07	42.30	37.14	43.60	40.53	3.68	6.75	MN
$M_{LG}$	225.42	164.12	154.86	194.40	207.16	207.16	180.14	18.26	45.28	MNm
$F_{H,FT}$	9.19	6.95	6.12	8.08	7.50	8.08	7.16	1.11	2.03	MN
$V_{FT}$	50.70	46.31	42.53	45.02	40.52	46.31	43.60	4.39	7.10	MN
$M_{FT}$	193.03	138.68	136.79	162.31	182.32	182.32	155.03	10.71	38.00	MNm

When comparing the RSA results of the Spring5 and Spring15 simulations there is very little difference in the maximum loads on the structure apart from the  $V_{LG}$  and  $V_{FT}$ . The vertical forces of the Spring5 case are higher than the Spring15 case while the horizontal forces and moments are very similar.

Comparing the results of the THA simulations for the Spring5 and Spring15 case it is clear that not only is there a difference in the vertical forces, but that the horizontal forces also show a significant change, while the moments remain very similar. When comparing the Spring15 to the Spring15ISO case for the THA simulations, the vertical forces differ significantly while the the horizontal forces and moments are quite similar.

### 7.3. Effect of time development

One of the advantages of using time history analysis over response spectrum analysis is time development. This section demonstrates the effect of time development on the magnitude of the forces and moments. As discussed in Section 6.3:  $F_H$  is the resultant of the horizontal components  $F_X$  and  $F_Y$ , and  $M$  is the resultant of moments  $M_X$  and  $M_Y$ . The maximum horizontal force  $F_{H,max}$  and maximum moment  $M_{max}$  are found differently in the RSA and THA method.

**RSA**  $F_{H,max}$  is found from  $F_{X,max}$  and  $F_{Y,max}$ ;  $M_{max}$  is found from  $M_{X,max}$  and  $M_{Y,max}$  Eqs. (6.2) and (6.3)

**THA**  $F_H$  and  $M$  are calculated for each time step.  $F_{H,max}$  and  $M_{max}$  are the maximum value of the respective time series. Eqs. (6.4) and (6.5)

As there is no time development in the RSA method both  $F_{X,max}$  and  $F_{Y,max}$  occur instantaneously. By looking at the results of the THA simulations in time it is observed that  $F_{X,max}$  and  $F_{Y,max}$  do not occur simultaneously, and therefore finding the maximum value of  $F_H$  in time should result in a lower value of  $F_{H,max}$ . Analogously the same is true for the moment  $M$  and  $M_{max}$ .

To assess the effect of time development on the magnitude of the action effects, the two methods of finding  $F_{H,max}$  and  $M_{max}$  are applied to the THA simulations for a fair comparison. This is done at the LowerGuide for the Fixed, Pinned, Spring5 and Spring15 soil structure condition for the FKS01 time history record.

#### Fixed connection

The results found in time are displayed in Figs. 7.31 and 7.33. The results found using the maximum X and Y components are displayed in Figs. 7.32 and 7.34.

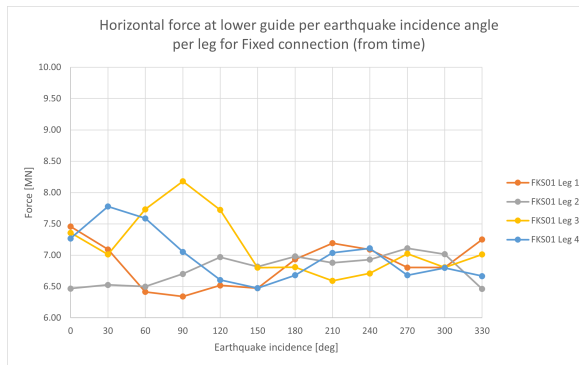


**Figure 7.31:** Max  $F_{H,LG}$  per leg per FKS01 EQ incidence angle found in time for the Fixed connection

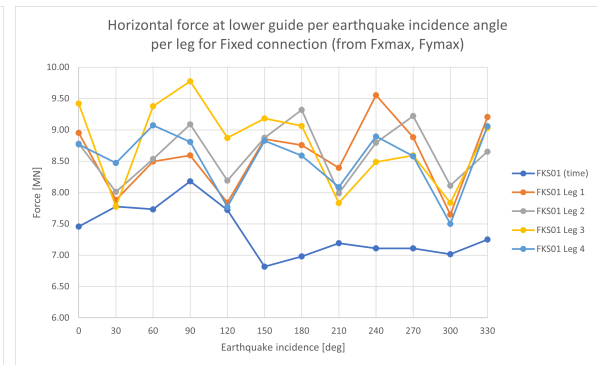


**Figure 7.32:** Max  $F_{H,LG}$  per leg per FKS01 EQ incidence angle found from  $F_{X,max}$ ,  $F_{Y,max}$  for the Fixed connection

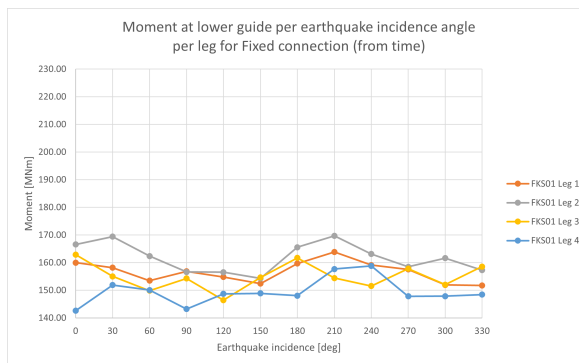


**Figure 7.33:** Max  $M_{LG}$  per leg per FKS01 EQ incidence angle found in time for the Fixed connection

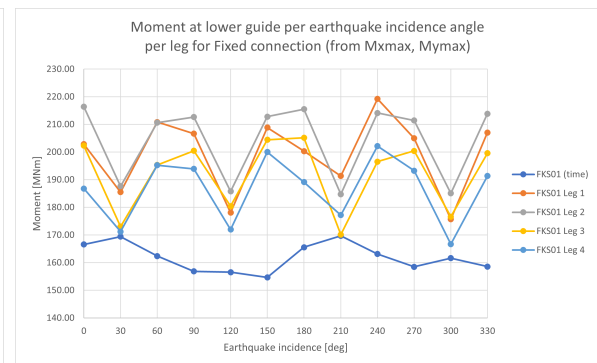


**Figure 7.34:** Max  $M_{LG}$  per leg per FKS01 EQ incidence angle found from  $M_{X,max}$ ,  $M_{Y,max}$  for the Fixed connection

### Pinned connection

The results found in time are displayed in Figs. 7.35 and 7.37. The results found using the maximum X and Y components are displayed in Figs. 7.36 and 7.38.

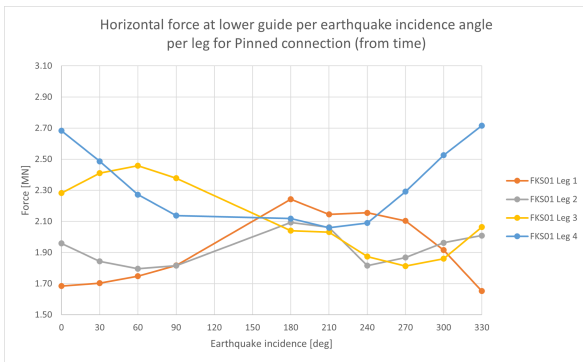


**Figure 7.35:**  $Max F_{H,LG}$  per leg per FKS01 EQ incidence angle found in time for the Pinned connection

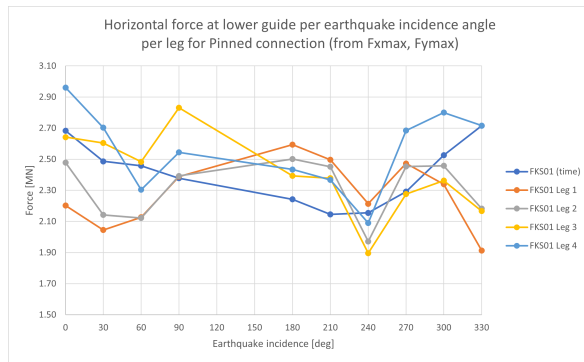


**Figure 7.36:**  $Max F_{H,LG}$  per leg per FKS01 EQ incidence angle found from  $F_{X,max}$ ,  $F_{Y,max}$  for the Pinned connection

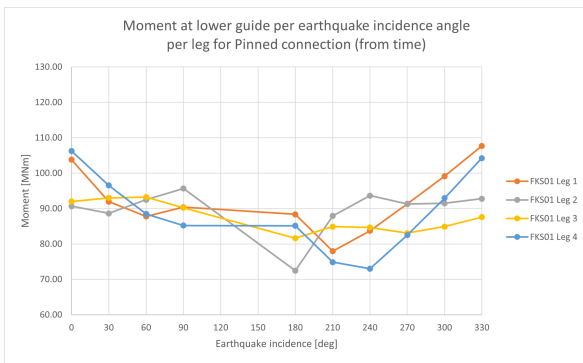


**Figure 7.37:**  $Max M_{LG}$  per leg per FKS01 EQ incidence angle found in time for the Pinned connection

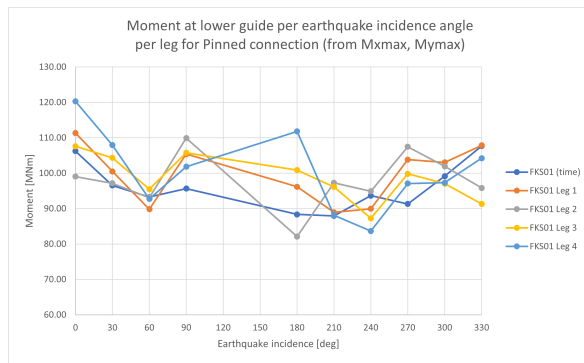


**Figure 7.38:**  $Max M_{LG}$  per leg per FKS01 EQ incidence angle found from  $M_{X,max}$ ,  $M_{Y,max}$  for the Pinned connection

### Spring5 connection

The results found in time are displayed in Figs. 7.39 and 7.41. The results found using the maximum X and Y components are displayed in Figs. 7.40 and 7.42.

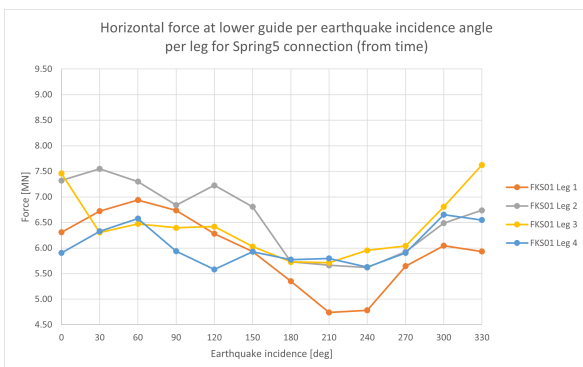


**Figure 7.39:**  $Max F_{H,LG}$  per leg per FKS01 EQ incidence angle found in time for the Spring5 connection

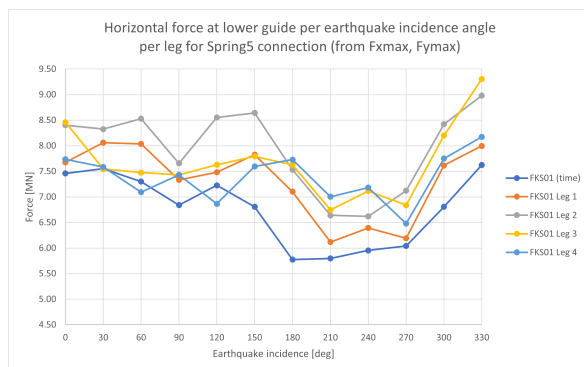


**Figure 7.40:**  $Max F_{H,LG}$  per leg per FKS01 EQ incidence angle found from  $F_{X,max}$ ,  $F_{Y,max}$  for the Spring5 connection

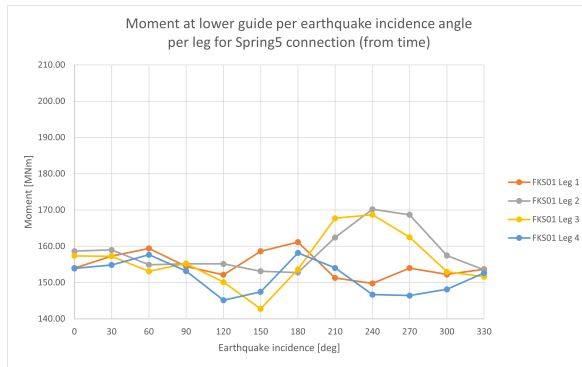


**Figure 7.41:** *Max  $M_{LG}$  per leg per FKS01 EQ incidence angle found in time for the Spring5 connection*

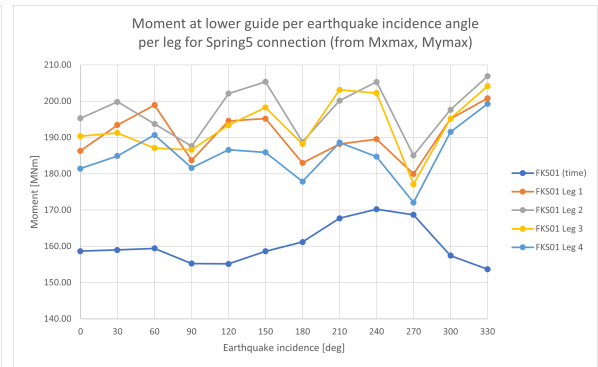


**Figure 7.42:** *Max  $M_{LG}$  per leg per FKS01 EQ incidence angle found from  $M_{X,max}$ ,  $M_{Y,max}$  for the Spring5 connection*

### Spring15 connection

The results found in time are displayed in Figs. 7.43 and 7.45. The results found using the maximum X and Y components are displayed in Figs. 7.44 and 7.46.

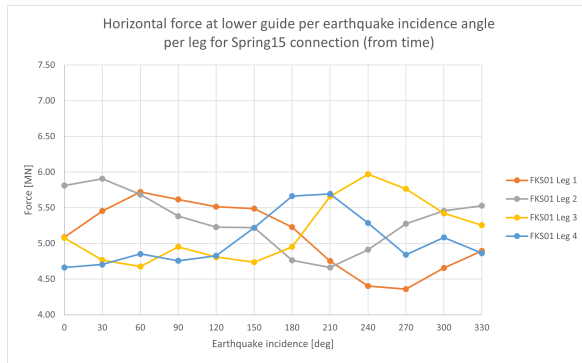


**Figure 7.43:** *Max  $F_{H,LG}$  per leg per FKS01 EQ incidence angle found in time for the Spring15 connection*

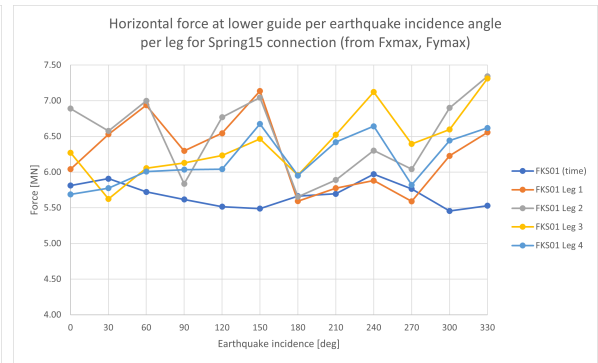


**Figure 7.44:** *Max  $F_{H,LG}$  per leg per FKS01 EQ incidence angle found from  $F_{X,max}$ ,  $F_{Y,max}$  for the Spring15 connection*

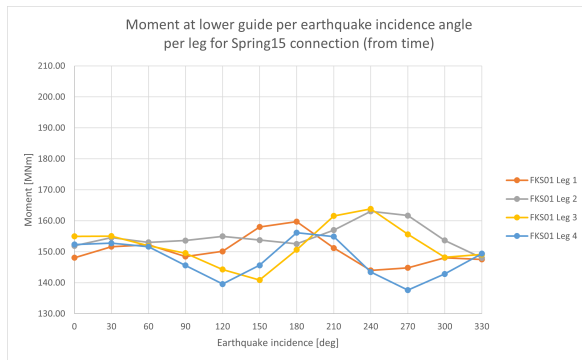


**Figure 7.45:** *Max  $M_{LG}$  per leg per FKS01 EQ incidence angle found in time for the Spring15 connection*

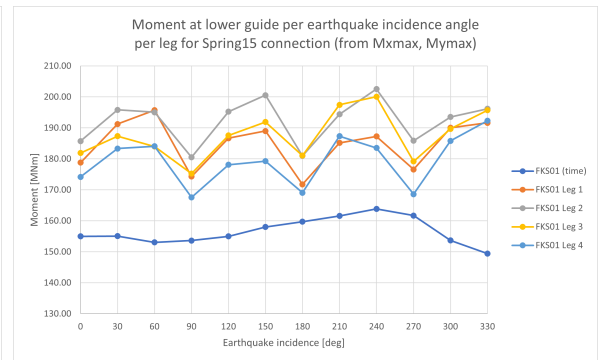


**Figure 7.46:** *Max  $M_{LG}$  per leg per FKS01 EQ incidence angle found from  $M_{X,max}$ ,  $M_{Y,max}$  for the Spring15 connection*

## 7.4. Remarks on simulations

As discussed in Section 6.5 the solution algorithm used for the THA simulations is the Modified Newton method. When this method does not converge to a solution an alternative solution algorithm is used. The model is programmed to consequently use the Newton with Initial Tangent method followed by the Broyden method. For the following cases one of the alternate solution methods was used:

- Fixed RSN73 dir 4,11
- Spring5 RSN73 dir 2,4,5
- Spring15 RSN73 dir 2
- Spring15ISO RSN73 dir 2

Not all simulations were able to converge to a solution. Of the ten cases nine belonged to the Pinned soil-structure connection type. For the following cases no solution was found:

- Pinned FKS01 dir 5,6
- Pinned RSN33 dir 6
- Pinned RSN57 dir 7,8,9
- Pinned RSN73 dir 1,5,7
- Spring15 RSN33 dir 2

When comparing the resulting forces and moments of the different soil-structure connection types in Section 7.1 it can be seen that the Pinned connection generally has the lowest action effects. This coincides with ISO 19905 which states that "A pinned spudcan model, in general, produces an unconservative representation of the earthquake demand on the jack-up" [6]. Looking at the Spring15 simulation results in Section 7.1, the RSN33 time history record produces the lowest action effects. As the cases that did not converge to a solution belonged to those that generally produced the lowest action effects no further analysis was performed.



# 8

## Discussion

This chapter discusses the results and findings from the previous chapters and relates them to the objectives of this research. Section 8.1 discusses the choice of structural model and the influence on the response of the jack-up and the resulting action effects. Section 8.2 discusses the bias caused by using the DRS for time history record selection and scaling, and the importance of correct period range for spectrum matching. The limitations of the SSI performed in this research are discussed in Section 8.3. The choice of soil-structure connection in the simulations and the use of the SRSS rule in RSA are discussed in Section 8.4. The simulation results, the effects of the number of THR and angle of incidence, and the effect of time development are discussed in Section 8.5.

### 8.1. Structural model

The jack-up used for the development and benchmarking of the new procedure is based on the GJ3750-C. It consists of a hull, four tubular legs, and four continuous jacking systems; the general configuration and dimensions were discussed in Section 3.1. A lumped parameter beam model of the jack-up, consisting of nodes and elements, was created for use in the simulation programs Minifem and OpenSees. The choices made in the structural model influence the response of the jack-up and the resulting action effects. This section discusses the hull model and the leg model including the leg-hull interface.

#### 8.1.1. Hull model

The hull model in this research was taken directly from the model used in the existing ELE-screening RSA procedure, and is depicted in Fig. 8.1. As discussed in Section 3.2 it consists of four edge beams connected by the hull corner nodes and four cross beams connecting the corner nodes to a hull centre node. The location of the hull corner nodes coincide with the centre of the legs in the jack-houses. 50% of the elevated mass is concentrated in the centre node while the remaining mass is distributed over the four corner nodes. The required eccentricity of the elevated weight is modelled by distributing the mass of the four corner nodes to produce an equivalent moment. The edge beams are modelled to represent the structural properties of the hull. The sole function of the cross beams is to connect the hull centre node to the hull and should not affect the stiffness of the hull. This is done by applying releases at the hull centre node.

This bar stool model is adequate for static analyses, however in dynamic analysis it does not represent reality well. This is evident from the mode shapes. Figure 8.2 shows the fourth eigenmode of the jack-up with spring soil-structure connection as vertical relative displacement of the centre node. Effectively the centre node is acting as a tuned mass damper system causing an inaccuracy in the model. This vertical resonance was observed in all time domain simulations in OpenSees. With 50% of the hull weight placed at the hull centre node there is a high mass participation in this mode. Coupled with the lowest damping value in the 4th mode, due to the manner in which Rayleigh damping is implemented (discussed in Section 3.3), this has a significant impact on the motion of the structure and the resulting action effects found in the simulation results.

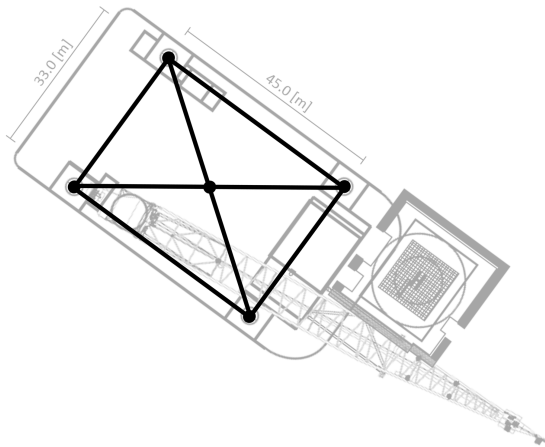


Figure 8.1: Structural model of the hull

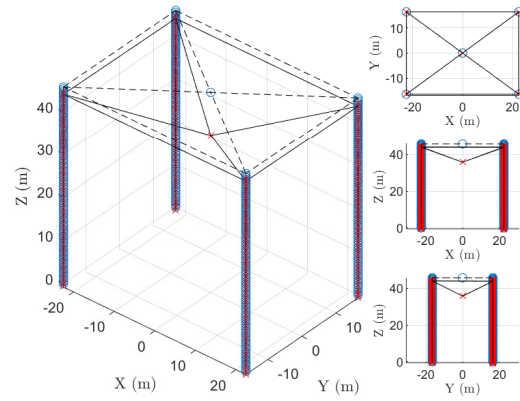


Figure 8.2: Mode 4 of spring case

This arrangement of nodes and elements also does not allow for effects such as hull sagging and the influence of this phenomenon on the legs to be captured by the model. The effects of modelling the structure in this manner were observed early on and discussed; the decision was made that this fell outside the scope of this research and would be picked up in a different study by Linthorst[22]. Since the same model is used in the RSA and THA simulations it is assumed this should allow for a fair comparison between the two methods. Caution should be used when making any statements regarding the absolute values of the (vertical) forces and moments, and it is advised to improve the structural model before use in practical applications.

The new structural model should allow for a more realistic weight distribution and a better representation of the internal load transfer. It is assumed that by following the major structural components of the hull a more realistic internal load transfer is achieved. The basis of two possible models are presented in Figs. 8.3 and 8.4. Nodes can be added along the horizontal and vertical elements of both models in order to create a representative mass distribution. An optimum would need to be found between the number of nodes and elements and the resulting increase in compute time. The model in Fig. 8.3 is a simple extension of the barstool model that would allow for a better mass distribution to more accurately represent the physical structure, however it does not follow the major structural components of the hull. The model in Fig. 8.4 would allow a better representation of the internal load transfer because it includes the jack-houses and major bulkheads in the structural model. A similar model is used by Linthorst[22] in his study on seismic analysis of cranes on jack-ups which uses the new ELE-screening THA procedure and the OpenSees tool developed in this research.

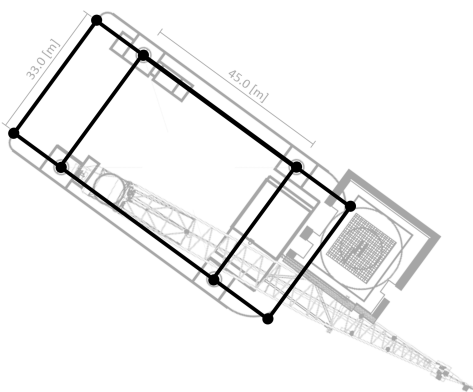


Figure 8.3: Basis for new structural model 1

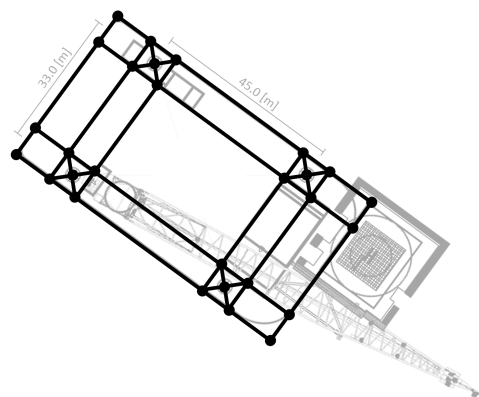


Figure 8.4: Basis for new structural model 2

### 8.1.2. Leg model

The legs of the jack-up are modeled as equivalent beams with corresponding bending stiffness and moment of inertia properties. The mass of the legs and the spudcan, including added mass, are lumped into the

various leg nodes. How the bending stiffness, moment of inertia, and mass are calculated for the different parts of the leg is described in detail in Section 3.2.

Simplifications were made in the structural model of the legs to ensure a fair comparison between the results of the RSA and THA methods. Due to a software limitation in the program used for the RSA simulations, the part of the leg above the hull can not be included in the structural model of the legs. As a result the mass of the leg above the hull is lumped to the highest node of the leg which is located on hull level at the lower guide. The overall leg length is 86[m], and in the chosen operational condition the length of the leg above the hull is 40,3[m]. This means that almost half the structural mass of the leg is lumped to the leg-hull node.

Not modeling the legs above the hull and lumping the mass of the legs above the hull to the node at the lower guide is not an accurate representation of reality. This approximation has an influence on the dynamic behaviour of the structure. The mode shapes and mass participation per mode of the jack-up are different. As the simulations run in this research were focussed on the difference between the RSA and THA method of analysis for earthquake response of the structure, and the same model is used for both, the effect of modelling the legs above the hull was not researched further. The THA tool built in OpenSees is designed to be able to model the legs above the hull and it is recommended this is done in practical applications for an accurate representation of the jack-up. Modelling the legs above the hull would also allow for a more detailed structural model of the leg-hull interface connection to be used. The existing structural model for the leg and leg-hull interface is depicted in Fig. 8.5. A more detailed model of the leg and leg-hull interface connection that incorporates the jack-house in the structural model is depicted in Fig. 8.6. This is an extension of the new structural model proposed in Fig. 8.4.

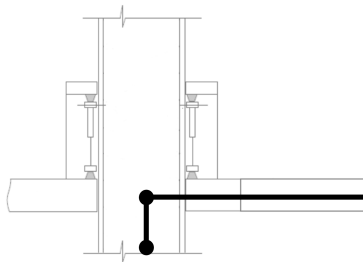


**Figure 8.5:** *The existing structural model of the leg and leg-hull interface at the jack-house*

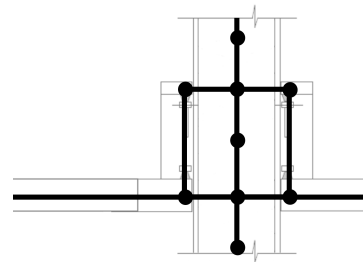


**Figure 8.6:** *Proposed new structural model of the leg and leg-hull interface incorporating the jack-house*

## 8.2. Ground motions

The input ground motions of the THA simulations are spectrum matched acceleration time history records. This section discusses the effects of using the DRS for time history record selection and modification, and the importance of a correct period range for spectrum matching.

### 8.2.1. THR selection and spectrum matching bias

ISO requires that earthquake time history records shall be selected such that they represent the dominating ELE events[2]. As discussed in Section 4.4 initial selection is based on an approximate match to the earthquake magnitude and the spectral shape. The most important factor in selecting ground motions for scaling to a target spectrum is spectral shape over the period range of interest[14]. The response spectrum used for this research is the ISO design response spectrum.

The DRS is generated with data from a generic PGA map that provides seismic information in terms of expected peak ground acceleration. Other characteristics of the ground motion such as strong motion shaking and energy content in different frequencies are lost when using PGA maps. Directivity effects can be captured, provided that the spectra generated in different directions are distinctly different. This is however not reflected in current seismic design codes including ISO. Seismic analysis is site-specific while the DRS is not; it is generic and does not represent the dominating ELE events. By using the DRS to select the THR results in a bias. It was found that in literature often the same earthquake time history records were used and the assumption is this is because they fit a particular spectrum well. Spectrum matching a THR results in a synthetic

time signal. By spectrum matching to the DRS the THR will reflect the properties of the DRS. The horizontal THR pairs used in this research are distinctly different, however they are spectrum matched to the same DRS. At this point it is not known how this affects the directivity effects or the phase information of the time signals.

This research was focussed on developing a new ELE screening procedure using THA and benchmarking it against the existing procedure that uses RSA. In the RSA method the ISO DRS is used, hence for a fair comparison of the two methods the decision was made to use the DRS for THR selection and scaling despite the limitations that come with its use. When applying the ELE-THA method in practice the choice can be made to use a different response spectrum depending on the situation and local requirements. NIST suggests constructing a site-specific spectrum from a probabilistic seismic hazard analysis for the location[14]. This is already employed in the non-linear ALE THA procedure described in Section 2.2.

### 8.2.2. Period range for spectrum matching

When spectrum matching the acceleration time history records to the design response spectrum it is important to choose a suitable period range over which spectrum matching takes place. In ASCE 7-16 this period range is defined as  $0.8T_{lower}$  to  $1.2T_{upper}$ ; Eurocode 8 prescribes a period range for spectrum matching in a similar manner. ASCE 7-16 and Eurocode 8 are focused on buildings which generally have a shorter fundamental period compared to jack-ups. Using the ASCE 7-16 period range for structures with a long fundamental period, such as the jack-up with pinned soil-structure connection, results in a large period interval over which to match time history records to the design response spectrum. An inverse relationship was observed between period range and matching quality. Using the ASCE 7-16 period range for the pinned condition resulted in poorly matched records, and in some instances spectrum matching was not possible. It was therefore chosen to select a period range for spectrum matching that includes the fundamental period of the structure and ensures an acceptable matching quality. Instead of  $1.2T_{upper}$  this resulted in  $1.03T_{upper}$  for the pinned case and  $1.17T_{upper}$  for the fixed and spring case.

Note that, as described in Section 6.1, the pinned case is not an accurate representation of the physical condition and was chosen as an edge case for this research. For the Fixed and the Spring case, which more accurately describe the physical condition, the ASCE 7-16 period range can be applied for spectrum matching without issue.

When the fundamental period of the structural model is changed, for instance when taking different soil spring stiffnesses, it is important to ensure the input time traces are matched to the corresponding period range. During the initial testing phase of the new method, simulations were run in which time history records were spectrum matched over an incorrect period range. The resulting response spectrum of the spectrum matched THR was significantly lower than the design response spectrum at the periods of the first two modes. It should also be noted that the first two modes of the structure constituted approximately 70% of the mass participation. The action effects found from the THA using these incorrectly matched time traces were unrealistically low. Incorrect matching of the time histories can result in an unsafe assessment of the structure.

### 8.3. Soil-structure interaction

In seismic design codes the seismic input is described as free-field motion at the ground surface. This is a simplification as the presence of a structure on the soil alters free-field ground motion directly beneath that structure; it creates an induced motion. The reaction of the soil also changes the vibration characteristics of the structure resting on top of it. In engineering practice this soil-structure interaction is often neglected due to: structural period elongation which moves the natural periods of the structure further from the energy containing periods of the ground motion, and extra damping caused by radiation of waves carrying energy away from the vibrating structure. An increased fundamental period and effective damping due to SSI lead to reduced forces in the structure. As discussed by Mylonakis and Gazetas these assumptions do not always hold true, in certain seismic and soil environments an increase in the fundamental natural period of a moderately flexible structure due to SSI may have a detrimental effect on the imposed seismic demand[23]. For completeness a soil model needs to be included in the structural model of the system being analysed, and soil-structure interaction needs to be included in the analysis. When this is not done an SSI analysis should be performed to demonstrate that the exclusion of SSI effects in the earthquake analysis does not result in an unsafe assessment of the structure

In Chapter 5 a soil-structure interaction analysis was performed on an equivalent single degree of freedom system which demonstrated the validity of the soil-structure interface model used in the new ELE-screening procedure. The analysis also demonstrated that the induced motion from soil-structure interaction is negligible for the cases considered and hence the free-field acceleration could be used.

The simulations were run for the site specific condition detailed in Section 4.1, a stiffer soil, and a softer soil by varying the dynamic shear modulus as shown in Table 5.1. The corresponding shear wave velocity determines the site class used to select the correction factors in the construction of the ISO DRS as described in Section 4.2. The soft soil condition has a shear wave velocity that is lower than the threshold value of the lowest site class E ( $120 \leq \bar{v}_s \leq 180 [m/s]$ ). Taking class E for the soft soil condition results in a significant change in  $C_v$ , the correction factor applied to the velocity part (longer periods) of the response spectrum. Analogously for the stiff soil condition there would be a decrease in  $C_v$ , and also a slight increase in  $C_a$ , the correction factor applied to the acceleration part (shorter periods) of the response spectrum. With a different DRS there will also be different spectrum matched time history records. This has however not been applied in the SSI analysis performed in this research. The input time trace was kept the same for all three cases considered. Note that for the soft soil condition the increase in the long period part of the response spectrum is in the range of the fundamental period of the structure. Most of the mass participation is also in the high period range of the response spectrum.

The type of foundation and how it is modelled strongly influences the resulting soil-structure response. The impedance of foundations with irregular geometries and complicated soil properties generally have a stronger frequency dependence than those that are circular or square on a homogeneous half space [24]. The cross-coupling soil impedance  $G_{xr}$  is almost zero for shallow rigid foundations resting on the surface of the soil, and non-zero when the foundation is partly or fully embedded into the soil. The foundation of the jack-up was modelled as flat circular plates resting on top of a homogenous half space. It was therefore assumed that there is no cross-coupling soil impedance, and hence the dynamic stiffness matrix is diagonal. This is an accurate representation for the jack-up and operational condition considered in this research, however in practice the spudcans of the jack-up are generally embedded in the soil as described in Section 3.1. In the operational condition the support point of the jack-up is located at 0.8 [m] above the spudcan tip. This is the maximum bearing area of the spudcan. The spudcan tip is embedded 3 [m] into the soil, so that the support point is located 2.2 [m] below seabed level. The level of penetration and backfill of the spudcan will influence the cross-coupling soil impedance.

It should be noted that the simulations were performed for a specific jack-up with a particular foundation type. For different jack-ups, or even similar jack-ups with different foundations or in different soil conditions a soil-structure interaction analysis should be performed with the appropriate soil and structure model.

The purpose of this type of jack-ups is wind turbine installation. The wind turbines have a higher exposure to earthquakes as they are located on site during their entire service life while the jack-up is only on location for installation in as short a time as possible. For water depths that fall within the operational envelope of the jack-up, wind turbines generally use a piled foundation type. As the pile is embedded in the soil these type of foundations have strong soil structure interaction. It is therefore reasonable to assume that a SSI analysis will have been performed by the owner/operator of the offshore wind farm. It is advised to establish engineering resource sharing, such as detailed soil models, as part of the work package to facilitate operational safety.

## 8.4. Simulation cases

Simulations were run to assess the performance of the new ELE-screening procedure. Details of these simulations are given in Chapter 6. This section discusses the choice of soil-structure connections used and the application of the SRSS rule in the RSA simulations.

### 8.4.1. Soil-structure connection

The jack-up is modelled with circular footings resting on a homogenous half-space. The interface of the spudcan with the underlying soil is modelled with equivalent springs and dampers as discussed in Section 3.4. In the usual procedure for SSA of a jack-up a representative soil condition is taken from where the unit will operate. Simulations are run with these values for the soil-structure connection. Additional simulations are run with higher and lower fixity values.

For the simulations in this research the Spring soil-structure connection was used to represent the in-situ soil condition. The Fixed and Pinned soil-structure connection were selected to represent an extreme low and high fixity condition respectively, with the intention of creating an envelope. It is recognised now that the Pinned connection is not the most accurate representation of a low fixity condition as it does not allow for translational movement. To have a true low fixity condition there should be no rotational resistance and low resistance in displacement directions. This can be achieved with springs of different stiffness for the horizontal and vertical translation directions. Due to the shape of the spudcan there will always be some degree of resistance/fixity. In the case where there is no or very low rotational resistance the soil is also expected to have low bearing capacity. In such soils the linear soil approximations would not be valid due to different soil-structure interaction. The Fixed connection is an accurate representation of an extreme high fixity condition, however it will very rarely occur with a spudcan foundation. Jack-ups with a caisson or suction bucket style foundations have a high degree of fixity and can be modelled with a fixed connection. Those types of foundations have different SSI and the assumptions and approximations made in this research do not hold.

The Pinned low fixity condition and the Fixed high fixity condition are not representative for the structure under consideration. When performing SSA of a jack-up with spudcans the soil-structure connection should be modelled with the use of springs of different stiffnesses to represent the in situ soil conditions and higher/lower fixity conditions.

### 8.4.2. SRSS rule in RSA

In the RSA simulation process in Minifem described in Section 6.4 the individual responses per mode are statistically combined to obtain the most probable peak response using the modal combination rule *square-root-of-sum-squares* (SRSS). Eurocode 8 states that when two nodes have closely spaced natural periods the SRSS rule is unconservative and more accurate rules shall be applied[7]. Two natural periods,  $T_i$ ,  $T_j$ , may be considered as closely spaced natural periods if they satisfy the condition in Eq. (8.1).

$$\frac{0.1}{0.1 + \sqrt{\zeta_i \zeta_j}} \leq \rho_{ij} = T_i / T_j \leq 1 + 10\sqrt{\zeta_i \zeta_j} \quad (8.1)$$

Where  $\zeta_i$  and  $\zeta_j$  are the viscous damping ratios of modes  $i$  and  $j$  respectively. The natural periods and damping ratios of the fixed, pinned, and spring model are given in Tables 8.1 to 8.3 for the first 10 modes of the jack-up. Applying Eq. (8.1) to the data in these tables shows that all three models have closely spaced natural periods. This is most significant for modes 1 and 2 which constitute approximately half the total mass participation.

Using SRSS for modal combination in the RSA simulations in Minifem results in an unconservative assessment of the structure. Although this could be critical in practical applications of the RSA method it does not negatively influence the comparison of the two methods in this research. The action effects found using the RSA method with SRSS for a model with closely spaced natural periods are smaller than if an appropriate modal combination rule were used. As a result the difference in magnitude of action effect between the RSA method and THA method found in this research is larger in reality than what is found from the simulation results. The performance gain of the new ELE-screening method using THA is larger than demonstrated in this research. When performing RSA simulations for a structure with closely spaced natural periods it is im-

**Table 8.1:** Natural periods and damping ratios of the Fixed model for the first 10 modes

mode	$T$	$\zeta$
[-]	[s]	[-]
1	2.56	0.050
2	2.55	0.050
3	1.67	0.037
4	0.74	0.029
5	0.27	0.048
6	0.27	0.049
7	0.27	0.049
8	0.26	0.050
9	0.26	0.050
10	0.26	0.050

**Table 8.2:** Natural periods and damping ratios of the Pinned model for the first 10 modes

mode	$T$	$\zeta$
[-]	[s]	[-]
1	5.35	0.050
2	5.30	0.050
3	3.91	0.039
4	0.74	0.030
5	0.40	0.047
6	0.40	0.048
7	0.38	0.049
8	0.38	0.049
9	0.38	0.049
10	0.37	0.050

**Table 8.3:** Natural periods and damping ratios of the Spring15 model for the first 10 modes

mode	$T$	$\zeta$
[-]	[s]	[-]
1	3.42	0.050
2	3.40	0.050
3	2.16	0.036
4	0.78	0.031
5	0.37	0.048
6	0.36	0.049
7	0.35	0.049
8	0.35	0.049
9	0.35	0.050
10	0.35	0.050

portant to use an appropriate modal combination rule such as *complete quadratic combination* (CQC). Use of SRSS for modal combination needs to be clarified in the ISO codes and guidance given on alternate methods such as CQC.

Note that according to Chopra the SRSS and CQC methods would be most accurate for ground motions with wide-banded frequencies and long duration of strong ground motions several times longer than the natural period of structures not having too light damping ( $>0.5\%$ ). If the ground motions are of short duration impulsive or contain many cycles of essentially harmonic excitations, the two modal combination methods will become less accurate [11].

## 8.5. Simulation results

This section examines and discusses the simulation results presented in Chapter 7. The global maximum action effects from the RSA and THA simulations are analyzed and compared for the different simulation cases. The impact of the number of time history records and the earthquake angle of incidence on the results are discussed, and the advantage of using THA over RSA for seismic analysis are demonstrated by examining the effects of time development on the resulting forces and moments.

### 8.5.1. Global maximum action effects

The quantities used for unity checks are the global maximum action effects found from the simulations. Table 8.4 provides an overview of the global maximum action effects of the Fixed, Pinned, Spring5, Spring15, and Spring15ISO simulation results in Section 7.1.  $THA_{max}$  is the maximum value found from all THA simulations,  $THA_{avg}$  is the average of the global maximum value found from each of the four time history records,  $\Delta_{max}$  is the difference between RSA and  $THA_{max}$ , and  $\Delta_{avg}$  is the difference between RSA and  $THA_{avg}$ .

**Table 8.4:** Global maximum action effects from the Fixed, Pinned, Spring5, Spring15, and Spring15ISO simulations

FIXED	RSA	FKS01	RSN33	RSN57	RSN73	$THA_{max}$	$THA_{avg}$	$\Delta_{max}$	$\Delta_{avg}$	
$F_{H,LG}$	10.87	8.18	7.38	11.00	8.54	11.00	8.77	-0.13	2.10	MN
$V_{LG}$	50.87	48.15	44.21	45.52	42.89	48.15	45.19	2.72	5.68	MN
$M_{LG}$	222.15	169.69	168.19	228.44	183.32	228.44	187.41	-6.28	34.75	MNm
$F_{H,FT}$	11.91	9.73	10.10	11.49	9.70	11.49	10.25	0.42	1.66	MN
$V_{FT}$	53.46	51.18	47.41	48.24	46.11	51.18	48.23	2.28	5.23	MN
$M_{FT}$	316.76	239.43	231.23	312.35	258.10	312.35	260.28	4.41	56.48	MNm
PINNED	RSA	FKS01	RSN33	RSN57	RSN73	$THA_{max}$	$THA_{avg}$	$\Delta_{max}$	$\Delta_{avg}$	
$F_{H,LG}$	4.26	2.72	2.67	1.83	7.01	7.01	3.56	-2.75	0.70	MN
$V_{LG}$	48.99	43.71	44.65	41.44	45.80	45.80	43.90	3.19	5.09	MN
$M_{LG}$	204.62	107.70	91.55	81.66	329.27	329.27	152.54	-124.65	52.07	MNm
$F_{H,FT}$	4.60	3.01	3.22	2.03	7.66	7.66	3.98	-3.06	0.62	MN
$V_{FT}$	51.58	45.87	50.95	43.97	47.82	50.95	47.15	0.63	4.43	MN
$M_{FT}$	0.00	0.01	0.06	0.01	0.02	0.06	0.02	-0.06	-0.02	MNm
SPRING5	RSA	FKS01	RSN33	RSN57	RSN73	$THA_{max}$	$THA_{avg}$	$\Delta_{max}$	$\Delta_{avg}$	
$F_{H,LG}$	8.45	7.62	7.03	7.44	8.10	8.10	7.55	0.34	0.90	MN
$V_{LG}$	50.93	58.17	50.03	51.90	49.63	58.17	52.43	-7.24	-1.50	MN
$M_{LG}$	226.25	170.20	168.34	202.10	212.00	212.00	188.16	14.25	38.10	MNm
$F_{H,FT}$	9.47	8.45	8.41	9.82	10.52	10.52	9.30	-1.05	0.17	MN
$V_{FT}$	54.77	62.49	55.73	55.37	54.96	62.49	57.14	-7.72	-2.37	MN
$M_{FT}$	193.38	141.51	146.72	165.39	183.78	183.78	159.35	9.60	34.03	MNm
SPRING15	RSA	FKS01	RSN33	RSN57	RSN73	$THA_{max}$	$THA_{avg}$	$\Delta_{max}$	$\Delta_{avg}$	
$F_{H,LG}$	8.20	5.97	5.50	6.87	6.62	6.87	6.24	1.33	1.96	MN
$V_{LG}$	47.28	48.67	40.02	47.98	40.86	48.67	44.38	-1.39	2.90	MN
$M_{LG}$	225.42	163.88	157.22	194.41	207.06	207.06	180.64	18.36	44.78	MNm
$F_{H,FT}$	9.19	7.41	6.18	8.84	7.49	8.84	7.48	0.35	1.71	MN
$V_{FT}$	50.70	51.11	42.38	51.07	44.73	51.11	47.32	-0.41	3.38	MN
$M_{FT}$	193.03	138.09	139.04	161.64	182.23	182.23	155.25	10.79	37.78	MNm
SPRING15ISO	RSA	FKS01	RSN33	RSN57	RSN73	$THA_{max}$	$THA_{avg}$	$\Delta_{max}$	$\Delta_{avg}$	
$F_{H,LG}$	8.20	5.92	5.49	6.52	6.63	6.63	6.14	1.57	2.06	MN
$V_{LG}$	47.28	43.60	39.07	42.30	37.14	43.60	40.53	3.68	6.75	MN
$M_{LG}$	225.42	164.12	154.86	194.40	207.16	207.16	180.14	18.26	45.28	MNm
$F_{H,FT}$	9.19	6.95	6.12	8.08	7.50	8.08	7.16	1.11	2.03	MN
$V_{FT}$	50.70	46.31	42.53	45.02	40.52	46.31	43.60	4.39	7.10	MN
$M_{FT}$	193.03	138.68	136.79	162.31	182.32	182.32	155.03	10.71	38.00	MNm

### Spring15

As detailed in Section 6.1 the Spring15 simulation best describes the jack-up and representative soil condition under consideration. The results in Figs. 7.19 to 7.24 from Section 7.1 and the data in Table 8.4 show that the action effects from time history analysis are generally lower than those from response spectrum analysis for the Spring15 case. This performance improvement is mainly observed for the shear force  $F_H$  and the moment  $M$  at both the lower guide and footing, and is in the order of 10 to 20 percent. Figs. 8.7 and 8.8 show that the normal force  $V$  found from THA is smaller than from RSA for 69 percent of the Spring15 simulations. The expectation was that the results would be fairly similar for both methods. On average there is approximately a seven percent performance improvement for  $V$  when using the new procedure with THA. Due to the structural model being used this result may possibly not accurately represent reality. As detailed in Section 8.1 the bar stool model exhibits vertical oscillation of the hull center node which can impact the motion of the structure and the resulting action effects. The results for  $V$  need to be verified with simulations using a more accurate structural model of the jack-up. No absolute conclusions can be made about  $V$  based on the simulation results, however they do allow relative effects of parameters on  $V$  to be examined.

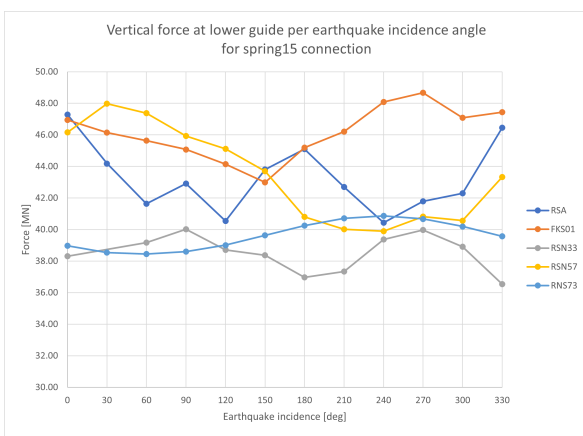


Figure 8.7: Max normal force  $V_{LG}$  at the lower guide per EQ incidence angle for the Spring15 connection

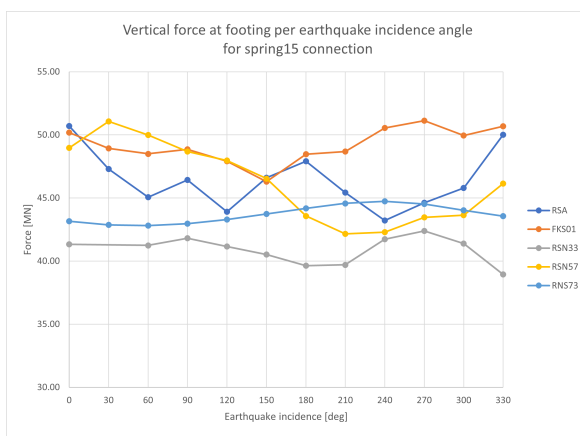


Figure 8.8: Max normal force  $V_{FT}$  at the footing per EQ incidence angle for the Spring15 connection

### Fixed, Pinned, Spring5

The Fixed, Pinned, and Spring5 cases have the same level of damping allowing a one to one comparison. The results in Table 8.4 show that a stiffer soil-structure connection results in higher action effects for  $F_H$  and  $M$ . This is not true for  $V$  as the Spring5 results are larger than the Fixed and Pinned results. This is due to the Spring5 case allowing translational displacement while the Fixed and Pinned cases do not. It is also assumed that the mode4 oscillation causes a resonance with the Spring5 soil-structure connection resulting in higher forces. The THA results of the Fixed, Pinned, and Spring5 cases are generally smaller than the RSA results. The exception is  $V$  in the Spring5 case where the results from THA are larger than from RSA. This is caused by the mode4 oscillation combined with the Rayleigh damping implementation, explained in Section 3.3, in which mode4 has a lower damping ratio. This effect will be negated by using the updated structural model from Section 8.1. The Pinned results in Table 8.4 show that the action effects  $F_H$  and  $M$  from both RSA and THA simulations are much smaller than the Fixed and Spring results. Compared to Spring15, which best represents the jack-up under consideration, the Pinned results are approximately 50 to 100 percent smaller. These findings are in accordance with ISO 19905 10.7 which states that a pinned spudcan model, in general, produces an unconservative representation of the earthquake demand on the jack-up[6]. Conversely the Fixed results for  $F_H$  and  $M$  are approximately 30 to 100 percent larger compared to Spring15. It should be noted here that as discussed in Section 8.4 the Fixed and Pinned condition are not representative for the structure under consideration and these type of foundations have different SSI. They do however clearly demonstrate the effects of a higher and lower fixity condition.

## Spring15ISO

The Spring15ISO condition was included in the simulations to analyze the difference between using the ISO DRS and the Minifem DRS. Due to a limitation in the RSA software, the Minifem vertical DRS is constructed using a constant scale factor, as described in Section 4.3, and consequently is larger than the codes prescribe. The ISO vertical DRS is constructed using a period dependent scale factor. The Fixed, Pinned, Spring5, and Spring15 cases used the Minifem DRS in both the RSA and THA procedure, facilitating a fair comparison between the two methods.; while the Spring15ISO case used the ISO DRS in the THA procedure. Note that in the THA procedure the DRS is used for spectrum matching the time history records. Since the difference between the Spring15 and Spring15ISO results would only be caused by the different vertical DRS used, the expectation was that  $F_H$  and  $M$  would be very similar, while  $V$  was expected to be noticeably lower in Spring15ISO. As the RSA results of Spring15 and Spring15ISO are identical by definition, the easiest parameters to compare the two cases are the  $\Delta_{max}$  and  $\Delta_{avg}$  in Table 8.4. This shows that while  $F_H$  and  $M$  are similar, there is a notable difference in the results for  $V$  which conforms to the expectation. The foundation bearing capacity of a jack-up subject to an ELE event is assessed using  $V_{FT}$ . A decreasing value of  $V$  results in increased operability of the jack-up. It is recommended the RSA software is improved to use the correct vertical design response spectrum, constructed using a period dependent scale factor.

### 8.5.2. Number of THR

Earthquakes are stochastic phenomena which is why design codes prescribe a minimum amount of appropriately scaled time history records to be used in the analysis of a structure. Eurocode-8 requires three time history records to be used [7] while ISO requires four sets of time history records be used to capture the randomness in seismic motions [2].

This research follows the ISO framework and four distinct sets of time history records were used in the simulations. How they were selected is described in Section 4.4. If only three distinct sets of THR were used as prescribed by EC-8 there would be a significant difference in the results found for the Fixed and Pinned condition. For the Pinned connection this is clearly visualized in Figs. 8.9 and 8.10. If the RSN73 THR were omitted in the Pinned THA simulations, the difference between the RSA and THA results would be in the order of 100% for the shear force and bending moment in the legs.

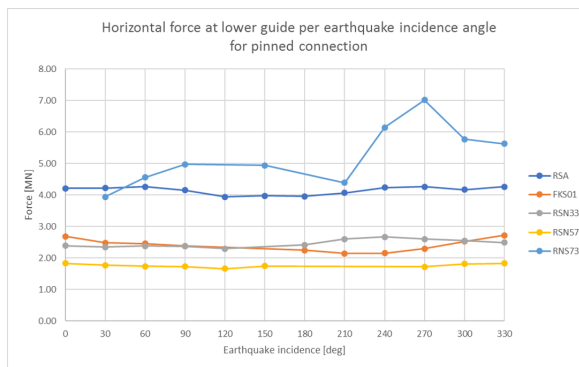


**Figure 8.9:** Max shear force  $F_{H,LG}$  at the lower guide per EQ incidence angle for the Pinned connection

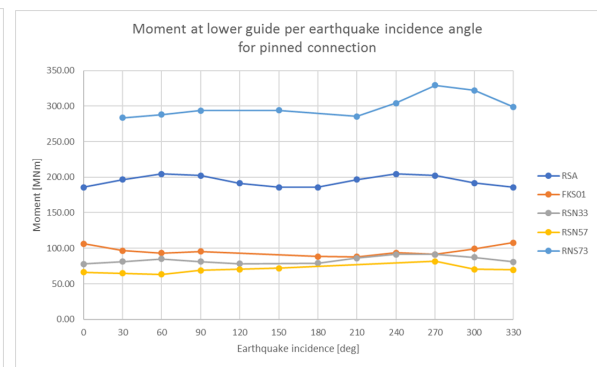


**Figure 8.10:** Max moment  $M_{LG}$  at the lower guide per EQ incidence angle for the Pinned connection

A similar situation can be seen in Figs. 8.11 and 8.12 for the Fixed connection. If the RSN57 THR were omitted in the Fixed THA simulations, the difference between the RSA and THA results would be in the order of 25% for the shear force and bending moments in the legs. As mentioned several times the Pinned and Fixed connection are not representative for the jack-up under consideration, however the Spring15 condition, which is representative, shows the same principle in Figs. 8.13 and 8.14. Omitting the RSN57 THR for the shear force in Fig. 8.13, or the RSN73 THR for the moment in Fig. 8.14 would lead to significant changes in the results.

While the time history records are all matched to the same Design Response Spectra, the simulation results in Section 7.1 clearly show that the respective resulting action effects of the four different THR vary in magnitude per case. For example RSN33 consistently results in the lowest values of  $F_H$  and  $M$ . It is also evident that some THR have larger resulting action effects in certain planes than others, or for different soil-structure

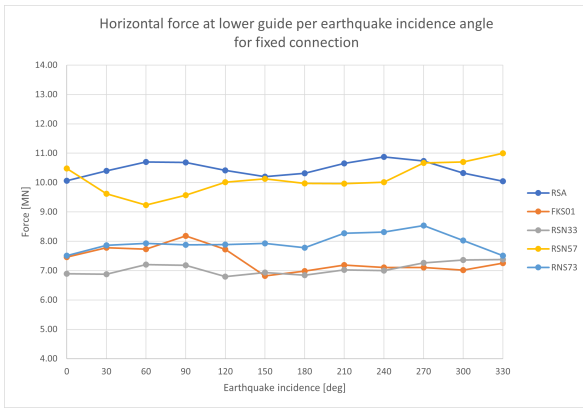


**Figure 8.11:** Max shear force  $F_{H,LG}$  at the lower guide per EQ incidence angle for the Fixed connection

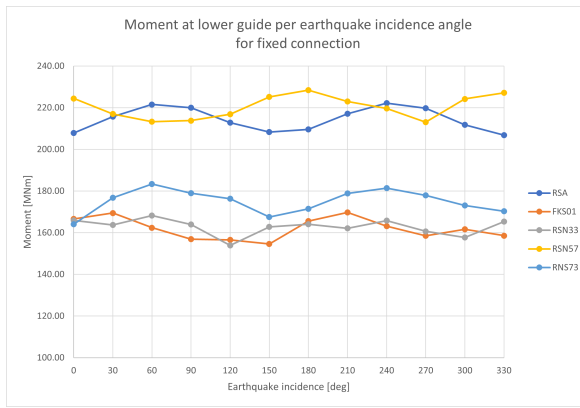


**Figure 8.12:** Max moment  $M_{LG}$  at the lower guide per EQ incidence angle for the Fixed connection

connection types. In most cases FKS01 results in the largest normal force in the leg  $V$ , while the shear force in the leg  $F_H$  and bending moment  $M$  are generally among the lowest. RSN57 results in the lowest values of  $F_H$  and  $M$  for the Pinned connection as seen in Figs. 8.9 and 8.10, while simultaneously resulting in the highest values of  $F_H$  and  $M$  for the Fixed connection as seen in Figs. 8.11 and 8.12. This emphasizes the need to use a sufficient number of THR to reduce statistical uncertainty in the analysis. As discussed in Section 4.4 adopting an ensemble of earthquakes reduces the effect of frequency content and of particular characteristics of the individual earthquake ground motions[4]. It is recommended to use more earthquake time history records to get a more realistic representation and ensure a safer assessment of the structure.

### 8.5.3. Earthquake angle of incidence

The four distinct sets of time history records used for the simulations were applied and rotated around the structural model in increments of 30 degrees, as described in Section 6.2, resulting in 12 simulation cases per THR, each being defined by their angle of incidence. This was done in accordance with literature suggesting that additional analyses need to be done to demonstrate suitable performance in weaker directions when a structural design is asymmetric in geometric configuration or directional capacity, and according to ISO for time history analyses this may require different orientations of the earthquake horizontal records to demonstrate performance requirements[2].

Rotating the time history records around the structural model as described results in 48 simulations from four earthquakes; without rotating there would only be four. Since the spectrum matched ground motions can be considered synthetic earthquakes, they can be manipulated to create other synthetic earthquakes. This creates more data points for the analysis of the structure.

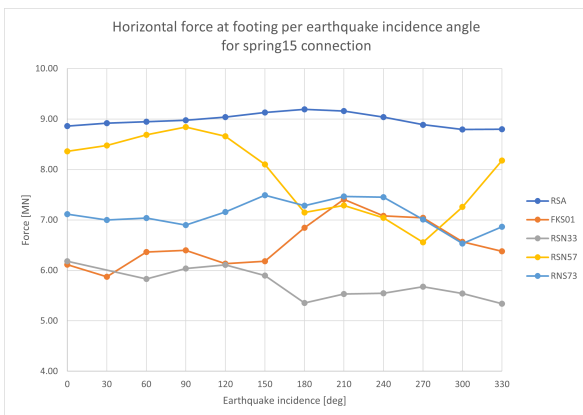


**Figure 8.13:** Max shear force  $F_{H,FT}$  at the footing per EQ incidence angle for the Spring15 connection

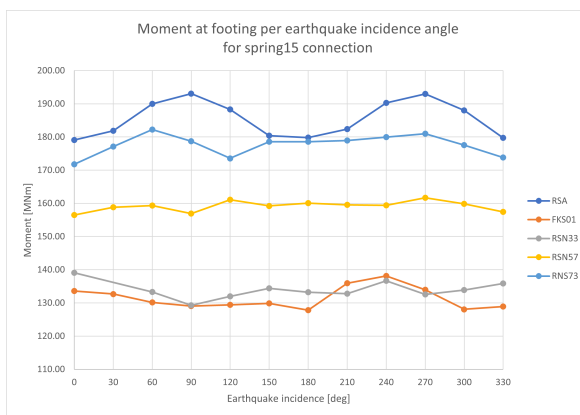


**Figure 8.14:** Max moment  $M_{FT}$  at the footing per EQ incidence angle for the Spring15 connection

The maximum shear force and the maximum moment for the Spring15 connection are shown in Figs. 8.13 and 8.14 respectively. It is evident from inspection that the maximum action effect caused by one THR does not necessarily occur at the same angle of incidence as for another THR, or even at the same angle of incidence as the RSA result. This can also be seen for the Fixed, Pinned, Spring5, and Spring15ISO conditions in Section 7.1. The graphs of the RSA simulation results in Section 7.1 suggest that there are predetermined critical angles of incidence. This term is used to denote the angle of incidence at which the maximum value of an action effect occurs for a given THA or RSA simulation. In Fig. 8.14 these can be seen at 90 and 270 degrees. The shape of the RSA graphs look very similar for the different soil-structure connections, especially for the maximum moments both at the lower guide and the footing. The THA results do not indicate a critical angle of incidence, nor are the graphs for the different soil structure connections similar in shape. It is recommended this observation is verified with a more representative structural model of the jack-up as described in Section 8.1. The relationship for non equivalent critical angles of incidence is given in Eq. (8.2) where  $\angle_i$  is the angle of incidence in degrees, eq1 represents one THR, and eq2 a different THR.

$$\angle_i(THA_{max}(eq_1)) \neq \angle_i(THA_{max}(eq_2)) \neq \angle_i(RSA_{max}) \quad (8.2)$$

If the THR were not rotated around the structure the results would only be at zero degrees angle of incidence. Inspecting the graphs it is clear that the average found from those 4 values,  $THA_{avg}(\angle_i = 0)$ , would be lower than  $THA_{avg}$  as calculated in Section 8.5. Similarly if all 48 data points would be used to calculate the average this would result in a lower value of  $THA_{avg}$ . The method of calculating  $THA_{avg}$  used in this report results in the most conservative interpretation of the average values of the simulations as used in Table 8.4.

Jack ups are movable structures and can be positioned in the most favorable orientation with regards to prevailing or expected wind and wave loading directions, and seabed topography. Similarly if the jack up would have predetermined critical angles of incidence it can be oriented such that these do not coincide with the direction to fault locations suspected of most probable earthquake origination; ensuring the most favorable orientation with regards to seismic loading.

#### 8.5.4. Time development THA

To assess the effect of time development on the magnitude of the action effects, the two methods of finding  $F_{H,max}$  and  $M_{max}$  were applied to the THA simulations. Section 6.3 describes how the first method finds these quantities in time while the second uses the maximum X and Y components. The results per leg are displayed in Section 7.3 for the Lower Guide, Fixed, Pinned, Spring5, and Spring15 soil-structure connection, and the FKS01 time history record. The Lower Guide was chosen since the results at the Footing for the Pinned connection are zero. Spring15ISO was omitted as the  $F_H$  and  $M$  results are near identical to Spring15. The simulation results confirm the expectation that the forces and moments found in time are lower than those found using the maximum X and Y components. When comparing the graphs of the Fixed, Pinned, Spring5, and Spring15 cases in Section 7.3 the results suggest that a stiffer soil-structure connection leads to a greater difference between the two methods. They also suggest that the difference is larger for  $M$  than for  $F_H$ .

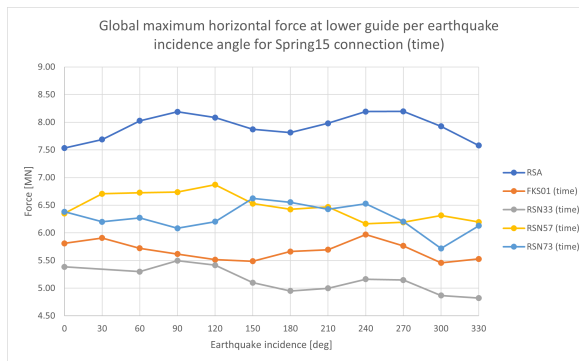


Figure 8.15: Max shear force  $F_{H,LG}$  at the lower guide per EQ incidence angle for the Spring15 connection (time)

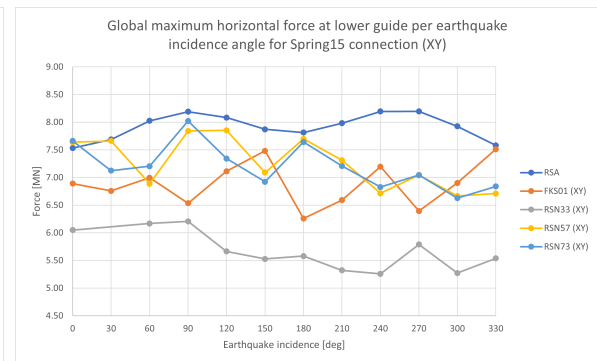
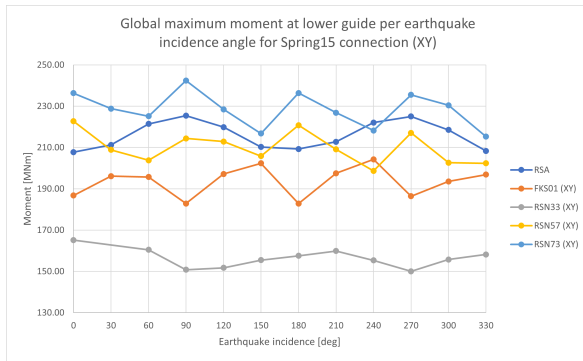
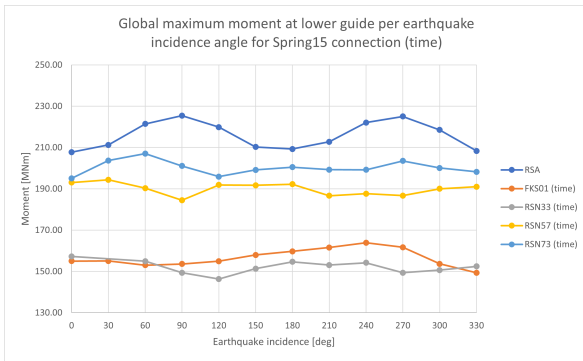


Figure 8.16: Max shear force  $F_{H,LG}$  at the lower guide per EQ incidence angle for the Spring15 connection (XY)

Figs. 8.15 and 8.17 show the Spring15 global maximum of  $F_H$  and  $M$  respectively from the RSA results and the THA results in time, denoted by the suffix (time), for all four time history records. Figs. 8.16 and 8.18 show the



**Figure 8.17:** Max moment  $M_{LG}$  at the lower guide per EQ incidence angle for the Spring15 connection (time) **Figure 8.18:** Max moment  $M_{LG}$  at the lower guide per EQ incidence angle for the Spring15 connection (XY)

Spring15 global maximum of  $F_H$  and  $M$  respectively from the RSA results and the THA results found from the maximum X and Y components, denoted by the suffix (XY), for all four time history records. Inspection of the graphs shows that the THA (XY) results for  $F_H$  and  $M$  are much closer to the RSA results, and in some cases they are larger. Fig. 8.18 shows that RSN73 (XY) has higher values of  $M_{LG}$  than RSA for all but one angle of incidence; RSN57 (XY) is larger for one angle of incidence. Excluding RSN33 (XY), the average of the THA (XY) results closely approximate the RSA results. This similarity was expected as both use SRSS of the maximum X and Y components to calculate the resultant  $F_H$  and  $M$ . Since similar input produces similar output it validates the THA model and simulation created in OpenSees. The difference in magnitude of action effect between RSA, THA (time), and THA (XY) is best demonstrated in Figs. 8.19 and 8.20, which show the FKS01 results from all three methods in one graph. This clearly demonstrates the effect of time development on the magnitude of the action effects  $F_H$  and  $M$  per individual earthquake time history record. Similar graphs can be found in Appendix F for all the THR used in this research. It should be noted that while most THR see a significant improvement, these gains are not universal. RSN33 sees a much smaller improvement relative to the other THR.

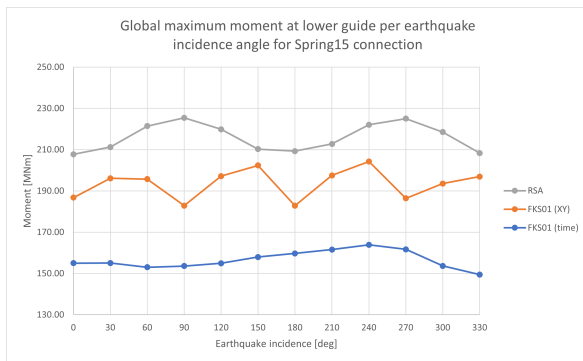
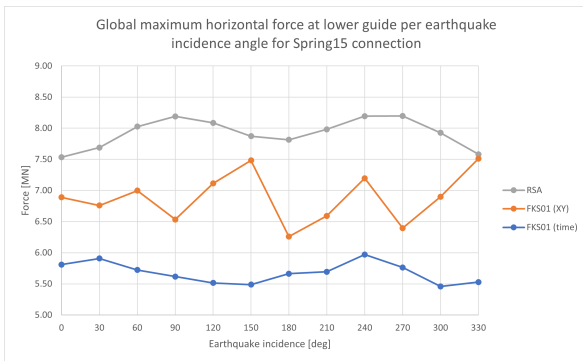


**Figure 8.19:** Max shear force  $F_{H,LG}$  at the lower guide per EQ incidence angle for the Spring15 connection; FKS01

**Figure 8.20:** Max moment  $M_{LG}$  at the lower guide per EQ incidence angle for the Spring15 connection; FKS01

Another advantage of using a model with time development is the ability to distinguish between short peak loads and sustained loads. Since the ELE-screening looks at the global maximum forces and moments for unity checks, the difference of short peak and sustained loading was not researched further. When expanding the model for non-linear time-history analysis this becomes more relevant.



# 9

## Conclusion and Recommendations

The aim of this research was to improve the accuracy of earthquake screening for OWTI jack-ups in order to increase their geographic operability. The objectives that were set to achieve this aim consisted of the development of a new earthquake screening procedure, building a tool to perform this procedure, developing procedures and tools for time history record selection and modification, and benchmarking the new screening procedure against the existing one. Several research questions were formulated in order to evaluate whether the objectives were achieved. This chapter concludes the report by answering the research questions and providing recommendations for future work.

### 9.1. Conclusion

This section answers the following research questions:

- RQ. 1** What are the advantages and limitations of the different earthquake analysis procedures?
- RQ. 2** Is the barstool structural model of the jack-up that was used for RSA adequate for THA?
- RQ. 3** What are requirements for using spectrum matched THR in ELE-screening?
- RQ. 4** Do soil-structure interaction effects need to be included in ELE-screening with THA?
- RQ. 5** Does the jack-up have predetermined critical angles of earthquake incidence?
- RQ. 6** What are the benefits of time development in seismic analysis?
- RQ. 7** Does the new ELE-screening procedure result in lower action effects?
- RQ. 8** Does the new ELE-screening procedure achieve the aim of this research?

### RQ1: What are the advantages and limitations of the different earthquake analysis procedures?

Earthquake analysis is performed as part of the site-specific analysis of jack-ups for locations with known seismic activity. In this research the analysis is performed according to the ISO codes due to its international applicability and because many local seismic codes follow a similar procedure. An overview of the main advantages and limitations of the existing earthquake analysis procedures are given in Table 9.1.

**Table 9.1:** Advantages and limitations of the ELE-screening method using RSA and the ALE method using THA

Assessment	Analysis	Advantages	Limitations
ELE	RSA	+ Computationally efficient + Straight forward method	- No sign information - No time development - No non-linearities
ALE	THA	+ Very detailed + Non-linearities + Sign information + Time development	- Requires PSHA - Requires DSHA - Complex method - Computationally very demanding - Requires detailed soil modelling

ELE-screening using RSA is a straight forward and simple method, however it can be considered conservative as it is designed to produce higher utilization results than more detailed assessments. The non-linear ALE method is comprehensive and has a high level of detail however it is complex and requires additional analyses to be performed, and detailed site-specific data. The so called conservatism of the ELE RSA procedure and the complexity of the ALE THA procedure led to the development of the new ELE-screening procedure with linear THA.

### RQ. 2 Is the barstool structural model of the jack-up that was used for RSA adequate for THA in the new ELE-screening procedure?

To assess the performance of the new ELE-screening procedure using THA against the existing ELE-screening procedure using RSA, an earthquake analysis was performed using both methods. The same structural model should be used to ensure a fair comparison. The barstool structural model from previous RSA studies was used; modifying the existing RSA tool fell outside the scope of this research

Due to a software limitation in the program used for RSA simulation, the part of the leg above the hull can not be modeled and is lumped to the leg-hull node at the lower guide in the RSA procedure. This changes the mass distribution and moment of inertia of the leg. Consequently, the dynamic behavior of the structure changes; the mode shapes and mass participation per mode of the jack-up are different. The hull is modeled by four corner nodes and one hull center node connected by beams. This barstool model is adequate for static analyses, however mode shape analysis shows it does not represent reality well. The fourth eigenmode shows a trampolining of the center node, effectively acting as a tuned mass damper system. This vertical resonance was observed in all time domain simulations and with 50% of the hull mass modeled at the center node there is high mass participation in this mode. Due to the implementation of Rayleigh damping this mode also has the lowest damping value. This has a significant impact on the motion of the structure and the resulting action effects found from simulations.

The bar stool structural model does not lead to a realistic representation of the structural response of the jack-up and should not be used in the THA ELE-screening procedure. When performing seismic analysis of jack-ups a more accurate structural model should be used for both the RSA and THA procedures. The basis for two such models has been discussed in this research.

### **RQ. 3 What are requirements for using spectrum matched THR in ELE-screening?**

The as-recorded time history records selected for spectrum matching should not be shallow or near field. The selected records should be decomposed to their principal axes before spectrum matching. Spectrum matching modifies properties of individual time history records and produces synthetic time signals. The response spectrum used for THR selection and matching introduces bias. The spectra and time history records used for ELE-screening should be selected such that they represent the dominating ELE events.

While the time history records were all matched to the same design response spectra, the simulation results clearly show that the respective resulting action effects of the different THR vary in magnitude. It is also evident that some THR result in larger action effects in certain planes than others, or for different soil-structure connection types. This emphasizes the need to use a sufficient number of THR to reduce statistical uncertainty in the analysis. Adopting an ensemble of earthquakes reduces the effect of frequency content and of particular characteristics of the individual earthquake ground motions. The use of more earthquake time history records should result in a better representation and assessment of the structure.

It is critical to ensure spectrum matching is performed over a suitable period range. This range depends on the fundamental period of the structure. When the fundamental period of the structural model is changed, for instance when taking different soil spring stiffnesses, the input time traces should be matched to the corresponding period range. Incorrect matching of the time histories can result in an unsafe assessment of the structure.

### **RQ.4 Do SSI effects need to be included in ELE-screening with THA?**

In engineering practice soil-structure interaction is often neglected due to: structural period elongation which moves the natural periods of the structure further from the energy containing periods of the ground motion, and extra damping caused by waves radiating energy away from the vibrating structure. An increased fundamental period and effective damping generally lead to reduced member forces, however in certain seismic and soil environments an increase in the fundamental natural period of a moderately flexible structure due to SSI may have a detrimental effect on the imposed seismic demand; excluding SSI effects would lead to an unsafe assessment of the structure. In order to determine whether SSI effects need to be included in the ELE-screening THA simulations, an SSI analysis was performed on an equivalent single degree of freedom system of the OWTI jack-up structural model used in this research. The SSI simulations were run using the same site-specific parameters as the ELE-screening simulations; the dynamic shear modulus of the soil was then varied to assess the effects of a stiffer and softer soil.

The analysis showed that, for the site-specific condition, the response of the jack-up was larger in the simulations that excluded SSI than in the simulations that included SSI. The analysis also showed that the SSI induced motion beneath the structure was several orders of magnitude smaller than the free-field ground motion. The use of linear springs and dampers to model the soil-structure interface connection was validated. Excluding SSI effects would not result in an unsafe assessment of the structure. Whether soil-structure interaction effects need to be included when performing ELE-screening with linear time history analysis depends on the properties of the soil and the structure, and needs to be verified with an SSI analysis of the jack-up for the site-specific operational conditions.

### **RQ. 5 Does the jack-up have predetermined critical angles of earthquake incidence?**

In seismic analysis of structures that are asymmetric in geometric configuration or directional capacity, additional simulations need to be performed to demonstrate suitable performance in weaker directions. For THA this may require different orientations of the horizontal earthquake THR to demonstrate performance requirements.

Seismic analysis of jack-ups using the RSA procedure suggests the existence of predetermined critical angles of earthquake incidence. These are the angles of incidence that result in the highest forces and moments on the structure. If jack-ups were to have predetermined critical angles of earthquake incidence, resulting in the highest action effects, the THA simulations would only have to be run for those particular orientations of horizontal THR pair. The THA simulation results do not support this idea of predetermined critical angles of earthquake incidence. The maximum action effect caused by one THR does not necessarily occur at the same

angle of earthquake incidence as for another THR, nor the same angle of incidence as the RSA result. When performing ELE-screening of jack-ups with THA, simulations should be run for different angles of earthquake incidence by rotating the horizontal THR pair around the structure.

### **RQ. 6: What are the benefits of time development in seismic analysis?**

The main advantage of using a model with time development for ELE-screening is a reduction in resulting seismic action effects. In THA the maximum action effects  $F_H$  and  $M$  are found in time rather than from their maximum  $X$  and  $Y$  components, as is the case with RSA. Since the maximum  $X$  and  $Y$  components do not necessarily occur simultaneously, finding the maximum resultant in time should result in lower action effects. This is also clearly demonstrated in the simulation results in this research.

Another advantage of using a model with time development is the ability to distinguish between short peak forces or moments, and sustained forces or moments. Since ELE-screening only looks at the global maximum forces and moments for unity checks this was not researched further. When expanding the model to the non-linear time-history analysis ALE assessment this becomes more relevant.

### **RQ. 7 Does the new ELE-screening procedure result in lower action effects?**

For the comparison of the RSA and THA method of ELE-screening, the Spring15 simulation case best describes the jack-up and representative soil condition under consideration. Analyses of the global maximum action effects from the simulations suggests that there is a performance improvement in the order of 10 to 20 percent when using the new ELE-screening procedure with THA in stead of RSA. This performance improvement is mainly observed for the shear force  $F_H$  and the moment  $M$  at both the lower guide and footing. A small improvement in the normal force  $V$  is also observed, however due to the structural model used in the simulations this may not accurately represent reality. The bar stool model exhibits vertical oscillation of the hull center node which impacts the motion of the structure and the resulting action effects. The results need to be verified with simulations using a more accurate structural model of the jack-up.

Note that the performance improvement demonstrated in this research is based on the RSA and THA simulation results. The SRSS rule for modal combination was used in the RSA simulation process, even though the jack-up has many closely spaced natural periods. When two nodes have closely spaced natural periods the SRSS rule is unconservative and more accurate rules shall be applied [7]. The actions effects found from the RSA simulations are smaller than they would be if an appropriate modal combination rule were used. Consequently, the performance gain of the new ELE-screening procedure with THA is expected to be greater than that demonstrated in this research.

### **RQ. 8 Does the new ELE-screening procedure achieve the aim of this research?**

The aim of this research was to improve the accuracy of earthquake screening of OWTI jack-ups in order to increase their geographic operability. A new ELE-screening procedure that uses time history analysis was developed and benchmarked against the existing procedure that uses response spectrum analysis. The use of THA introduces sign information and time development into the ELE-screening procedure. The expectation was that this increase in modeling accuracy would result in lower action effects from seismic excitation. This was confirmed by the simulation results, which indicate a reduction in the order of 10 to 20 percent of the global maximum shear force and moment in the legs at the lower guide and footing. A small improvement in the global maximum normal force was also observed. The ELE-screening procedure with THA can be used to demonstrate compliance with earthquake performance requirements when a jack-up does not satisfy the ELE-screening assessment criteria using RSA. Since safe operation can now be demonstrated for more areas, the geographic operability of OWTI jack-ups is increased.

The inclusion of a soil-structure interaction analysis in the new ELE-screening procedure also improves the accuracy of earthquake screening of jack-ups. Since the SSI analysis in this research is only used to demonstrate that, for the cases considered, the exclusion of SSI effects would not result in an unsafe assessment of the structure, it does not directly improve the geographic operability of jack-ups.

## 9.2. Recommendations

This section provides recommendations for further research and development.

### Structural model

**Improve the structural model of the jack-up** used for seismic analysis. The new structural model should allow for a more realistic weight distribution and a better representation of the internal load transfer. It is assumed that by following the major structural components of the hull a more realistic internal load transfer is achieved. The basis for such a model is discussed in this research, and a similar model is used by Linthorst[22] in his study on seismic analysis of cranes on jack-ups which uses the new ELE-screening THA procedure and the OpenSees tool developed in this research.

**Model the legs above the hull.** In this research the part of the legs above the hull were lumped to the leg-hull interface in both RSA and THA simulations. This was done to allow a fair comparison between the two methods, while a limitation in the RSA tool meant the leg above hull level could not be modeled. The THA tool in OpenSees does not have this limitation and the legs of the jack-up should accurately be included in the structural model.

### Groundmotions

**Generate distinctly different spectra** for the different directions in seismic analysis procedures. Directivity effects can be captured, provided that the spectra generated in different directions are distinctly different. This is however not reflected in current seismic design codes including ISO.

**Research the use of site-specific spectra** created from probabilistic seismic hazard analysis of the geographic location for spectrum matching of time history records. Using a site-specific spectrum will improve the accuracy of the seismic analysis.

**Automate spectrum matching process** of time-history records. Manually spectrum matching THR is a time consuming process. Considering that changing structural properties changes the period range for matching, changing site-specific conditions changes the target spectrum, and that an increase in the number of THR used in the ELE-screening with THA should result in a better representation and assessment of the structure, the spectrum matching process should be automated.

### SSI analysis

**Establish engineering resource sharing**, such as detailed soil model and site-specific data, as part of the work package to facilitate more accurate analysis, resulting in increased operational safety. This would be particularly useful for soil-structure interaction analysis.

**Create a more accurate and refined tool for SSI analysis** of jack-ups to determine whether the inclusion of SSI effects is required in THA simulations for ELE-screening. SSI is included in THA by modeling the structure and soil as an integrated system. The mesh size of the model should be small enough to capture the shortest wavelength and the soil domain should be large enough to model the longest wave length. A large model with a fine mesh is computationally very demanding. Being able to accurately determine whether SSI effects can be excluded from THA simulations will result in a reduction of engineering resources and risk, while increasing operational safety.

### ELE-screening with RSA

**Use complete quadratic combination (CQC)** instead of square root of sum squares (SRSS) for modal combination when performing ELE-screening with RSA for structures that have closely spaced natural periods, such as OWTI jack-ups. Implement the use of the CQC method in the RSA tool.

**Implement correct vertical DRS** in RSA tool. The vertical DRS was constructed from the horizontal DRS using a constant scale factor instead of a frequency dependent scale factor due to a limitation in the RSA tool. Using the correct vertical DRS results in lower action effects under ceteris paribus conditions.

### **ELE-screening**

**Adapt ELE-screening procedure to local design codes** for site-specific analysis. The new ELE-screening method was developed using the ISO standards due to their worldwide application, however the method can easily be adapted to conform to local design codes by using local design response spectra or local soil data. It is possible to perform an adapted version of the analysis for a geographic location using input data or requirements that conform to regional design codes.

**Incorporate SSI directly into ELE-screening tool** in OpenSees. The SSI analysis performed in this research showed that the response of the jack-up was larger in the simulations that excluded SSI than in the simulations that included SSI. Including SSI into the THA tool could reduce the calculated action effects, thereby further improving the geographic operability of the jack-up.

# A

## Rayleigh damping ratio

This appendix contains the graphs showing the damping ratios when Rayleigh damping is fitted to modes 1 and 4, and when fitted to modes 1 and 10, for the Fixed, Pinned, and Spring connections.

### Fixed connection

mode	freq [rad/s]	$\zeta$ (m1-m4)	$\zeta$ (m1-m10)
1	2.45	0.050	0.050
2	2.47	0.050	0.050
3	3.76	0.043	0.037
4	8.44	0.050	0.029
5	22.89	0.109	0.048
6	23.17	0.110	0.049
7	23.43	0.112	0.049
8	23.76	0.113	0.050
9	23.94	0.114	0.050
10	23.97	0.114	0.050

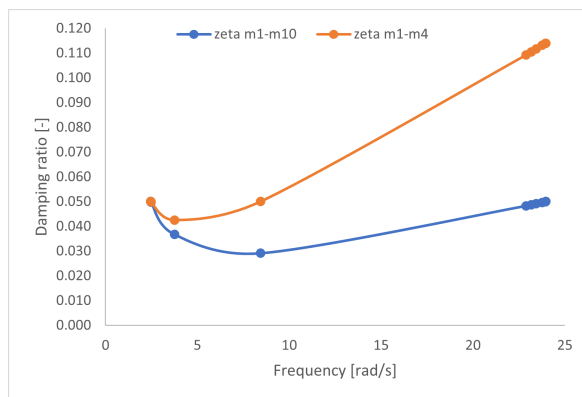


Figure A.1: Damping ratio when fitted to modes 1 and 4, and damping ratios when fitted to mode 1 and 10, for the Fixed condition

### Pinned connection

mode	freq [rad/s]	$\zeta$ (m1-m4)	$\zeta$ (m1-m10)
1	1.18	0.050	0.050
2	1.19	0.050	0.050
3	1.61	0.040	0.039
4	8.44	0.050	0.030
5	15.66	0.085	0.047
6	15.89	0.086	0.048
7	16.35	0.088	0.049
8	16.37	0.088	0.049
9	16.41	0.089	0.049
10	16.83	0.091	0.050

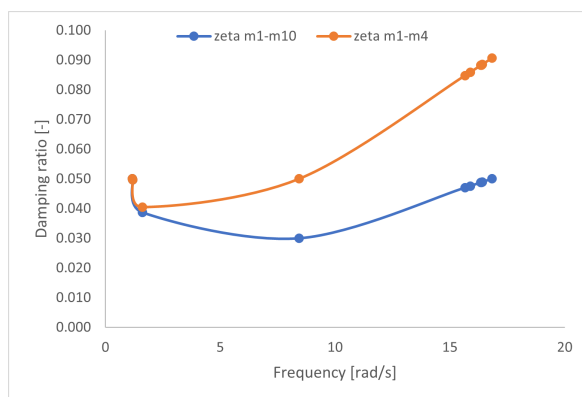
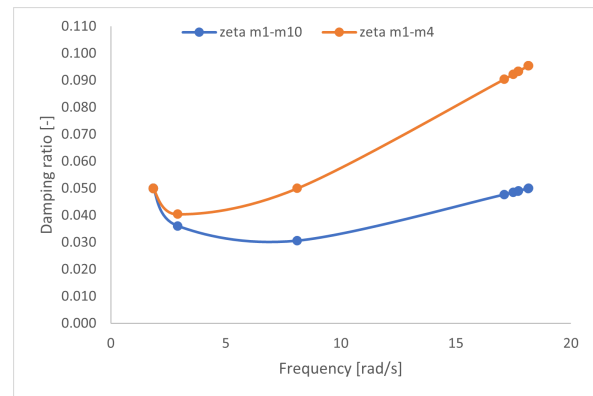


Figure A.2: Damping ratio when fitted to modes 1 and 4, and damping ratios when fitted to mode 1 and 10, for the Pinned condition

### Spring connection

mode	freq [rad/s]	$\zeta$ (m1-m4)	$\zeta$ (m1-m10)
1	1.84	0.050	0.050
2	1.85	0.050	0.050
3	2.90	0.040	0.036
4	8.10	0.050	0.031
5	17.10	0.090	0.048
6	17.50	0.092	0.049
7	17.71	0.093	0.049
8	17.72	0.093	0.049
9	18.15	0.095	0.050
10	18.16	0.095	0.050



**Figure A.3:** Damping ratio when fitted to modes 1 and 4, and damping ratios when fitted to mode 1 and 10, for the Spring conditions

# B

## Site seismic maps

Figures B.1 and B.2 display the generic seismic maps of spectral accelerations for offshore Japan. The acceleration values are expressed in g, correspond to 5% damped spectral accelerations on rock outcrop (site class A/B), and have a return period of 1000 years. The accelerations are designated  $S_{a,map}(0.2)$  and  $S_{a,map}(1.0)$  for a 0.2[s] and 1.0[s] oscillator period respectively. The areas that are classified as severe seismic areas for jack-ups and require site-specific assessment have been highlighted.

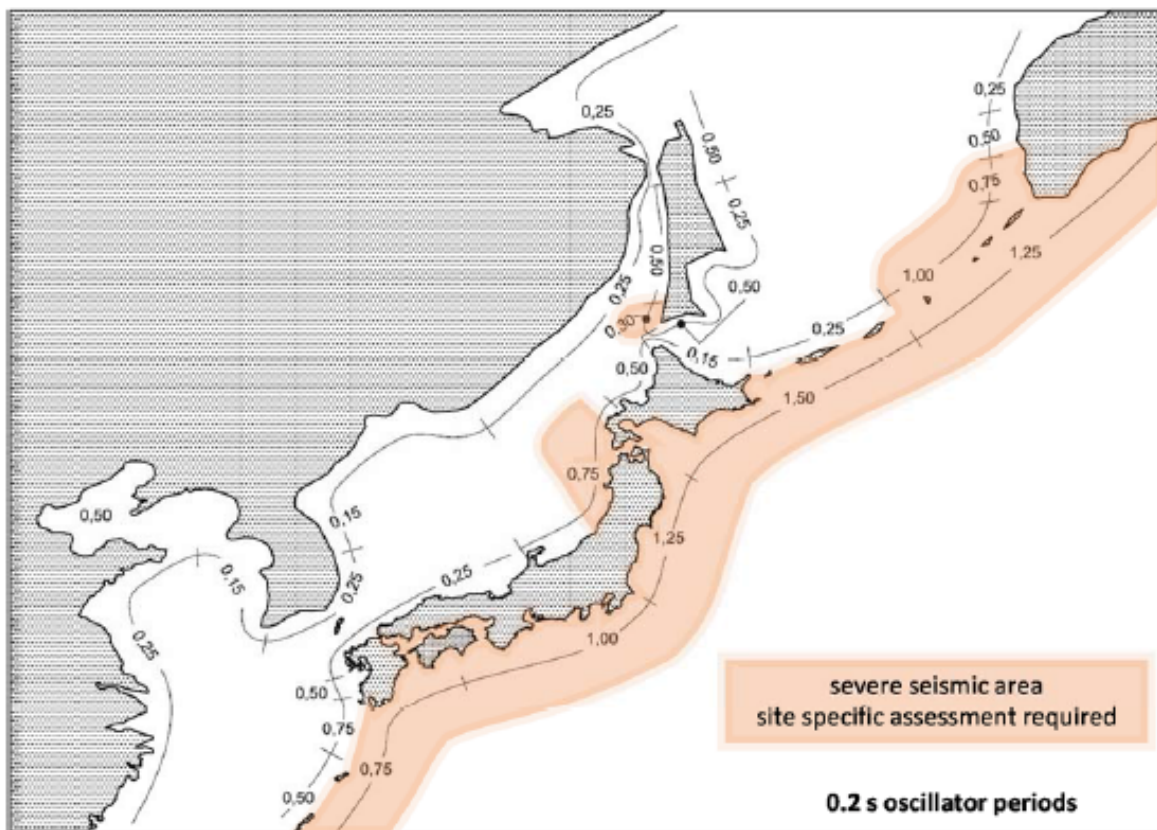


Figure B.1: Map of spectral accelerations offshore Japan for 0.2[s] oscillator period

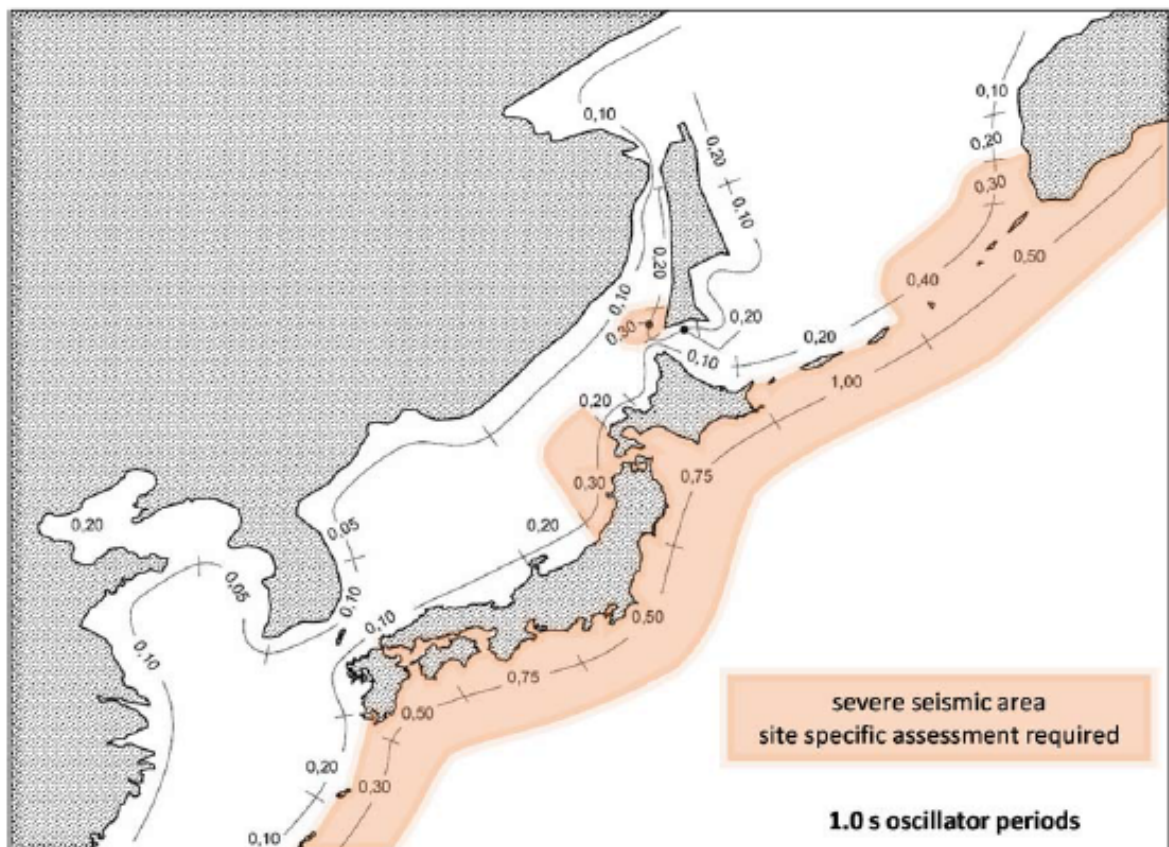


Figure B.2: Map of spectral accelerations offshore Japan for 1.0[s] oscillator period

# C

## Analysis methods

### C.1. Response spectrum analysis

One of the most widely used methods of analysis in earthquake engineering is response spectrum analysis. It is a linear-dynamic statistical analysis method that makes use of a response spectrum. It measures the contribution from each natural mode of vibration and combines them to calculate the most probable maximum seismic response of an elastic structure. The method is primarily limited to linear problems, however there have been several attempts to extend its application to non-linear problems [4]. The steps that make up a response spectrum analysis are:

- Derivation of the design response spectrum
- Solving the eigenvalue problem to determine the eigenfrequencies and eigenmodes
- Obtaining the peak response for each modal degree of freedom
- Statistically combining the individual responses to find the most probable peak response

When performing a response spectrum analysis the first step is to derive or define the design response spectrum. A response spectrum is a plot of the peak or steady-state response of a series of oscillators of varying period  $T_i$  for a chosen value of damping  $\zeta_i$ , that are forced into motion by the same base excitation. The response quantity can be either displacement, velocity, or acceleration. Figure C.1 shows a schematic illustration of how the displacement response spectrum of a SDOF with 2% damping is built up for the El Centro earthquake of 1940. The acceleration and velocity response spectra are constructed in the same manner.

A response spectrum represents one single excitation, or earthquake, and contains several fluctuations with peaks and troughs. In an earthquake assessment all possible earthquakes likely to occur in the location of interest need to be accounted for, which is why design response spectra are used. The design response spectra are usually generated from code provisions such as ISO [2] and EC8 [7], and represent an envelope of all likely responses for a location as a function of fundamental period and damping ratio. In the ISO response spectrum analysis procedure use is made of acceleration design response spectra. How the ISO acceleration design response spectra are constructed is discussed in Section 4.2. The base excitation is represented by two orthogonal horizontal acceleration design response spectra and one vertical acceleration design response spectrum.

The next step is to reduce a multi-degree of freedom (MDOF) system to a number of uncoupled SDOF systems which can each be solved by using the response spectrum. The MDOF is reduced using a normal mode analysis and transformation. The eigenfrequencies  $\omega_i$  and the normalised eigenshapes  $\Phi_i$  are obtained by solving the eigenvalue problem of the MDOF system. The equations of motion of the structure are then transformed to the modal domain. The equation of motion of an MDOF system with damping is given in Eq. (C.1). The eigenfrequencies are the positive roots of the characteristic equation given in Eq. (C.2). The assumption is made that the response can be expressed in terms of the undamped modes as given in Eq. (C.3), where  $\Phi$  is the real-valued eigenmatrix obtained by solving the undamped free vibration  $\mathbf{M}\ddot{\mathbf{x}} + \mathbf{K}\mathbf{x} = \mathbf{0}$ .

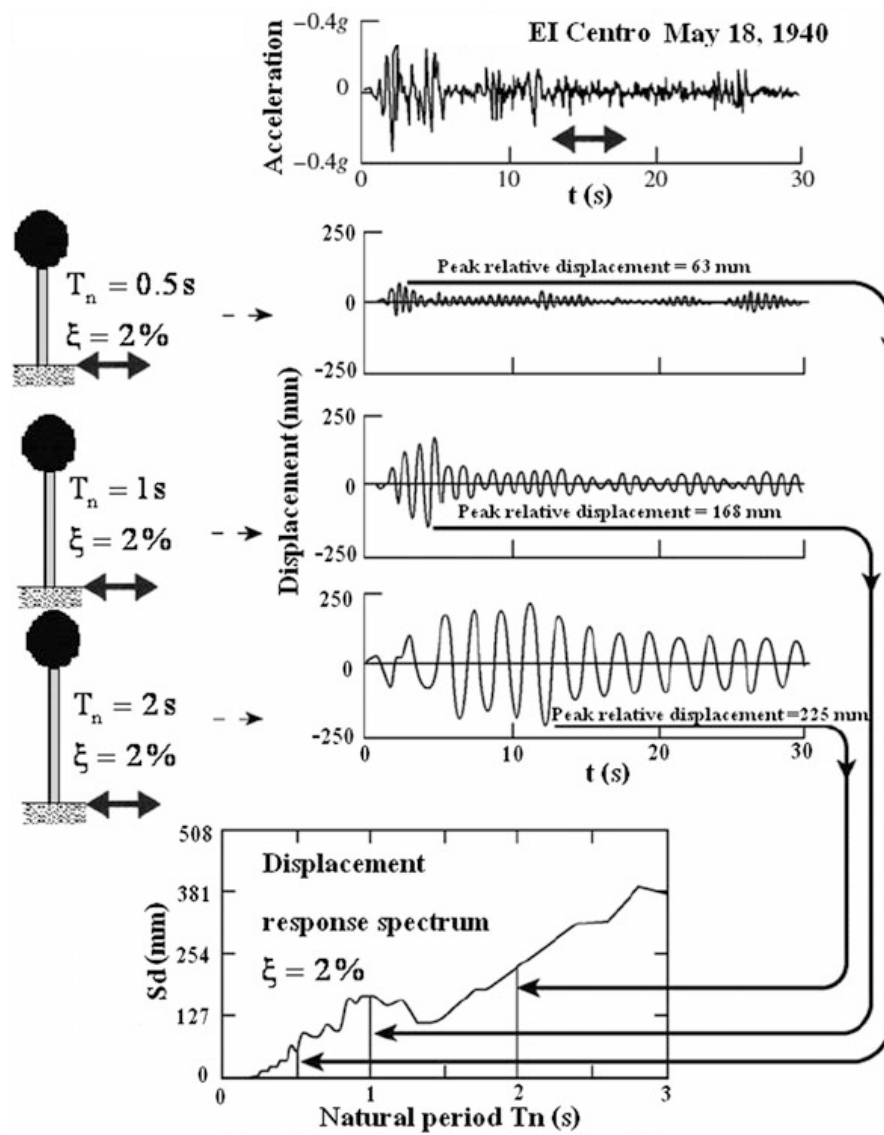


Figure C.1: Schematic illustration of the construction of the displacement response spectrum of a SDOF with 2% damping for the El Centro earthquake of 1940 [4]

$$\mathbf{M}\ddot{\mathbf{x}}(t) + \mathbf{C}\dot{\mathbf{x}}(t) + \mathbf{K}\mathbf{x}(t) = -\mathbf{M}\mathbf{r}\ddot{x}_g(t) \quad (\text{C.1})$$

$$\det(-\omega_i^2 \mathbf{M} + \mathbf{K}) = 0 \quad (\text{C.2})$$

$$\mathbf{x}(t) = \Phi \mathbf{u}(t) = \sum_{i=1}^N \hat{\Phi}_i u_i(t) \quad (\text{C.3})$$

Substituting the solution found for  $\mathbf{x}(t)$  from Eq. (C.3) into the equation of motion results in Eq. (C.4). Pre-multiplying this equation with the transpose of the eigenmatrix gives Eq. (C.5).

$$\mathbf{M}\Phi\ddot{\mathbf{u}}(t) + \mathbf{C}\Phi\dot{\mathbf{u}}(t) + \mathbf{K}\Phi\mathbf{u}(t) = -\mathbf{M}\mathbf{r}\ddot{u}_g(t) \quad (\text{C.4})$$

$$\mathbf{M}^* \ddot{\mathbf{u}}(t) + \mathbf{C}^* \dot{\mathbf{u}}(t) + \mathbf{K}^* \mathbf{u}(t) = -\Phi^T \mathbf{M} \mathbf{r} \ddot{u}_g(t) \quad (\text{C.5})$$

The modal mass matrix  $\mathbf{M}^*$  and modal stiffness matrix  $\mathbf{K}^*$  are diagonal, while the modal damping matrix  $\mathbf{C}^*$  is fully populated. Rayleigh damping is used to force a diagonalised modal damping matrix. Rayleigh damping is explained further in Section 3.3. A decoupled equation of motion is obtained for each modal coordinate  $u_i(t)$ ,  $i = 1, 2, \dots, N$  and given in Eq. (C.6), with  $\zeta_i$  and  $\Gamma_i$  given in Eqs. (C.7) and (C.8) respectively.

$$\ddot{u}_i(t) + 2\zeta_i \omega_i \dot{u}_i(t) + \omega_i^2 u_i(t) = -\Gamma_i \ddot{u}_g(t) \quad (\text{C.6})$$

$$\zeta_i = \frac{c_{ii}^*}{2m_{ii}^* \omega_i} = \frac{c_{ii}^*}{c_{ii,crit}^*} \quad (\text{C.7})$$

$$\Gamma_i = \frac{L_i}{m_{ii}^*} = \frac{\hat{\Phi}_i^T \mathbf{M} \mathbf{r}}{\hat{\Phi}_i^T \mathbf{M} \hat{\Phi}_i} \quad (\text{C.8})$$

$u_i(t)$  is the modal displacement response in the  $i^{th}$  mode

$\zeta_i$  is the modal damping ratio in the  $i^{th}$  mode

$\Gamma_i$  is the modal participation factor in the  $i^{th}$  mode

The maximum modal displacement response for each modal degree of freedom is then calculated in Eq. (C.9) using the the design response spectrum.

$$u_{i,max} = |u_i(t)|_{max} = |\Gamma_i S_d(\zeta_i, T_i)| \quad (\text{C.9})$$

The normal coordinate of each mode responds to the earthquake like a single degree of freedom oscillator. Each mode experiences a scaled version of the excitation determined by the participation factor. The maximum displacement response of the structure in the  $i^{th}$  mode is given in Eq. (C.10) and the maximum acceleration response of the structure in the  $i^{th}$  mode is given in Eq. (C.11)

$$x_{i,max} = \Phi_i u_{i,max} \quad (i = 1, 2, \dots, n) \quad (\text{C.10})$$

$$\ddot{x}_{i,max} = \Phi_i \Gamma_i S_a(\zeta_i, T_i) \quad (i = 1, 2, \dots, n) \quad (\text{C.11})$$

The next step is statistically combining the individual responses to obtain the most probable peak response. This is done using modal combination rules such as the absolute sum rule (ABBSUM), square-root-of-sum-of-squares rule (SRSS), and complete quadratic combination rule (CQC). The SRSS is given in Eq. (C.12)

$$\ddot{x}_{max} = \left( \sum_{i=1}^N (\ddot{x}_{i,max})^2 \right)^{\frac{1}{2}} = \left( \sum_{i=1}^N (\Phi_i \Gamma_i S_a(\zeta_i, T_i))^2 \right)^{\frac{1}{2}} \quad (\text{C.12})$$

Finally, to obtain the total structural response due to the seismic excitations from all three translational directions, spatial combination of response is required using methods such as SRSS or CQC [4].

## C.2. Time history analysis

Time history analysis, which is also referred to as response history analysis, is a method in which the state of a system is evaluated at successive time increments. The seismic input for time-history analysis are acceleration time history records. The response of the system is evaluated at each time step using the initial conditions of the previous time step and the loading history at the current time step.

The equation of motion and the initial conditions of a damped multiple degree of freedom system to an earthquake input acceleration  $\ddot{u}_g(t)$  are given in Eqs. (C.13) and (C.14) respectively.

$$\mathbf{M}\ddot{\mathbf{x}}(t) + \mathbf{C}\dot{\mathbf{x}}(t) + \mathbf{K}\mathbf{x}(t) = -\mathbf{M}\mathbf{r}\ddot{u}_g(t) \quad (\text{C.13})$$

$$\mathbf{x}(0) = \dot{\mathbf{x}}(0) = \mathbf{0} \quad (\text{C.14})$$

The equation of motion and initial conditions can be rewritten to state-space form, thereby going from a coupled system of 2nd order differential equations to a system of first order differential equations that can be solved by commercial software packages.

$$\mathbf{y}(t) = \dot{\mathbf{x}}(0) \quad (\text{C.15})$$

$$\dot{\mathbf{y}}(t) = \mathbf{M}^{-1}(-\mathbf{M}\mathbf{r}\ddot{u}_g(t) - \mathbf{K}\mathbf{x}(t) - \mathbf{C}\mathbf{y}(t)) \quad (\text{C.16})$$

$$\mathbf{x}(0) = \mathbf{0} \quad (\text{C.17})$$

$$\mathbf{y}(0) = \mathbf{0} \quad (\text{C.18})$$

# D

## Spectrum matching quality

The SeismoMatch spectrum matching software matches the earthquake time histories to the design response spectrum. An inverse relationship was observed between matching quality and period range over which the matching is performed,  $T_{min}$  to  $T_{max}$ . The match quality of the major, and intermediate principal axis component time traces to the 5% damped horizontal design response spectrum are given in Tables D.1 and D.2 respectively. The match quality of the minor principal axis earthquake component time traces to the 5% and 15% damped vertical design response spectrum are given in Tables D.3 and D.4 respectively. MMS stands for 'mean matched spectrum'.

**Table D.1:** Match quality of the major principal axis earthquake component time traces to the 5% damped horizontal design response spectrum

Tmin	Tmax	Accerlerograms	Average misfit	Maximum misfit	Max acceleration
0.1	3	p1RSN332_C	7.4%	34.3%	1.29
0.1	3	p1RSN737_L	4.4%	44.5%	1.26
0.1	3	p1RSN579_S	7.4%	59.2%	1.23
0.1	3	p1FKS012NS	7.1%	27.2%	1.38
0.1	3	MMS	3.9%	31.1%	1.19
0.1	4	p1RSN332_C	12.3%	48.3%	1.29
0.1	4	p1RSN737_L	5.8%	45.8%	1.26
0.1	4	p1RSN579_S	9.1%	62.8%	1.23
0.1	4	p1FKS012NS	4.9%	27.6%	1.38
0.1	4	MMS	5.2%	41.5%	1.19
0.1	5.5	p1RSN332_C	5.6%	54.0%	1.29
0.1	5.5	p1RSN737_L	7.7%	60.5%	1.26
0.1	5.5	p1RSN579_S	9.2%	65.3%	1.23
0.1	5.5	p1FKS012NS	3.9%	30.9%	1.38
0.1	5.5	MMS	4.7%	46.8%	1.08

**Table D.2:** Match quality of the intermediate principal axis earthquake component time traces to the 5% damped horizontal design response spectrum

Tmin	Tmax	Accerlerograms	Average misfit	Maximum misfit	Max acceleration
0.1	3	p2RSN332_C	5.6%	44.1%	1.22
0.1	3	p2RSN579_S	7.6%	61.5%	1.23
0.1	3	p2RSN737_L	4.3%	49.9%	1.33
0.1	3	p2FKS012EW	6.0%	21.1%	1.34
0.1	3	MMS	3.9%	43.5%	1.20
0.1	4	p2RSN332_C	24.8%	61.5%	1.28
0.1	4	p2RSN579_S	7.5%	62.2%	1.28
0.1	4	p2RSN737_L	6.3%	64.0%	1.33
0.1	4	p2FKS012EW	6.9%	34.4%	1.34
0.1	4	MMS	8.3%	53.9%	1.18
0.1	5.5	p2RSN332_C	26.2%	59.0%	1.29
0.1	5.5	p2RSN579_S	12.6%	60.0%	1.35
0.1	5.5	p2RSN737_L	9.2%	68.8%	1.33
0.1	5.5	p2FKS012EW	12.0%	37.1%	1.34
0.1	5.5	MMS	11.9%	54.4%	1.10

**Table D.3:** Match quality of the minor principal axis earthquake component time traces to the 5% damped vertical design response spectrum

Tmin	Tmax	Accerlerograms	Average misfit	Maximum misfit	Max acceleration
0.1	3	p3RSN332_C	5.6%	32.2%	1.06
0.1	3	p3RSN579_S	11.9%	57.7%	1.07
0.1	3	p3RSN737_L	5.7%	60.2%	1.03
0.1	3	p3FKS012UD	9.2%	36.1%	1.14
0.1	3	MMS	5.4%	39.2%	1.03
0.1	4	p3RSN332_C	8.0%	53.3%	1.12
0.1	4	p3RSN579_S	6.6%	51.3%	1.08
0.1	4	p3RSN737_L	6.3%	59.5%	1.03
0.1	4	p3FKS012UD	6.4%	29.4%	1.16
0.1	4	MMS	4.4%	44.5%	1.06
0.1	5.5	p3RSN332_C	10.5%	62.1%	1.12
0.1	5.5	p3RSN579_S	9.0%	55.0%	1.08
0.1	5.5	p3RSN737_L	16.5%	74.2%	1.03
0.1	5.5	p3FKS012UD	11.1%	37.9%	1.16
0.1	5.5	MMS	6.8%	53.7%	0.92

**Table D.4:** Match quality of the minor principal axis earthquake component time traces to the 15% damped vertical design response spectrum

Tmin	Tmax	Accerlerograms	Average misfit	Maximum misfit	Max acceleration
0.1	3	p3RSN332_C	4.0%	16.0%	0.92
0.1	3	p3RSN579_S	3.9%	16.0%	0.85
0.1	3	p3RSN737_L	5.4%	13.6%	0.88
0.1	3	p3FKS012UD	7.5%	25.7%	1.14
0.1	3	MMS	5.3%	11.2%	0.66
0.1	4	p3RSN332_C	6.3%	16.6%	0.92
0.1	4	p3RSN579_S	4.5%	22.8%	0.85
0.1	4	p3RSN737_L	5.0%	15.1%	0.88
0.1	4	p3FKS012UD	4.4%	16.9%	1.14
0.1	4	MMS	4.1%	10.7%	0.66
0.1	5.5	p3RSN332_C	7.5%	29.4%	0.92
0.1	5.5	p3RSN579_S	4.8%	22.2%	0.85
0.1	5.5	p3RSN737_L	2.9%	22.5%	0.88
0.1	5.5	p3FKS012UD	5.5%	15.7%	1.14
0.1	5.5	MMS	5.5%	17.9%	0.66



# E

## Eigenmodes

This appendix contains graphs of the first 10 eigenmodes of the jack-up model for the fixed, pinned, and spring15 case. For clarity the graphs have been plotted with 10x magnification factor. The blue circles connected by the dashed lines represent the nodes and beam elements of the undisturbed structure. The red crosses connected by the solid lines represent the nodes and beam elements of the structure in its eigenmode. For all soil structure connections the first two modes are lateral displacement of the hull and bending of the legs. The third mode is rotation of the hull around the vertical axis and bending of the legs, and the fourth mode is vertical displacement of the hull, but especially the hull centre node. The following higher order modes are bending of the legs in some cases in combination with rotation of the hull around the horizontal plane.

### E.1. Fixed case

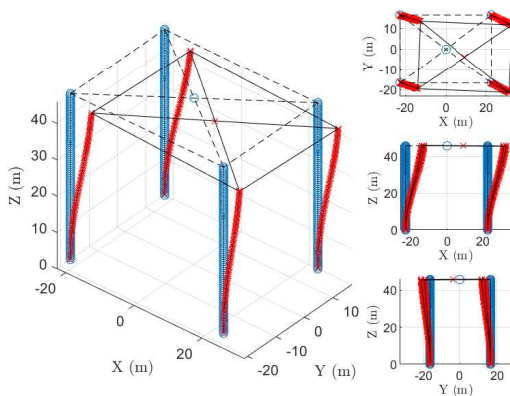


Figure E.1: Mode 1 of fixed case

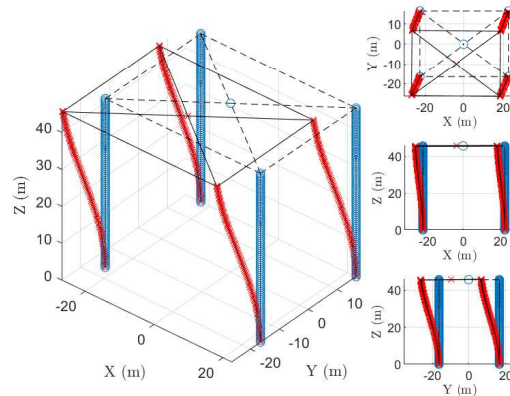


Figure E.2: Mode 2 of fixed case

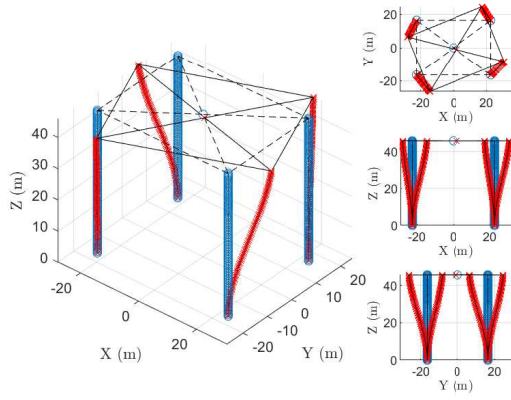


Figure E.3: Mode 3 of fixed case

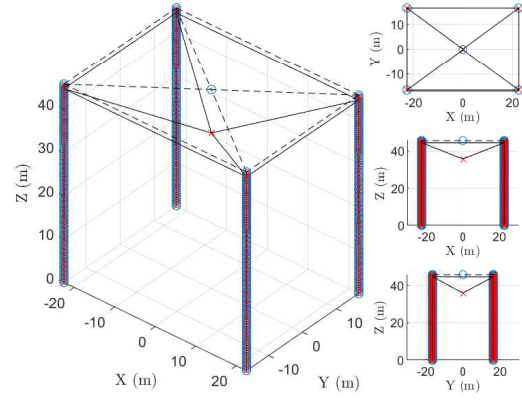


Figure E.4: Mode 4 of fixed case

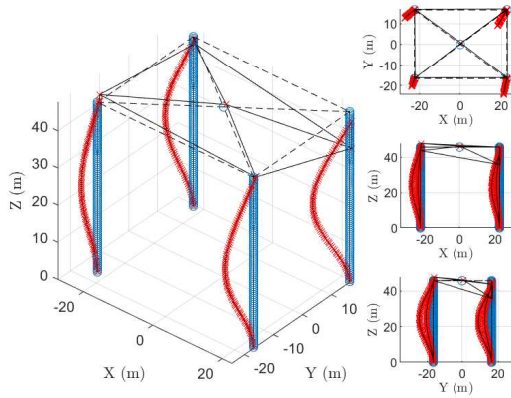


Figure E.5: Mode 5 of fixed case

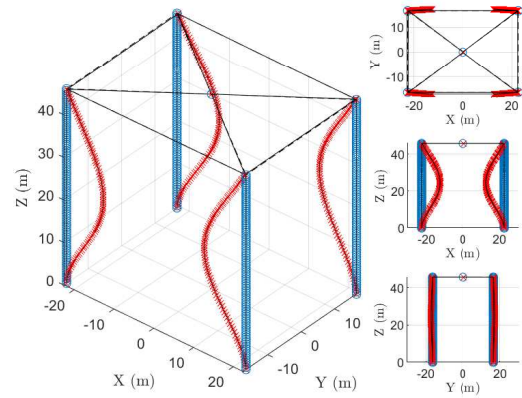


Figure E.6: Mode 6 of fixed case

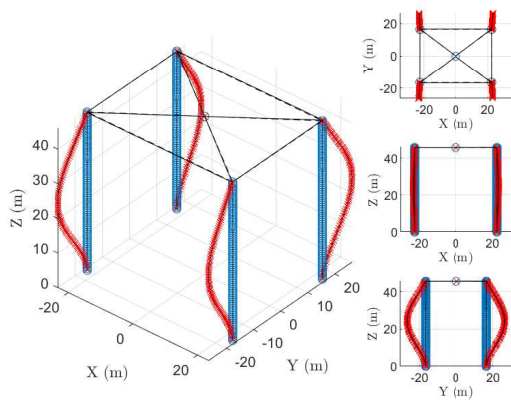


Figure E.7: Mode 7 of fixed case

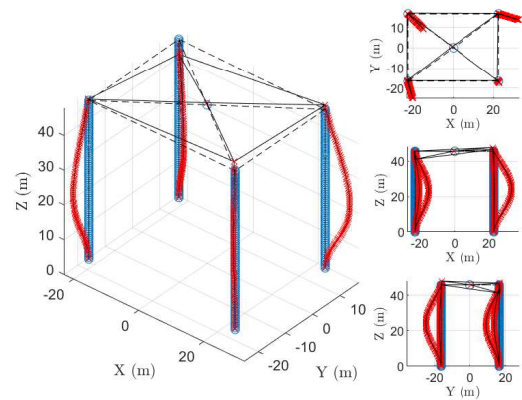


Figure E.8: Mode 8 of fixed case

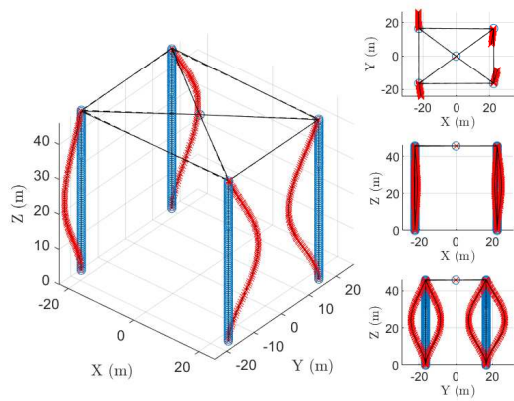


Figure E.9: Mode 9 of fixed case

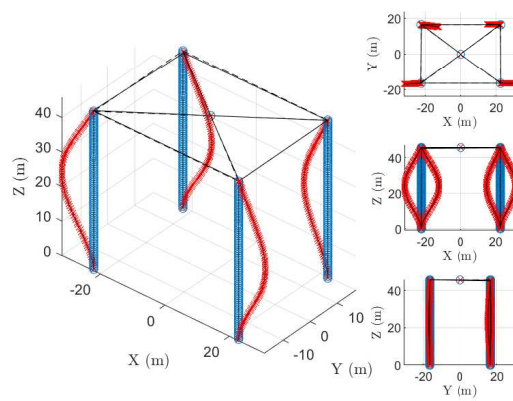


Figure E.10: Mode 10 of fixed case

E.2. Pinned case

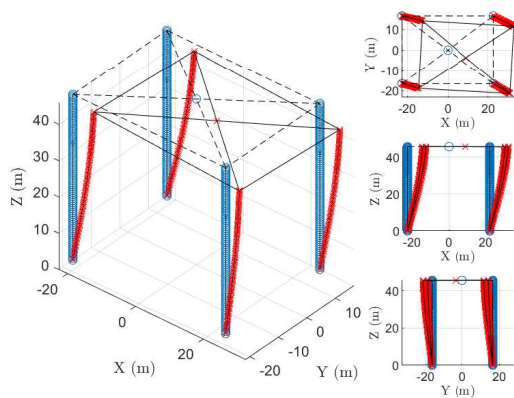


Figure E.11: Mode 1 of pinned case

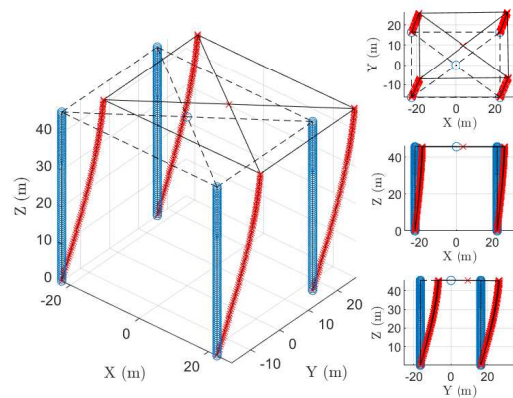


Figure E.12: Mode 2 of pinned case

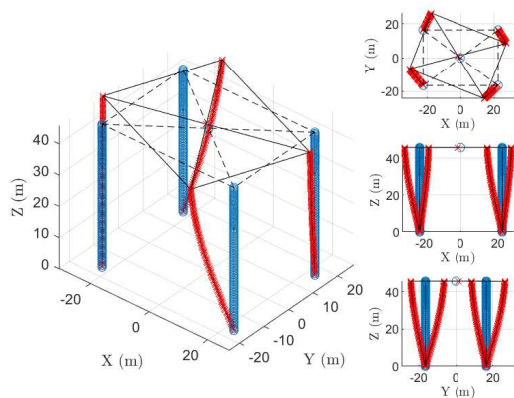


Figure E.13: Mode 3 of pinned case

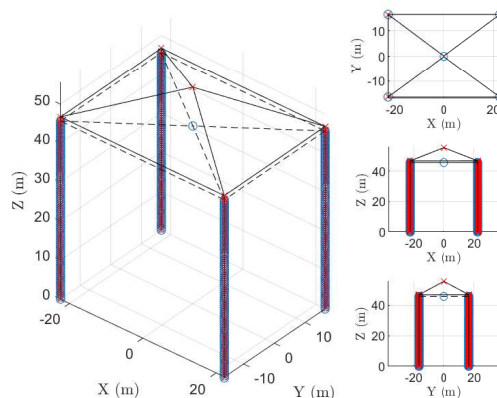


Figure E.14: Mode 4 of pinned case

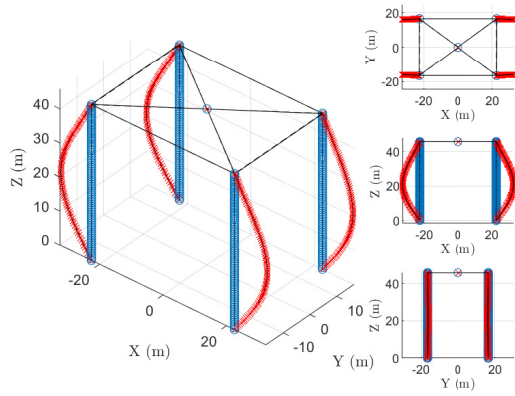


Figure E.15: Mode 5 of pinned case

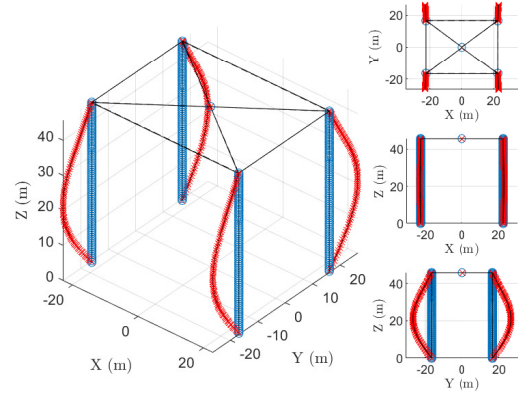


Figure E.16: Mode 6 of pinned case

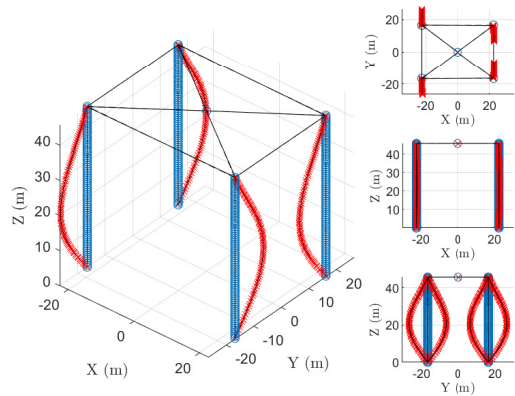


Figure E.17: Mode 7 of pinned case

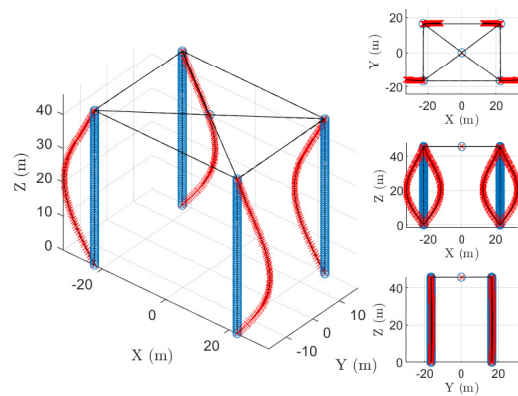


Figure E.18: Mode 8 of pinned case

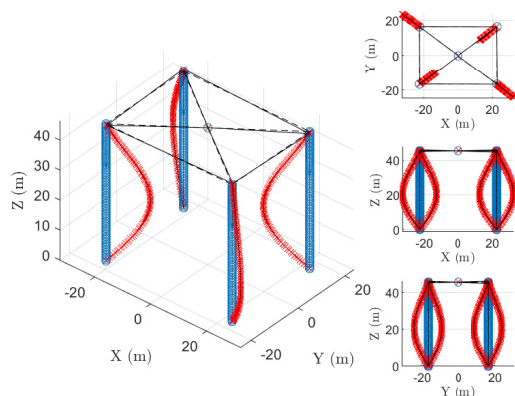


Figure E.19: Mode 9 of pinned case

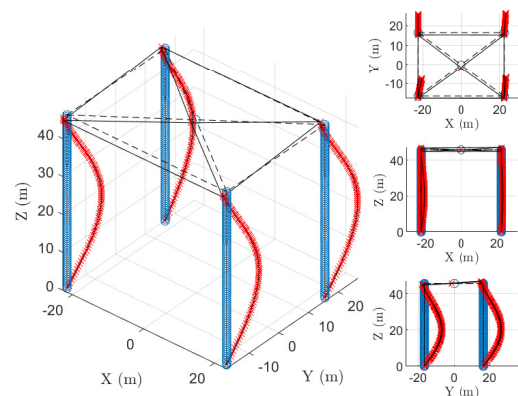


Figure E.20: Mode 10 of pinned case

### E.3. Spring case

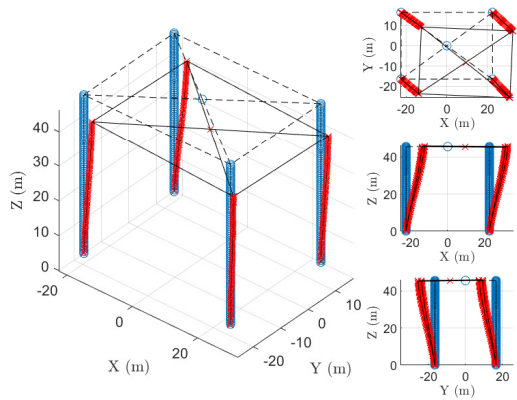


Figure E.21: Mode 1 of spring case

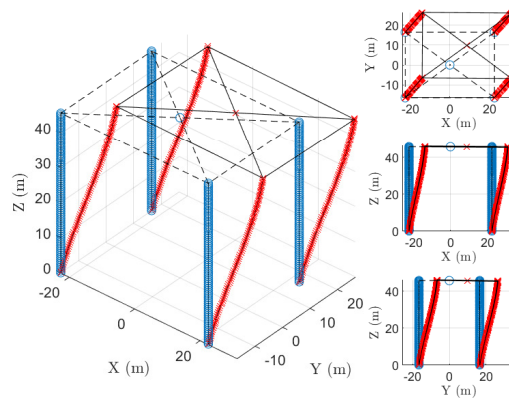


Figure E.22: Mode 2 of spring case

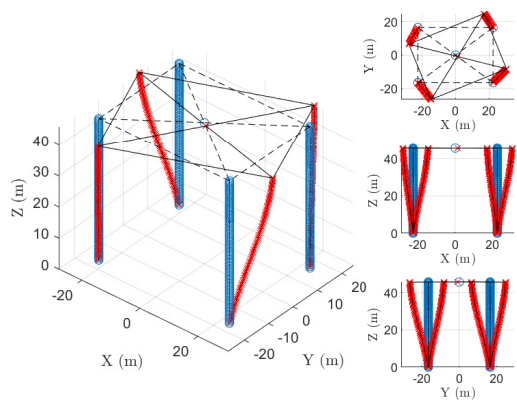


Figure E.23: Mode 3 of spring case

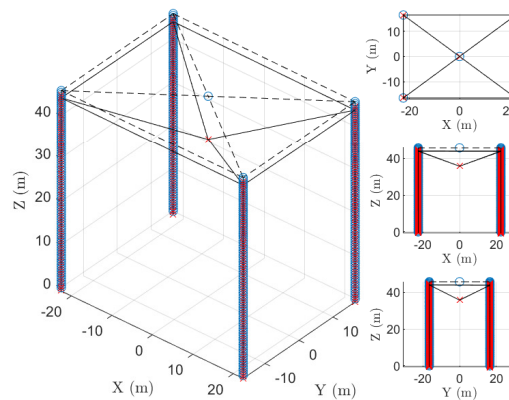


Figure E.24: Mode 4 of spring case

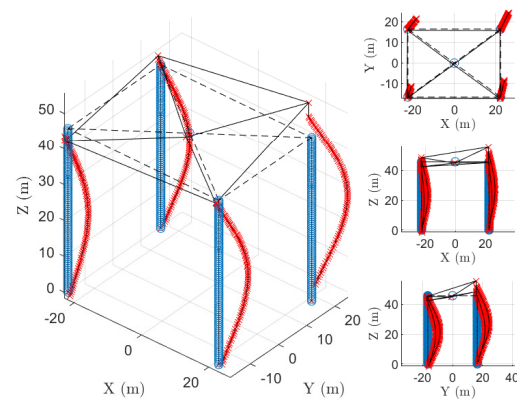


Figure E.25: Mode 5 of spring case

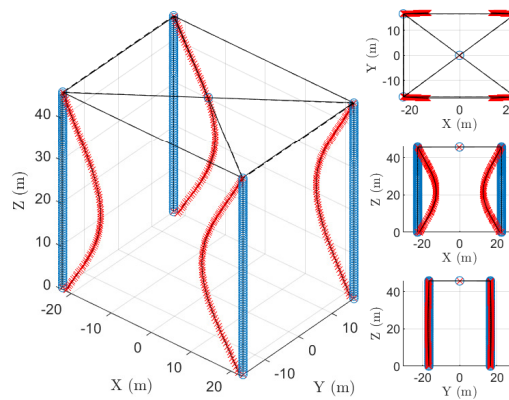


Figure E.26: Mode 6 of spring case

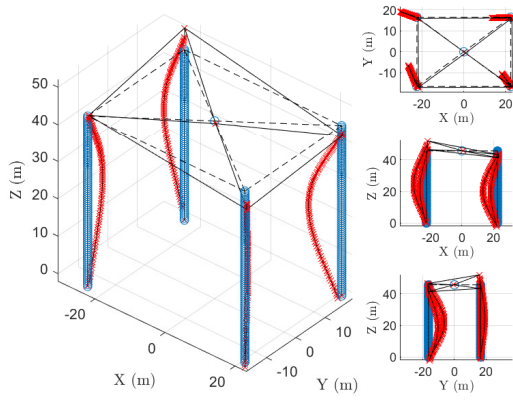


Figure E.27: Mode 7 of spring case

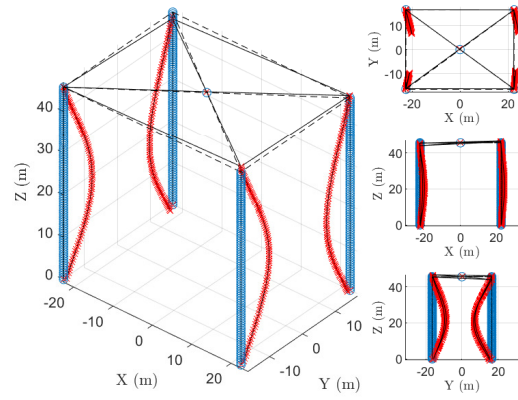


Figure E.28: Mode 8 of spring case

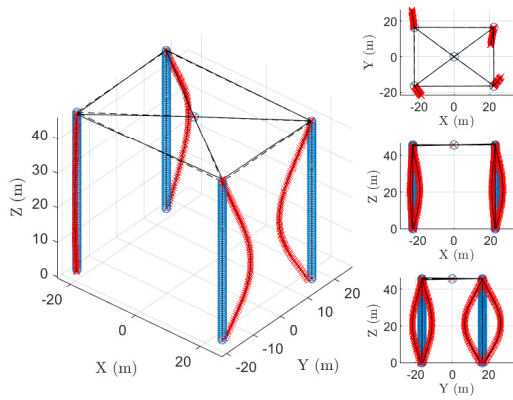


Figure E.29: Mode 9 of spring case

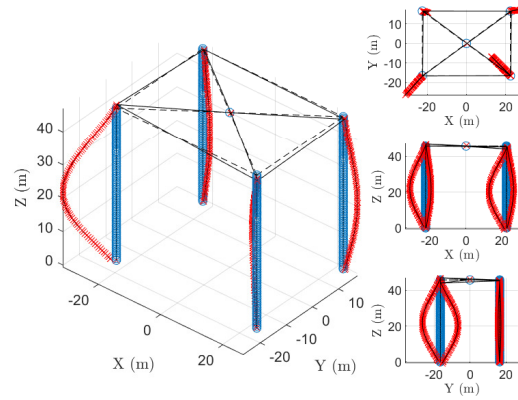


Figure E.30: Mode 10 of spring case

# F

## Time development graphs

This appendix contains the graphs of the maximum shear force  $F_{H,LG}$  and the maximum moment  $M_{LG}$  at the lower guide, per earthquake incidence angle, for the Spring15 connection for all four time history records. Each graph shows the RSA results, the THA results found in time, and the THA results found from the maximum X and Y component, as discussed in Section 8.5.4 Time development THA.

### FKS01

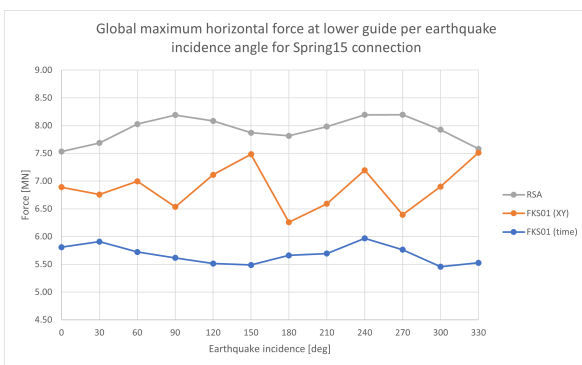


Figure F.1: Max shear force  $F_{H,LG}$  at the lower guide per EQ incidence angle for the Spring15 connection; FKS01

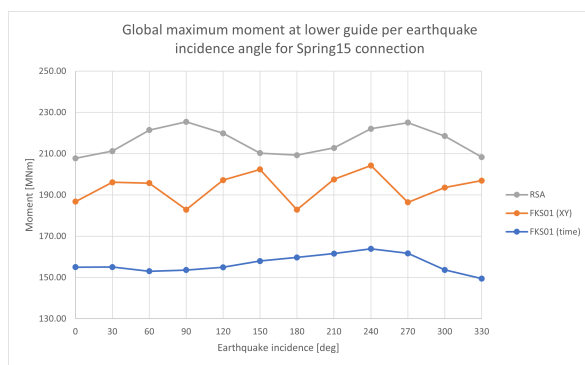
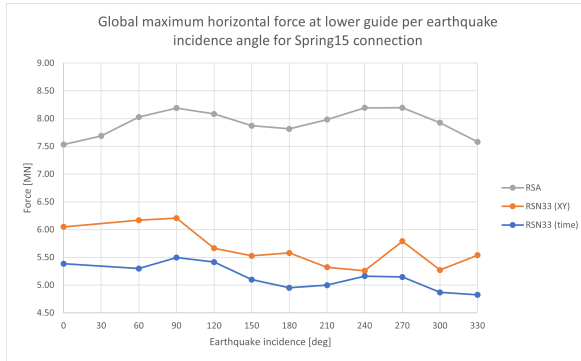
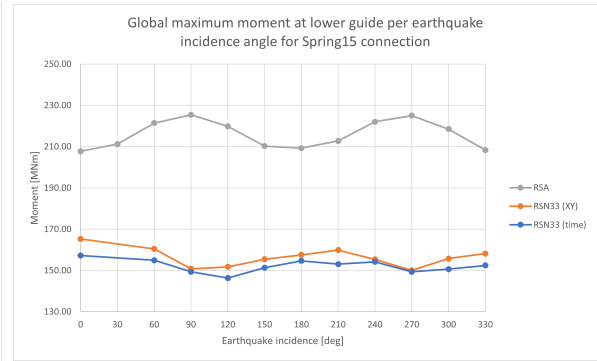


Figure F.2: Max moment  $M_{LG}$  at the lower guide per EQ incidence angle for the Spring15 connection; FKS01

**RSN33**



**Figure E3:** Max shear force  $F_{H,LG}$  at the lower guide per EQ incidence angle for the Spring15 connection; RSN33



**Figure E4:** Max moment  $M_{LG}$  at the lower guide per EQ incidence angle for the Spring15 connection; RSN33

**RSN57**

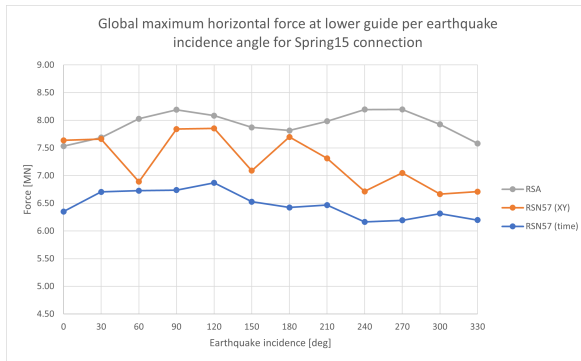


**Figure E5:** Max shear force  $F_{H,LG}$  at the lower guide per EQ incidence angle for the Spring15 connection; RSN57

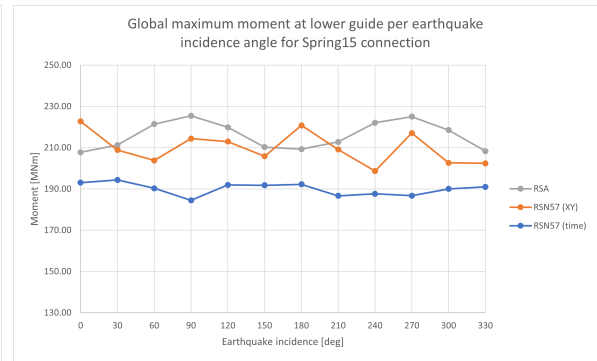


**Figure E6:** Max moment  $M_{LG}$  at the lower guide per EQ incidence angle for the Spring15 connection; RSN57

**RSN73**

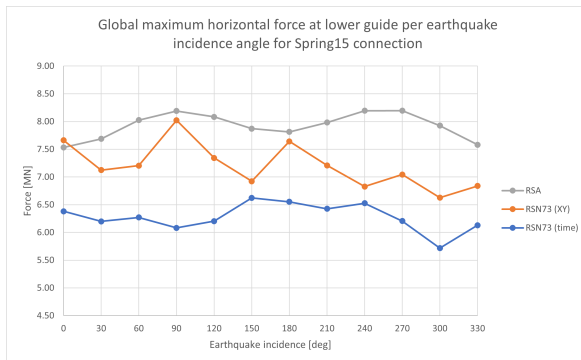


**Figure E7:** Max shear force  $F_{H,LG}$  at the lower guide per EQ incidence angle for the Spring15 connection; RSN73

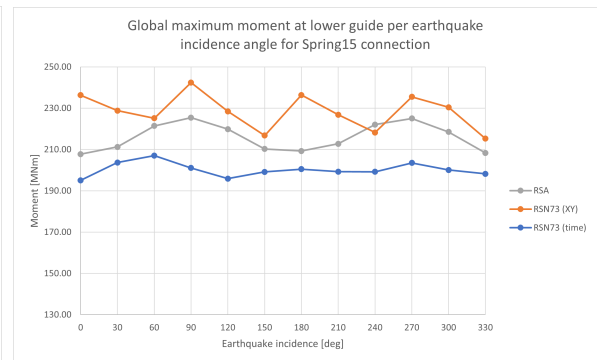


**Figure E8:** Max moment  $M_{LG}$  at the lower guide per EQ incidence angle for the Spring15 connection; RSN73

# Bibliography

- [1] Earth observatory of Singapore, “The great east japan (tohoku) 2011 earthquake: Important lessons from old dirt,” 2011.
- [2] ISO-19901-2, “Petroleum and natural gas industries - specific requirements for offshore structures - seismic design procedures and criteria.” Genève, Switzerland: the International Organization for Standardization, Nov. 2004.
- [3] R. W. Clough and J. Penzien, *Dynamics of structures*. Computers & Structures, Inc., 1995.
- [4] J. Jia, *Modern Earthquake Engineering*. Springer, 2017.
- [5] PEER, “Nga-west2 database,” 2014.
- [6] ISO-19905-1, “Petroleum and natural gas industries - site specific assessment of mobile offshore units - jack-ups.” Genève, Switzerland: the International Organization for Standardization, Jan. 2016.
- [7] “En 1998-1: Eurocode 8: Design of structures for earthquake resistance - part 1: General rules, seismic actions and rules for buildings.”
- [8] American Society of Civil Engineers, “Minimum design loads and associated criteria for buildings and other structures.” American society of civil engineers, 2017.
- [9] ISO-19902, “Petroleum and natural gas industries - fixed steel offshore structures.” Genève, Switzerland: the International Organization for Standardization, Dec. 2007.
- [10] “Opensees,” 2018.
- [11] A. K. Chopra, *Dynamics of structures - theory and applications to earthquake engineering, 4th edition*. Prentice Hall, 2010.
- [12] J. Lysmer and F. E. Richart, “Dynamic response of footings to vertical loading,” *Journal of soil mechanics and foundations division*, vol. 92, no. 1, pp. 65–91, 1966.
- [13] E. Kausel, *Advanced Structural Dynamics*. Cambridge University Press, 2017.
- [14] A. Whittaker, G. Atkinson, J. Baker, J. Bray, D. Grant, R. Hamburger, C. Haselton, and P. Somerville, “Selecting and scaling earthquake ground motions for performing response-history analyses,” 2011-11-15 2011.
- [15] gopisrt7, “readpeer.m.” Copyright (c) 2015.
- [16] G. Shin and O. Song, “A time-domain method to generate artificial time history from a given reference response spectrum,” *Nuclear Engineering and Technology*, vol. 48, no. 3, pp. 831 – 839, 2016.
- [17] F. Naeim and M. Lew, “On the use of design spectrum compatible time histories,” *Earthquake Spectra*, vol. 11, no. 1, pp. 111–127, 1995.
- [18] J. Hancock, J. Watson-Lamprey, N. A. Abrahamson, J. J. Bommer, A. Markatis, E. McCoyh, and R. Mendis, “An improved method of matching response spectra of recorded earthquake ground motions using wavelets,” *Journal of Earthquake Engineering*, vol. 10, no. sup001, pp. 67–89, 2006.
- [19] A. Tsouvalas, *CIE5260 Structural Response to Earthquakes*. Delft University of Technology, 2018.
- [20] G. Gazetas, *Foundation engineering handbook*, ch. 15: Foundation vibrations, pp. 553–593. Chapman and Hall, 1991.

- 
- [21] N. D. P. Barltrop and A. Adams, *Dynamics of fixed marine structures*. Elsevier, 1991.
- [22] J. Linthorst, "Seismic analysis of cranes on jack-ups,"
- [23] G. Mylonakis and G. Gazetas, "SEISMIC SOIL-STRUCTURE INTERACTION: BENEFICIAL OR DETRIMENTAL?," vol. 4, no. 3, pp. 277–301.
- [24] J. Wang, D. Zhou, W. Liu, and S. Wang, "Nested lumped-parameter model for foundation with strongly frequency-dependent impedance," *Journal of Earthquake Engineering*, vol. 20, no. 6, pp. 975–991, 2016.